Universitat Autònoma de Barcelona	UAB Universitat Autònoma de Barcelona	Departament de Química Facultat de Ciències

Doctorat en Química

Molecular Modelling

of Switchable [2]Rotaxanes

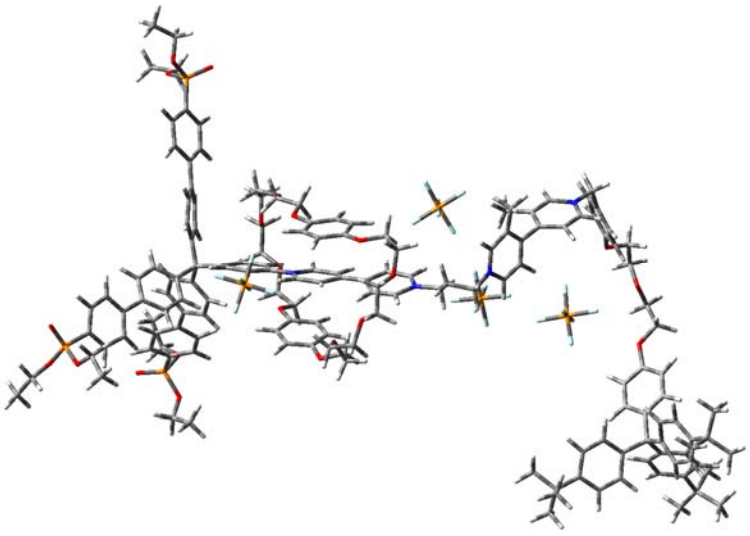

Javier Pérez Mirón

Supervised by Carlos Jaime Cardiel

PhD Thesis - March 2008

Universitat Autònoma de Barcelona	UAB Universitat Autònoma de Barcelona	Departament de Química Facultat de Ciències
Doctorat en Química		

Molecular Modelling

of Switchable [2]Rotaxanes

Javier Pérez Mirón

Supervised by Carlos Jaime Cardiel

PhD Thesis - March 2008

Universitat Autònoma de Barcelona

Unitat de Química Orgànica

Departament de Química

Universitat Autònoma de Barcelona

El Dr. Carlos Jaime Cardiel, catedràtic d'universitat del Departament de Química de la Universitat Autònoma de Barcelona

FA CONSTAR:

que la tesi doctoral que porta per títol "Molecular Modelling of Switchable [2]rotaxanes" ha estat realitzada sota la seva supervisió per Javier Pérez Mirón, llicenciat en Química, i es presenta en aquesta memòria per tal d'optar al grau de Doctor de la Universitat Autònoma de Barcelona dins el programa de Química.

I per a que així consti, signa la present.

Carlos Jaime Cardiel

Bellaterra, a 11 de gener de 2008.

‘*Here they come.*

And I’m not ready.

How could I be?

I’m a new teacher and learning on the job.’

Teacher Man by Frank McCourt

To my wife

Agradecimientos (Acknowledgments)

Tras acabar esta tesis, ahora es el momento de agradecer a mucha gente su apoyo y su compañía durante estos últimos años. La verdad es que han sido unos años de mi vida en los que he tratado de exprimir y disfrutar cada segundo. Los que me conocen bien saben que no me gusta la monotonía y durante la tesis he tenido tiempo para todo menos para aburrirme: mucho trabajo de investigación y de docencia, algunos viajes y algunos momentos de diversión.

En primer lugar, me gustaría dar las gracias a mi director de tesis Carlos Jaime por ayudarme a realizar este trabajo, por su apoyo incondicional a pesar de su *multitasking* y por todo lo que he aprendido y las oportunidades que me han surgido gracias a él. También quiero agradecer a Albert Virgili por darme la oportunidad de entrar en el grupo y por compartir tantos buenos momentos en la facultad junto con el resto de miembros del grupo.

Más allá de estas páginas que componen la tesis, hay escrita una historia de la vida de un estudiante que sólo unos pocos conocen. Muchas de estas páginas tienen acento irlandés quizás por mis viajes a esa isla misteriosa llamada Irlanda. El primero de esos viajes fue en agosto de 2004 y me acuerdo muy bien de los nervios que pasé: mi primera vez que cogía un avión, mi primera vez que visitaba la isla y mi primera vez que hablaba personalmente con el profesor Donald Fitzmaurice, el director del grupo irlandés con el que he colaborado durante todos estos años. Recuerdo mi *speaking* lento, trabado y muy rico en *spanglish*. La segunda vez que visité la isla fue en diciembre de ese mismo año. Durante una semana, además de trabajar y conocer a todos los integrantes del grupo de Nanoquímica, pude disfrutar del magnífico paisaje y conocer muchos de los tesoros que guarda Irlanda. Al año siguiente, pasé dos meses en Dublín trabajando en la UCD. En poco tiempo me adapté al estilo y ritmo de vida irlandés. Sin embargo, añoré el buen tiempo de España y sobretodo, eché de menos a mi familia y amigos. Un año más tarde, el destino quiso que volviera de nuevo a la isla mágica y verde. Esa última estancia en Irlanda tuvo lugar del 1 de abril al 1 de mayo del 2006. Tengo que reconocer que durante todos esos meses no aprendí mucho de química. Sin embargo, volví a España cargado de experiencias inolvidables y con una madurez notable. Me gustaría terminar de hablar de mis aventuras en tierras irlandesas

agradeciendo a Jacek Stolarczyk todo su apoyo durante todos los meses que he estado en Irlanda y me gustaría mencionar al resto de miembros del grupo de Nanoquímica (especialmente a Keith, Elena y Amro) con quienes he pasado ratos muy divertidos y agradables.

En el laboratorio de la Universidad Autónoma de Barcelona he pasado muchas horas durante todos estos años donde he compartido ratos de "bricomanía" y tertulias con Itzi, Miguel y Kepa: mis maestros de AMBER y MacroModel. Muchas gracias por vuestra ayuda especialmente a Kepa, quien más me ha ayudado en el mundo de los cálculos y las computadoras. Me gustaría agradecer también a Petko Ivanov, Toni Llobet y David Rodríguez por haber podido colaborar con ellos.

También me gustaría mencionar al resto de miembros de mi laboratorio (Julen, Sergio, Raquel y Eva), a todos los amigos (Yoli, Manu, Irene, Sergio, Anabel, Arnau, Tony, David, Xavi, …), a los compañeros que tengo en toda la torre de química y a los profesores que han trabajado junto a mí en estos años de investigación y docencia. Tengo que reconocer que dar clases no ha sido una tarea fácil, pero he de agradecer a mis alumnos su compresión, su participación y el respeto que me han tenido en la clase o en el laboratorio.

Finalmente, me gustaría que estas últimas líneas de agradecimiento fueran para mi mujer Yanira y mi familia. Si estoy aquí es gracias a ellos.

Muchas gracias a todos.

TABLE OF CONTENTS

PURPOSES

INTRODUCTION

RESULTS

PURPOSES

'May the road rise to meet you.
May the wind be always at your back.
May the sun shine warm upon your face.
And rains fall soft upon your fields.
And until we meet again.
May God hold you in the hollow of His hand.'

Irish Blessing

1 PURPOSES

The purpose of this PhD thesis is to examine by computational methods a number of novel [2]rotaxanes that have been synthesised and characterized by Prof. Fitzmaurice's Group at the University College Dublin (UCD), Dublin, Ireland.

Essentially, the main points to address are the following:

1.- Studying of the [2]pseudorotaxanes shown in Scheme 1-1. It is an important step forward as the viologen stations (essentially the axle of the pseudorotaxane) constitute the building blocks of more complex rotaxanes and provide insights into the energetics and strength of the interactions between the crown ether ring and the stations. We want to determine the dynamic structure of the pseudorotaxanes in acetonitrile and methanol solutions (changing also the counterions, PF_6^- and Br^-), calculate the association constants for pseudorotaxanes (viologen-crown complex) and determine the energy profile for the movement of the crown along the axle of the pseudorotaxane.

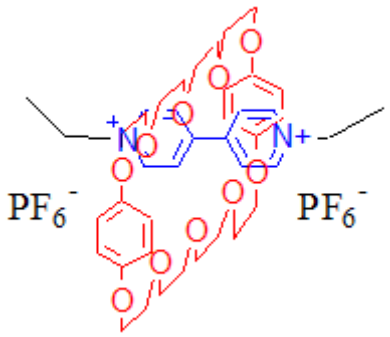

Scheme 1-1.- Example of a [2]pseudorotaxane studied

2.- Studying of the [2]rotaxane shown in Scheme 1-2. It contains two viologen stations which exhibit different levels of affinity towards the crown ether, two bulky stoppers (including one which could be used to attach the rotaxane to the surface of an electrode or semiconductor nanoparticle) and a crown ether. The two viologen stations are connected through a flexible aliphatic linker.

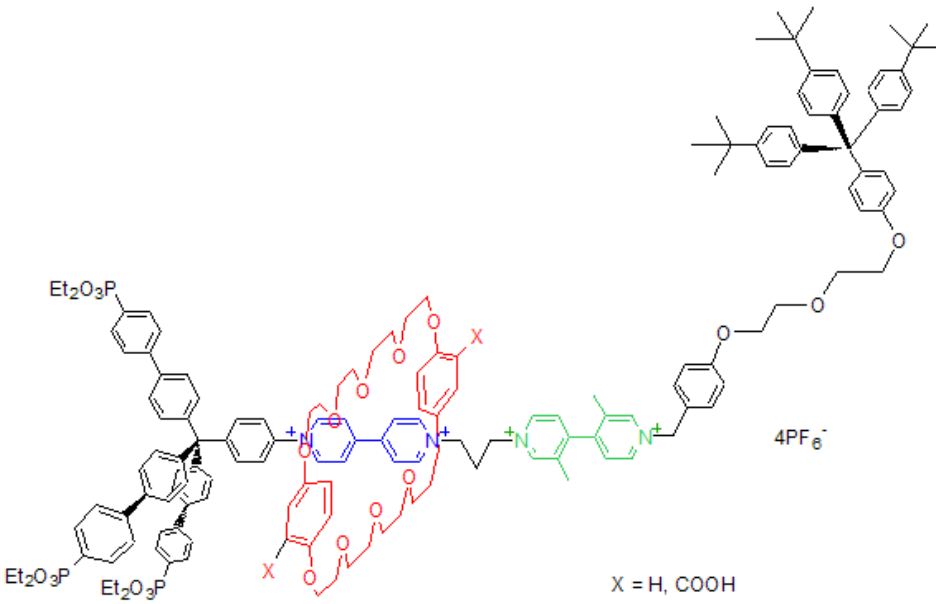

Scheme 1-2.- General scheme of the [2]rotaxanes studied

We want to complete the modelling of the structural and dynamical properties of such [2]rotaxane and to compare the results with experimentally determined solution structures. The experimental results were obtained using NMR, optical absorption spectroscopy and cyclic voltammetry.

3.- Studying of the shuttling phenomenon of the [2]rotaxane induced by stepwise reduction of the viologen stations. Firstly, we shall calculate the structure and energy of singly reduced pseudrotaxanes (i.e. cation radical viologens).

4.- Extension of the study shown previosly to full two-station rotaxanes undergoing four successive steps of reduction. It will be a critical observation from the molecular dynamics simulations at which stage of the reduction the crown moves to the second station, as envisaged in Scheme 1-3.

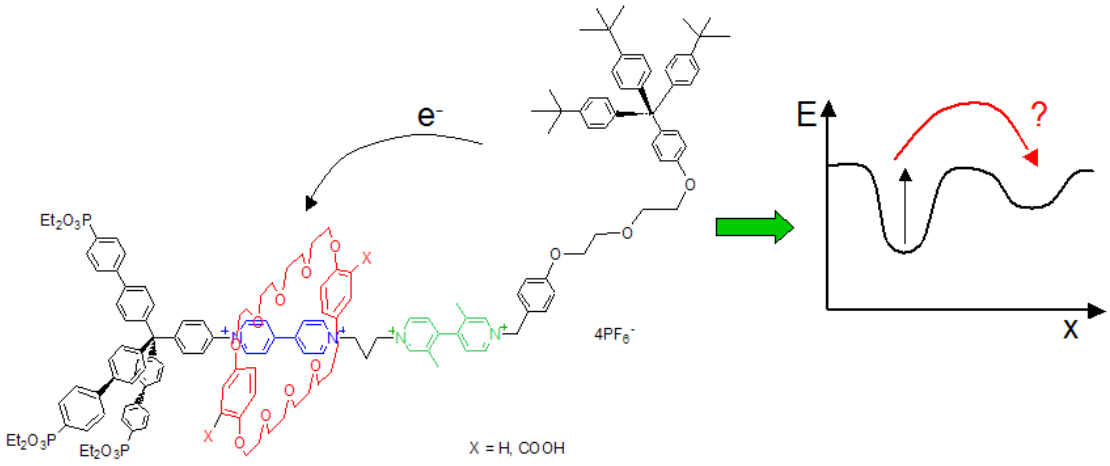

Scheme 1-3

All four steps of reduction (from 4+ to 0 net charge) are of great interest to study the shuttling phenomenon. It is however known from electrochemical data that the movement of the ring should happen when the interaction between the first station and the ring is decreased, i.e. after second or third step. Therefore if the time constraints do not allow us to study all four steps, we will limit our studies to the first three steps. If time permits, we will continue to execute the last step.

Hence, this collaboration will provide insights on the underpinning of the rational design of [2]rotaxanes and related supermolecules capable of functioning as bi-stable switches for use in the next-generation electronics. [1]

[1] a) Prasanna de Silva, A.; McClenaghan, N. D. *Chem. Eur. J.* **2004**, *10*, 574. b) Balzani, V.; Clemente-Leon, M.; Credi, A.; Ferrer, B.; Venturi, M.; Flood, A; Stoddart, J. F. *Proc. Nat. Acad. Sciences*, **2006**, *103*, 1178.

INTRODUCTION

'When Irish eyes are smiling,
sure it's like a morning spring.
In the lilt of Irish laughter
You can hear the angels sing.
When Irish hearts are happy,
all the world seems bright and gay.
And when Irish eyes are smiling,
They'll steal your heart away!

Traditional Irish Folk Song

2 INTRODUCTION

2.1 SUPRAMOLECULAR CHEMISTRY

2.1.1 From Molecular to Supramolecular Chemistry

Supramolecular chemistry refers to the area of chemistry which focuses on the study of systems which contain more than one molecule, and it aims to understand the structure, function, and properties of these assemblies.

The domain of supramolecular chemistry came of age when Donald J. Cram, Charles J. Pedersen and Jean-Marie Lehn were jointly awarded the Nobel Prize for Chemistry in 1987 (see Scheme 2-1) in recognition of their work on "host-guest" assemblies (in which a host molecule recognizes and selectively binds a certain guest). The field of supramolecular chemistry was defined by Lehn as 'chemistry beyond the molecule', and involves investigating new molecular systems in which the most important feature is that the components are held together reversibly by intermolecular forces, not by covalent bonds.

Scheme 2-1.- Nobel Chemistry Laureates in 1987

For many years, chemists have synthesized molecules and investigated their physical and chemical properties. Interest in supramolecular chemistry arose when chemistry became relatively mature subject and the synthesis and properties of molecular compounds had become well understood.

Its development requires the use of all resources of molecular chemistry combined with the designed manipulation of non-covalent interactions so as to form supramolecular entities, supermolecules possessing features as well defined as those of molecules themselves (see Scheme 2-2).

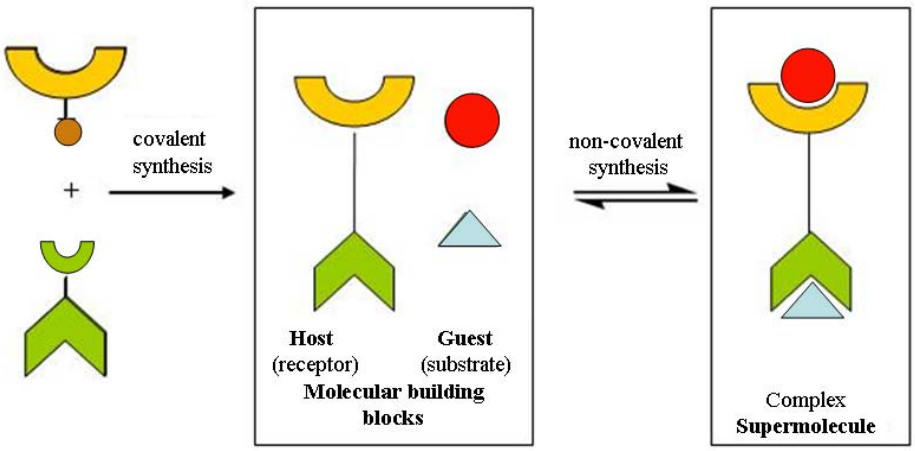

Scheme 2-2.- Supramolecular Chemistry

Lehn said that supermolecules are to molecules and the intermolecular bond what molecules are to atoms and the covalent bond (see Scheme 2-3).

MOLECULAR CHEMISTRY	→	SUPRAMOLECULAR CHEMISTRY
Covalent Bond Formation		Non-covalent Bond Formation

Scheme 2-3.- Differences between molecular chemistry and supramolecular chemistry

Since many years, chemists are trying to design artificial molecules capable of displaying processes of highest efficiency and selectivity. However, it is needed the correct manipulation of the energetic and stereochemical features of the non-covalent, intermolecular forces (electrostatic interactions, hydrogen bonding, van der Waals forces etc.) within a defined molecular architecture.

The basic functions of supramolecular species are molecular recognition, transformation and translocation. These species can be organized to create polymolecular assemblies and phases (layers, membranes, vesicles, liquid crystals, etc.) or functional supermolecules that may lead to the development of molecular devices.

Supramolecular chemistry has been applied to the development of new materials. Moreover, it is often used to develop new functions that cannot appear from a single molecule such as magnetic properties, light responsiveness, catalytic activity, chemical sensors, etc. Supramolecular chemistry is also important to the development of new pharmaceutical therapies by understanding the interactions at a drug binding site.

Green chemistry is also another of its applications where reactions have been developed which proceed in the solid state directed by non-covalent bonding. That kind of procedures is very desirable because the use of solvents during the production of chemicals can be reduced. [2]

2.1.2 Molecular Recognition in Supramolecular Chemistry

The knowledge of molecular recognition started when Charles J. Pedersen discovered crown ether in 1967.

Molecular recognition has been defined by Lehn as a process involving both binding and selection of substrate(s) by a given receptor molecule, as well as possibly a specific function.

A supermolecule, which is a well defined complex of molecules held together by noncovalent bonds, is characterized by its thermodynamic and kinetic stability and selectivity. The size, shape and position of the binding sites within the active site are

[2] a)Lehn, J.-M. Nobel lecture, December 8, **1987**. b) Lehn, J.-M. *Supramolecular chemistry: concepts and perspectives*. Wiley-VCH: Weinheim, **1995**.

ideal for specific substrate recognition. Thus, molecular recognition is a question of information storage and read out at the supramolecular level. [3]

These concepts were described by Emil Fischer in 1894 as the "Lock and Key " principle. The idea is represented in Scheme 2-4 where the arrangement of binding sites in the host (lock) is complementary to the guest (key) both sterically and electronically.

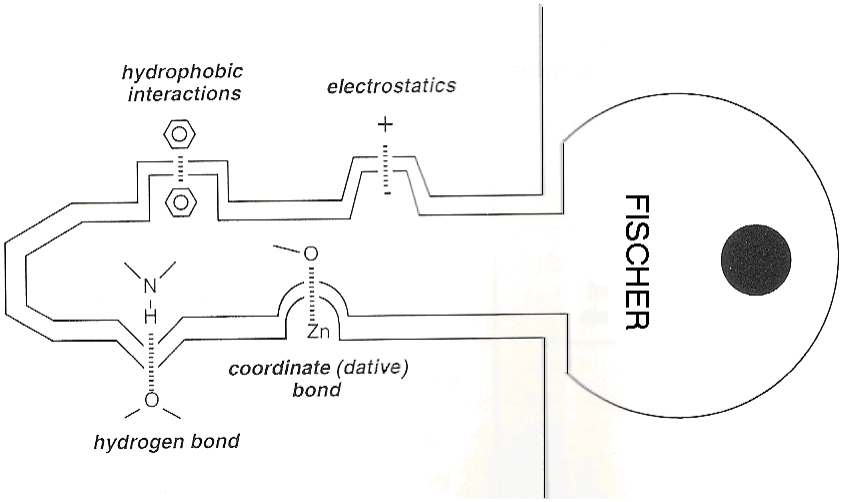

Scheme 2-4.- Lock and key principle

The ideas of molecular recognition and of receptor chemistry have been penetrating chemistry more and more over the last fifteen years, namely in view of its bioorganic implications, but more generally for its significance in intermolecular chemistry and in chemical selectivity.

2.1.3 Non-Covalent Interactions: the Main Forces at Supramolecular Chemistry

Supramolecular species are characterized both by the spatial arrangement of their component, their architecture or superstructure, and by the nature of the intermolecular bonds that hold these components together. They possess well-defined structural, conformational, thermodynamic, kinetic and dynamical properties.

[3] Cragg, P. J., *A Practical Guide to Supramolecular Chemistry*. Wiley-VCH: Weinheim, **2005**.

The "glue" used by supramolecular chemists to hold molecules together is non-covalent, and there are various types of interactions that can be utilized. They include:

- Electrostatics (ion-ion, ion-dipole and dipole-dipole);
- Hydrogen bonding;
- π-π Stacking interactions;
- Dispersion and induction forces (van der Waals forces);
- Hydrophobic or solvatophobic effects.

The strengths of many of the non-covalent interactions used by supramolecular chemists are generally much weaker than covalent interactions. However, the power of supramolecular chemistry lies in the combination of a number of weak interactions, allowing strong and selective recognition of specific guests to be achieved. [4]

2.1.4 Self-Processes

Processes that are directed by information held internally within a system are termed self-processes. These include self-assembly, self-organization, self-repair and self-replication. An important distinction is made between self-assembly and self-organization.

Supramolecular self-assembly concerns the spontaneous association of a few or many molecular components resulting in the generation of oligomolecular or polimolecular supermolecules such as molecular layers, films, membranes, etc. These assemblies are generated by spontaneous recognition-directed association under the intermolecular control of the non-covalent interactions.

[4] Beer, P. D.; Gale, P. A.; Smith, D. K., *Supramolecular Chemistry*. Oxford University Press: Great Britain, **1999**.

Self-organization can be considered as an ordered self-assembly process. It involves multicomponent systems that show a spontaneous emergence of order in either space or time or both by means of non-covalent interactions.

The use of molecular recognition events to direct self-assembly and self-organization of components has resulted in the creation of many interesting organic and inorganic architectures.

Self-assembly and self-organization are dominant processes in the chemistry of living biological systems as for example, the formation of the DNA double helix from two complementary deoxyribonucleic acid strands. Under the right conditions, the termodynamically stable double helix forms spontaneously and reversibly as the strands are mixed together and hydrogen bonds are formed between complementary base pairs. As a result of the reversibility of the process, it is possible to correct any errors that may have occurred during assembly. These assemblies have many potential uses ranging from information storage to drug delivery.

Construction of artificial supramolecular structures via self-organization needs suitably programmed molecular components and full control of all the weak intermolecular forces (including solute-solvent interactions) involved in the thermodynamically driven formation of the desired system. This task can be successfully fulfilled by careful chemical design of the molecular components. Several supramolecular structures have indeed been obtained by self-association and self-organization of artificial molecular components.

However, the construction of artificial supramolecular devices and machines by self-assembly and self-organization is a much more difficult job. The reason of this fact is that the various molecular components must be programmed to ensure their self-assembly into a structurally organized system and to ensure their function integration, as required by the operation the device or machine is expected to perform.[5]

[5] Balzani, A.; Credi, A.; Venturi, M. *Molecular Devices and Machines : a Journey into the Nano World*. Wiley-VCH: Weinheim, **2003**.

2.2 NANOCHEMISTRY

Nanochemistry can be defined briefly as the study of the synthesis and analysis of materials in the nanoscale range (1-100 nanometers), including large organic molecules, inorganic cluster compounds, and metallic or semiconductor particles.

Half a century ago, the Nobel Laureate in Physics, Richard Feynman outlined the foundations of nanoscience (the science of building devices from single atoms and molecules), and the promise that totally synthetic constructions could eventually be built with molecular scale precison. Nanoscience research has been rapidly increasing across the globe during the past decade. It is now widely accepted by the scientific, industrial, goverment and business communities, that nanoscience will be of integral importance in the development of future technologies. Nanoscience will be the engine that will drive the next industrial revolution.

For building devices, the electronic designer usually works using the top-down approach, creating machines each time smaller. In fact, lithographic techniques, used in the recent production of mini transistors made of silicon, are going to the top of its limits (see Scheme 2-5).

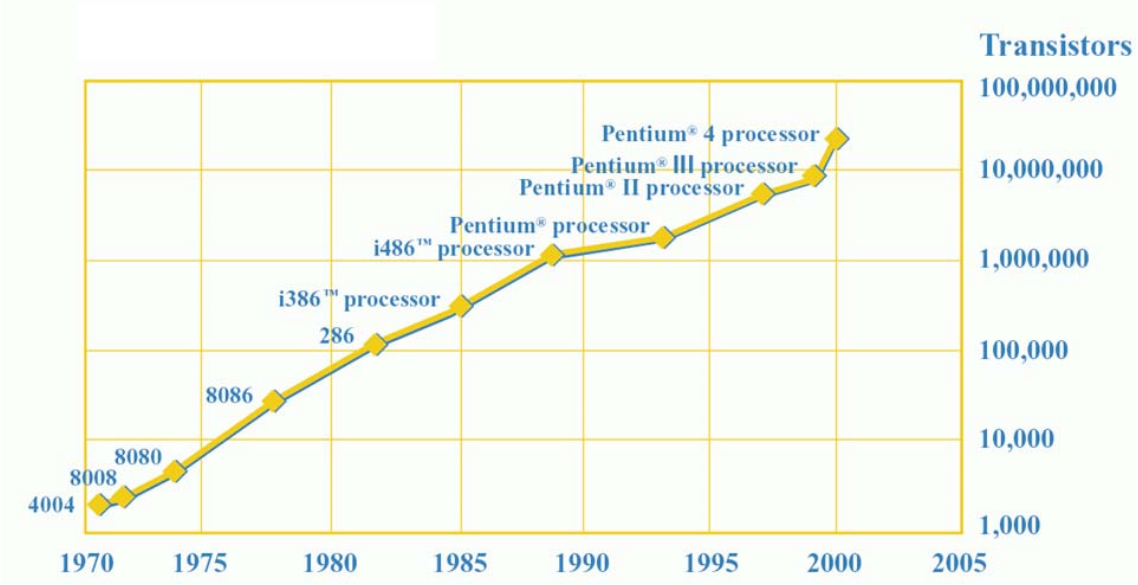

Scheme 2-5.- Moore's law

Therefore, “there is plenty of room at the bottom” for further miniaturization, as Richard P. Feynman[6] stated in a famous talk to the American Physical Society in 1959, but the top-down approach does not seem capable of exploiting such opportunity. To proceed towards further miniaturization, science and technology will have to find new ways.

An alternative and promising strategy towards technology on the nanometer scale is offered by the bottom-up (small-upward) approach, which starts from atom or molecules and builds up to nanostructures. Chemists, by the nature of their discipline, are already at the bottom, because we can manipulate atoms and molecules. We are, therefore, in the ideal position to develop bottom-up strategies for the construction of nanoscale devices and machines.

Nanoscience today is a creative amalgamation of bottom-up chemistry and top-down engineering techniques. We are currently witnessing an explosion of novel ideas and strategies for making and manipulation, visualizing and interrogation nanoscale materials and structures.

Nanochemistry is the utilization of synthetic chemistry to make nanoscale building blocks of different size and shape, composition and surface structure, charge and functionality. These building blocks may be useful in their own right. Or in a self-assembly construction process, spontaneous, directed by templates or guided by chemically or lithographically defined surface patterns, they may from architectures that perform an intelligent function and portend a particular use (termed “molecular devices"). [7]

2.2.1 Nanoscale Devices and Machines

A molecular machine can be defined as a particular type of molecular-level device in which the component parts can display changes in their relative positions as a

[6] Feynman, R. P. *Eng. Sci*. **1960**, *23*, 22.

[7] Ozin, G. A.; Arsenault, A. C. *Nanochemistry: A Chemical Approach to Nanomaterials*. RSC Publishing: Cambridge, **2005**.

result of some external stimulus, and as a consquence a net task is performed, something useful happens.

Such movements usually result in changes of some chemical and/or physical property of the supramolecular system, giving rise to a monitorable signal used to follow the operation of the machine. The reversibility of the movements, i.e., the possibility to restore the initial situation by means of an opposite control stimulus, is an essential feature of a molecular machine.

Analogously to what happens for macroscopic machines, the energy to make molecular machines work (that is, the stimuli which induce the molecular motions) can be supplied as light, electrical energy, or chemical energy. In most cases, the mechanical movements occur between two different, well defined and stable states, and are accompanied by on/off switching of some observable property, usually monitored by NMR, electronic absorption and luminescense spectroscopies, and by electrochemical techniques. For this reason, molecular machines can also be regarded as bistable devices for information storage.[8]

2.3 CATENANES, ROTAXANES AND PSEUDOROTAXANES

The synthesis of assemblies in which two molecular components are interlinked, but not chemically joined by covalent bonds, presents a considerable challenge to the supramolecular chemist. The catenanes, rotaxanes and pseudorotaxanes illustrate this callenge most clearly.

Catenanes (from Latin: *catena* (chain)) are molecular systems constituted of mechanically interlocked macrocyclic species.[9] Once a catenane has formed, the only

[8] a) Kay, E. R.; Leigh, D. A; Zerbetto, F. *Angew. Chem. Int. Ed.* **2007**, *46*, 72. b) Balzani, V.; Gomez-Lopez, M.; Stoddart, J. F. *Acc. Chem. Res*. **1998**, *31(7)*, 405. c) Balzani, V.; Credi A.; Venturi, M. *ChemPhysChem*, DOI: 10.1002/cphc.200700528.

[9] Balzani, V.; Credi, A.; Langford, S. J.; Raymo, F. M.; Stoddart, J.F.; Venturi, M. *J. Am. Chem. Soc*. **2000**, *122(14),* 3542.

way in which the rings can be removed from one another is by breaking one of the rings. A [*n*]catenane is composed of *n* interlocking macrocycles (Scheme 2-6).

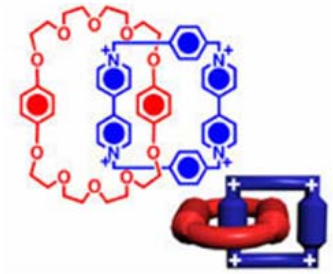

Scheme 2-6.- Example of a [2]catenane

Rotaxanes (from the latin words *rota*, wheel, and *axis*, axle) are constituted of a macrocyclic component through which a linear subunit (axle) is threaded. The ends of the axle are stoppered with bulky groups that prevent the macrocycle from slipping off. Therefore the individual components are permanently joined together, but are not linked by an actual covalent bond. The nomenclature [*n*]rotaxane refers to the total number of non-covalently linked components present in the rotaxane (Scheme 2-7).

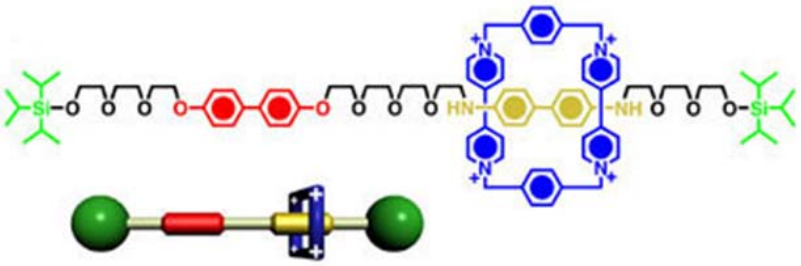

Scheme 2-7.- Example of a [2]rotaxane

Pseudorotaxanes are supramolecular systems composed of a thread-like species inserted through the cavity of a macrocycle. Since there are no stoppers at the ends of the thread, dissociation of the complex can occur, and the pseudorotaxane is always equilibrated with its components unthreaded. A [*n*]pseudorotaxane contains one linear and *n*-1 macrocyclic components (see Scheme 2-8).[10]

[10] Vignon, S. A.; Stoddart, J. F. *Collect. Czech. Chem. Commun*. **2005**, *70*, 1493.

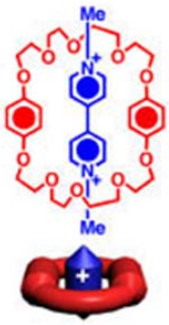

Scheme 2-8.- Example of a [2]pseudorotaxane

Obviously, the simplest molecular systems of this type are whose with *n*=2. We will deal in this thesis mainly with [2]pseudorotaxanes and [2]rotaxanes.

We want to mention also another class of interlocked molecules called suitanes (from English *suit*). It consists of two separate components – a body with two or more limbs whose torso carries a close-fitting, all-in-one suit, such that it encompasses the torso of the body. The *n* of suit[*n*]ane will indicate the number of protruding limbs. For example, in the Scheme 2-9 we can show the construction of a suit[5]ane composed by crown ethers with [24]crown-8 constitutions (red rectangles) and $-NH_2^+$- stations ("+" signs) on the linears (blue lines). [11]

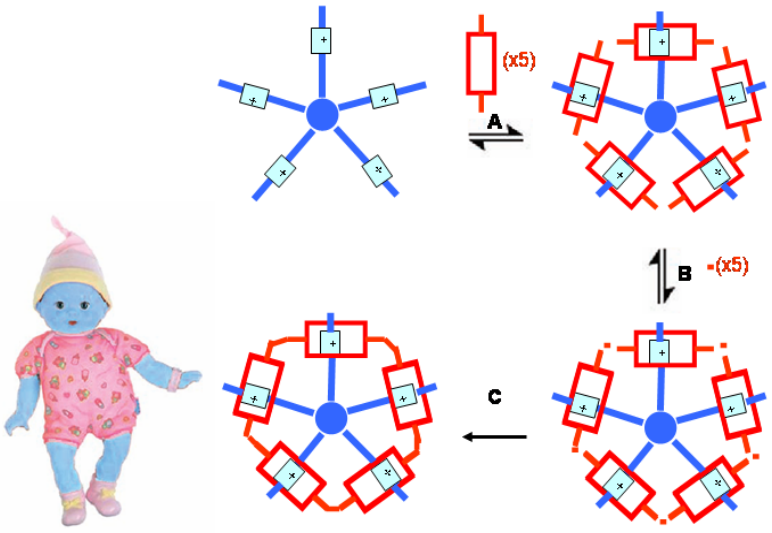

Scheme 2-9.- Representation of the construction of a suit[5]ane.

[11] Williams, A. R.; Northrop, B. H.; Chang, T.; Stoddart, J. F.; White, A. J. P.; Williams, D. *J. Angew. Chem. Int. Ed*. **2006**, *45*, 6665.

2.3.1 Synthesis of rotaxanes

There are different strategies for rotaxane synthesis.[12] The main approaches are the following: threading, slipping and clipping (see Scheme 2-10).

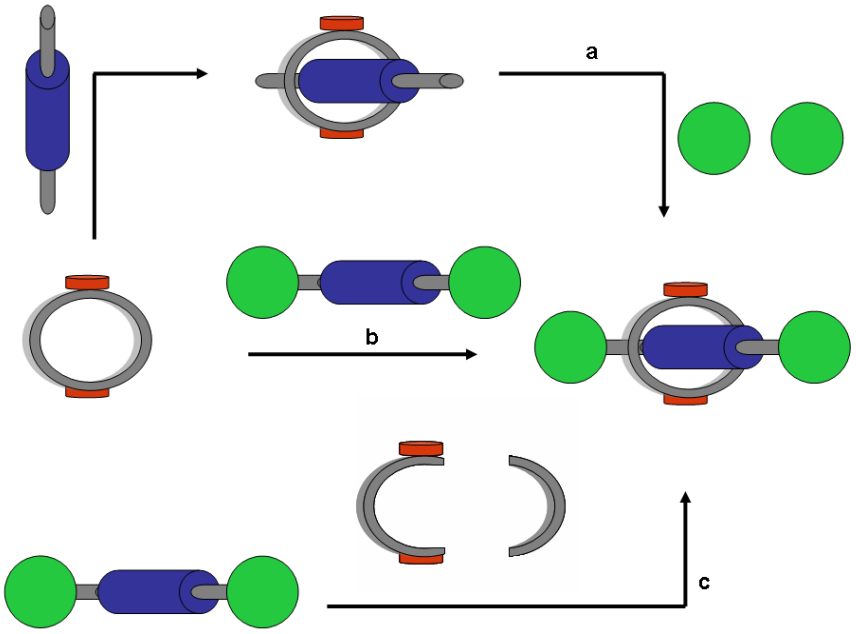

Scheme 2-10.- Synthesis of rotaxanes a) threading approach. b) slipping approach. c) clipping approach.

2.3.1.1 Threading approach

Threading involves mixing self-assembling linear and macrocycling components to form a pseudorotaxane. The ends of the lineal component are then stoppered to prevent the ring slipping off the axle, producing a [2]rotaxane (Scheme 2-10a).

[12] Gómez-López, M.; Preece, J. A.; Stoddart, J. F. *Nanotechnology*, **1996**, *7*, 183.

2.3.1.2 Slipping approach

In this approach, the macrocyclic and dumbbell-shaped components are synthesized separately. These two species are then heated together in solution, in order that the macrocycle slips over the stoppers of the dumbbell to form a rotaxane. When the reaction mixture is cooled down, the macrocycle is obliged to remain threaded on the dumbbell, as it is trapped in the thermodynamic minimum due to the non-covalent interactions between the dumbbell and the macrocyclic component. This approach requires that the bulky groups present at both ends of the dumbbell are tailored with respect to the size of the macrocycle, i.e., they must act as stoppers for the ring at room temperature, and let the ring slip over when the temperature is increased (Scheme 2-10b).

2.3.1.3 Clipping approach

The macrocyclization of the ring component is carried out in the presence of the performed dumbbell-shaped component, which then templates the formation of the macrocycle (Scheme 2-10c).

2.3.2 Switchable [2]rotaxane

A switchable [2]rotaxane contains two sites in the axle (stations) which can be recognized by the macrocycle. Moreover, the strengths of the non-covalent bonding interactions between two recognition sites with the ring component are quite different, and as a result, the ring component locates preferentially on the station that has stronger interactions with the ring. In such a system, when a suitable external stimulus -either chemical or physical- is applied, the binding preference of the two recognition sites is altered, as a consequence, the ring component shuttles from the original recognition site to another. In the ideal case, the properties of the two recognition sites can be shifted reversibly back to the original ones by another stimulus. Such a molecule constitutes a molecular shuttle.

In 1991, Pier Lucio Anelli, Neil Spencer and J. Fraser Stoddart reported the first molecular shuttle. It was based on a [2]rotaxane consisting of a linear dumbbell-shaped component, possessing two π-electron rich hydroquinone rings separated by a polyether chain and terminated by two bulky triisopropylsilyl groups as stoppers and a cyclic tetracationic cyclophane which was threaded on to the linear component (see Scheme 2-11). [13]

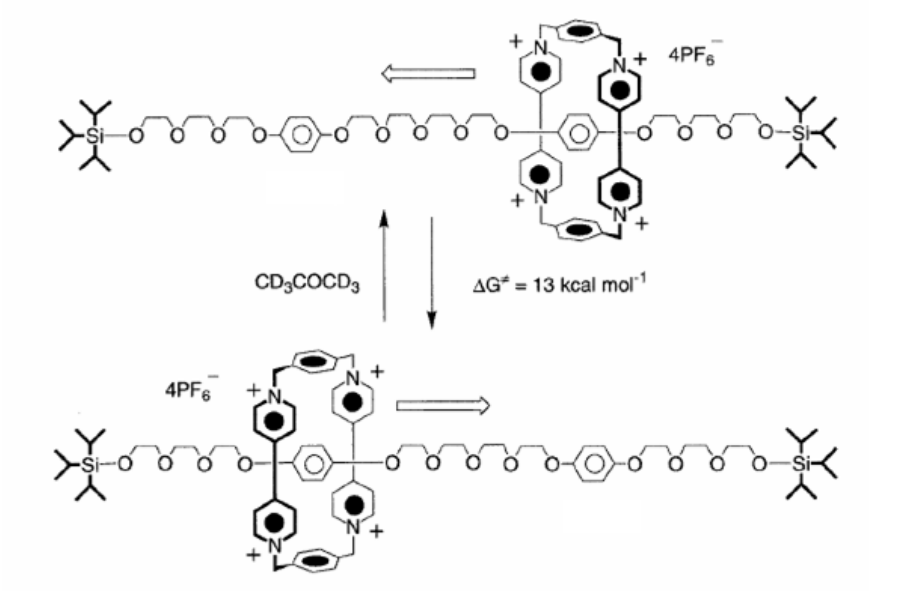

Scheme 2-11.- Graphical representation of the first molecular shuttle.

2.3.2.1 Driving forces of switchable rotaxanes

It can be seen that the external stimulus employed to effect the switching motion of a rotaxane must be able to weaken the relative binding forces which stabilize the initial state. Thus, the type of stimulus used depends on the nature of the binding forces. A chemical (acid/base), an entropic stimulation, or a solvent change can drive a molecular machine based on hydrogen-bonding; chemicals (oxidant/reducer), electrochemical (redox) processes, or photochemical (photoinduced redox) processes

[13] a) Anelli, P. R.; Spencer, N.; Stoddart, J. F. *J. Am. Chem. Soc*. **1991**, *113*, 5131. b) Balzani, V.; Gomez-Lopez, M.; Stoddart, J. F. *Acc. Chem. Res*. **1998**, *31(7)*, 405.

can power a molecular machine relying on donor/acceptor interactions. A photoisomerization process can also induce relative special changes among the components and thus can drive a molecular shuttle.

Like a macroscopic machine displaying intercomponental relative position changes when applying power, a switchable rotaxane performs shuttling motion in response to external stimuli. From this point of view, a molecular shuttle is also seen as a molecular machine, and the external stimuli are the driving forces, or energies supplies, of the machine system. [14]

2.3.2.1.1 Chemical energy

In the literature, we can find a lot of examples of this sort of switchable rotaxanes.[15] In fact, this is the most obvious way of supplying a molecular machine system. We can show in the Scheme 2-12 a chemically driven [2]rotaxane based on π-electron donor-acceptor interaction[16]. In the neutral state, the macrocycle positions itself over the 1,4,5,8-naphthalene-tetracarboxylate diimide (NpI) unit for its better electron-withdrawing ability than the pyromellitic diimide (PmI) unit. However, since the pole-dipole interactions involving Li^+ ions and the oxygen atoms in the polyether loops of the macrocycle are stronger in the case of a PmI encircled unit, addition of Li^+ ions to the neutral bistable [2]rotaxane induces the macrocycle to move from the NpI to the PmI recognition site. Upon removing the Li^+ ions by adding [12]crown-4, the switched state is restored to the ground state.

---

[14] Ballardini, R.; Balzani, V.; Credi, A.; Gandolfi, M. T.; Venturi, M. *Acc. Chem. Res*. **2001**, *34(6)*, 445.

[15] a) Ashton, P. R.; Ballardini, R.; Balzani, V.; Baxter, I.; Credi, A.; Fyfe, M. C. T.; Gandolfi, M. T.; Gómez-López, M.; Martínez-Díaz, M.-V.; Piersanti, A.; Spencer, N.; Stoddart, J. F.; Ventura, M., White, A. J. P.; Williams, D. J. *J. Am. Chem. Soc*. **1998**, *120*, 11932. b) Cao, J.; Feyfe, M. C. T.; Stoddart, J. F.. *J. Org. Chem*. **2000**, *65*, 1937. c) Bissell, R. A.; Córdova, E.; Kaifer, A. F.; Stoddart, J. F.. *Nature*, **1994**, *369*, 133.

[16] Iijima, T.; Vignon, S. A.; Tseng, H.-R.; Jarrosson, T.; Sanders, J. K. M.; Marchioni, F.; Venturi, M.; Apostoli, E.; Balzani, V.; Stoddart, J. F. *Chem-Eur. J*., **2004***, 10*, 6375.

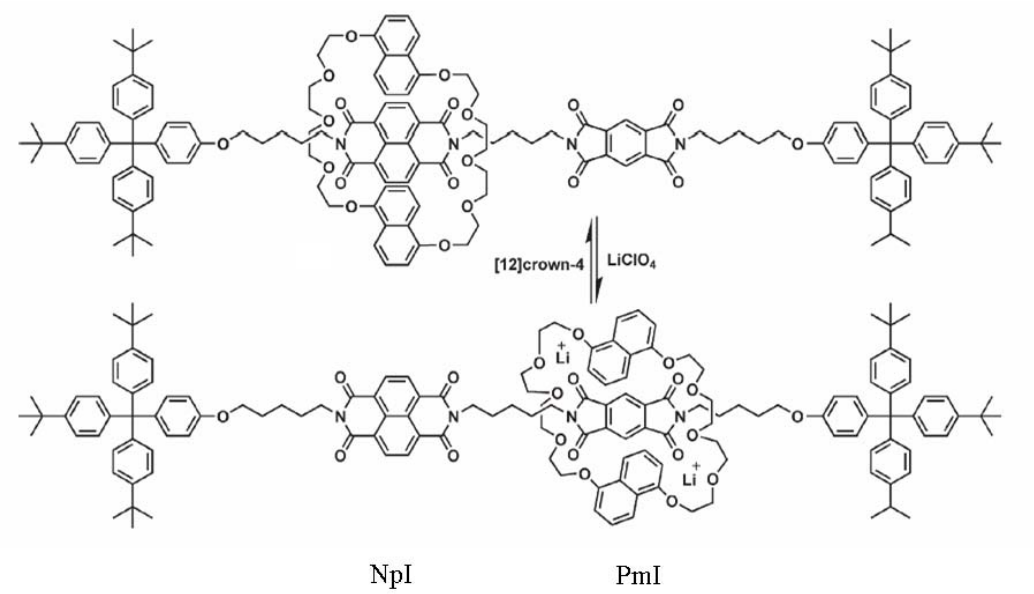

Scheme 2-12.- Representation of a chemically driven [2]rotaxane based on π-electron donor-acceptor interaction.

Another example of a chemically driven rotaxane based on hydrogen bonds and electrostatic interactions is shown in the Scheme 2-13a. It consists of a controllable, bistable [2]rotaxane, containing two different recognition sites (a dialkylammonium center and a bipyridinium unit) in its dumbbell-shaped component where the macrocycle can be recognized. The two different states of the molecule can be switched by a change of pH (see Scheme 2-13b). In acid, the preferred station for the ring to encircle is the -NH_2^+- center. This preference results from a combination of strong [N^+-H···O] hydrogen bonding and weak [C-H···O] interactions, which are much stronger than with some stabilizing [π-π] stacking forces (see Scheme 2-13b, initial state). However, on addition of a base (a tertiary amine) to the initial state of the molecule, the –NH_2^+-] center is deprotonated. The strong intercomponent hydrogen bonding is destroyed, and the ring moves to the bipyridinium unit, where it is stabilized by [C-H···O] and [π-π] stacking interactions (see Scheme 2-13b, final state).

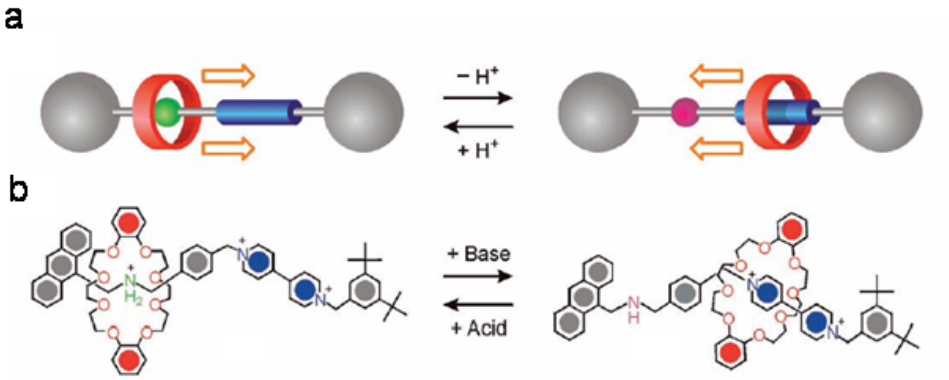

Scheme 2-13.- Molecular shuttle based on hydrogen bonds and electrostatic interactions. a) Schematic representation of the different states of the molecular shuttle. b) Molecular shuttle.

The [2]rotaxane shown before has been used for building the following molecular lift (see Scheme 2-14a).

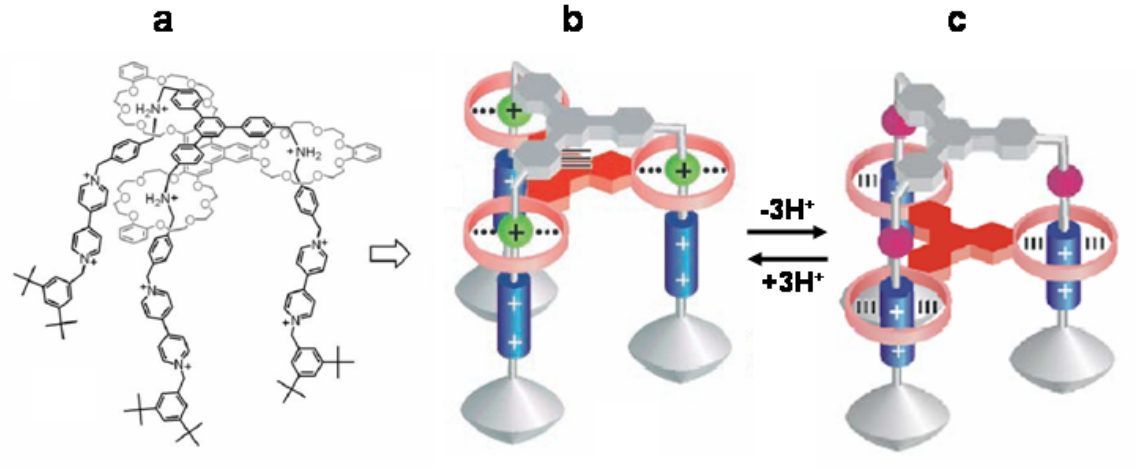

Scheme 2-14.- Molecular lift. a) trifurcated riglike component containing two different notches at different levels in each of its three legs that are interlocked by a platform. The platform is made up of loops in the form of the three macrocycles, fused trigonally to a central floor, that can be made to stop at the two different levels. The energy needed to raise and lower the platform between the two levels on the rig's legs is supplied by an acid-base reaction. b) State of the molecule in acid. The platform is in upper floor. c) Basically, the platform stays at the bottom floor.

The nanoscale lift is only 2.5 nm in height with a diameter of 3.5 nm. It has two different floors and the distance travelled by the platform is about 0.7 nm. The charge of one of the two stations is sensitive to pH changes and as a result the platform can move

between the two levels by adding acid or base. The authors of this device estimate that this molecular machine could develop forces up to around 200 pN. [17]

Like macroscopic internal combustion engines, the chemical driven molecular machine needs fresh reactants (fuel) at any step of its working cycle and produces waste products. It is obvious that the chemical driven molecular machine will not work properly if the waste products are accumulated, unless these wastes are expelled from the system.

2.3.2.1.2 Electrical energy

A molecular machine system based on π-electron donor-acceptor interaction can induce a forward motion by oxidation of the electron donation group or reduction of the electron-acceptor unit. These redox reactions can be performed by an electrical potential and the backward reaction to the original state can be simply obtained by reversing the potential.[18] One of the systems is the redox-controllable amphiphillic [2]rotaxane series based on the redox active tetrathiafulvalene (TTF) unit.

Scheme 2-15 presents a bistable rotaxane consisting of a 2,2'-bipyridine-containing thread and a ring incorporating both a bidentate chelate and a tridentate fragment.[19] Taking advantage of the fact that copper(I) prefers to form a 4-coordinate complex while copper(II) is apt to generate a 5-complex, the [2]rotaxane undergoes an electrochemically driven (oxidation of Cu^{+} or reduction of Cu^{2+}) pirouetting motion of the ring around the axis which takes place on the millisecond timescale.

---

[17] a) Balzani, V.; Credi, A.; Silvi, S.; Venturi, M. *Chem. Soc. Rev*., **2006**, *35*, 1135. b) Badjic, J. D; Balzani, V.; Credi, A.; Silvi, S.; Stoddart, J. F.. *Science.,* **2004**, *303*, 1845.

[18] a)Altieri, A.; Galti, F. G.; Kay, E. R.; Leigh, D. A.; Martel, D.: Paolucci, F.; Slawin, A. M. Z.; Wong, J. K. Y. *J. Am. Chem. Soc*., **2003**, *125*, 8644. b) Saha, S.; Flood, A. H.; Stoddard, J. F.; Impellizzeri, S.; Silvi, S.; Venturi, M.; Credi, A. *J. Am. Chem. Soc*. **2007**, *129(40)*, 12159.

[19] Poleschak, I.; Kern, J.-M.; Sauvage, J.-P.. *Chem. Commun*. **2004**, 474.

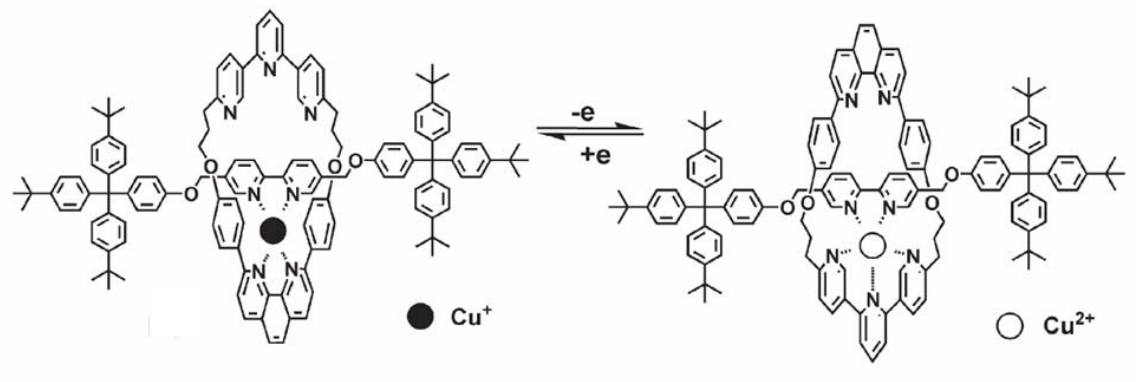

Scheme 2-15.- Electrochemically driven [2]rotaxane.

It is obvious that electrochemical inputs have advantages over chemical ones. An electrochemical stimulus can cause reversible switching processes by simply reversing the electrode couple to induce reversible redox reactions. No waste product is produced during the switching procedure. Besides, the supply of electrical potential can be switched on and off easily and rapidly. Furthemore, electronic devices can be easily fabricated with these electrochemically-triggered systems, directly without any signal transformation.

2.3.2.1.3 Solvent changes

In addition to the different kind of energy inputs described above, a simple solvent change can also be used to drive a molecular machine. If we make a search in the literature, there are not many examples of switchable rotaxanes solvent-tunable[20]. We present an example of a [2]rotaxane (see Scheme 2-16) which can perform solvent-induced shuttling movements. [21]

[20] Ghosh, P.; Federwish, G.; Kogej, M.; Schalley, A.; Haase, D.; Saak, W.; Lützen, A.; Gschwind, R. M. *Org. Biomol. Chem*. **2005**, *3*, 2691.

[21] Ros, T. D.; Guldi, D. M.: Morales, A. F.; Leigh, D. A.; Prato, M.; Turco, R.. *Org. Lett*., **2003**, *5*, 689.

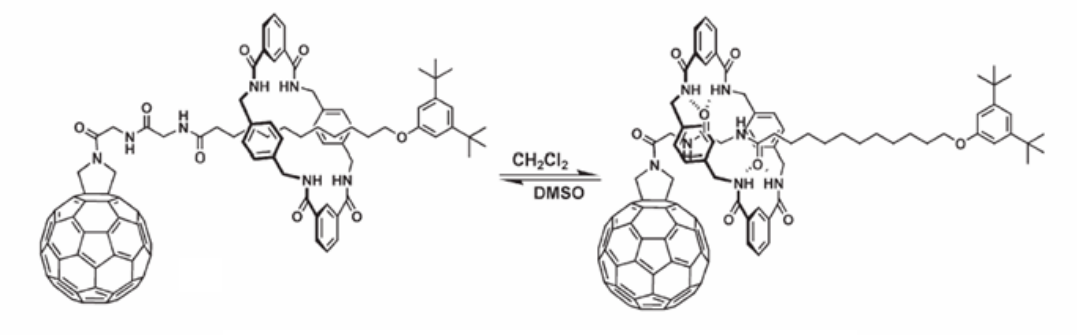

Scheme 2-16.- Solvent-tunable switchable rotaxane.

Although solvent change can drive a molecular shuttle, one solvent has to be removed before the other solvent is added to cause the switching motion. The need to carry out the solvent replacement process brings difficulties in the design and fabrication of solid molecular devices.

2.3.2.1.4 Thermal energy

The switching behavior of the ring component from one station to another rests on the free enthalpy change in the process, that is $\Delta G = \Delta H - T\Delta S$. So, if the entropy change is big enough, the switching process of the ring component from one recognition site to another can be reversed by increasing or lowering the temperature.[22] We show in Scheme 2-17 an entropy-driven [2]rotaxane.[23] At 308 K, the macrocycle sites over the succinamide station, this being entropically favorable. However, when the temperature is lowered to 258 K, both of the amides units—one in fumaramide and the other in succinamide—form hydrogen bonds with the macrocycle because of the stronger hydrogen bonding ability of amide-amide than ester-amide, and the alkyl chain adopts a folded "S-shape". The temperatures dependent co-conformational changes are reversible and chemical reaction is not involved.

[22] Jiang, L.; Okano, J.; Orita, A.; Otera, J. *Angew. Chem. Int. Ed*. **2004**, *43*, 2121.

[23] Bottari, G.; Dehez, F.; Leigh, D. A.; Nash, P. J.; Pérez, E. M.; Wong, J. K. Y.; Zerbetto, F.. *Angew. Chem. Int. Ed*., **2003**, *42*, 5886.

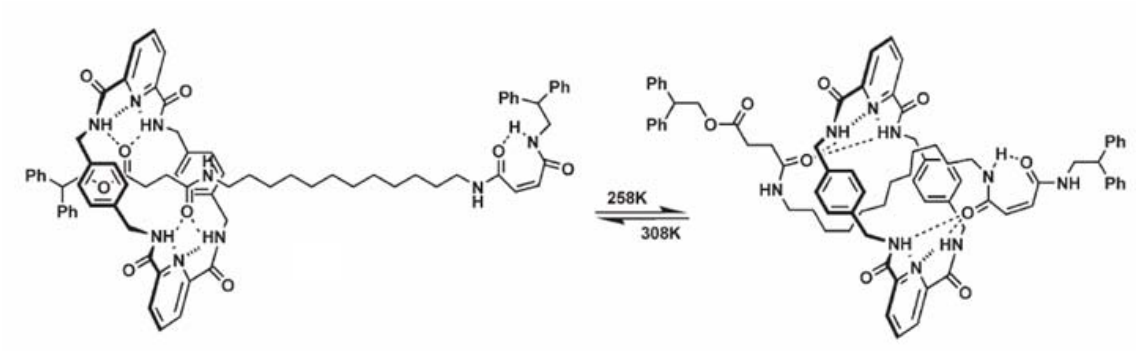

Scheme 2-17.- Entropy-driven rotaxane.

Heat is very interesting driving force because it does not produce any waste product like electrical power.

2.3.2.1.5 Light energy

Light energy can also be used to power a molecular machine[24] and it has more advantages with respect to the other types of driven molecular machine:

- Clean driving force
- Laser can be switched on and off easily and rapidly
- Laser beam can work in a very small space and very short time domains
- The excitation with photons can lead to a fast response.

Considering that the heart of a digital electronic computer is a group of switches that communicate via electrons flowing among them, an ensemble of molecular switches controlled by light which can communicate with one another could be used to build a binary computer. [25]

[24] Bottari, G.; Leigh, D. A.; Pérez, E. M. *J. Am. Chem. Soc*., **2003**, *125*, 13360.

[25] Gust, D.; Moore, T. A.; Moore, A. L., *Chem. Commun*., **2006**, 1169.

An example of the light-driven molecular machines is the rotaxane shown in the following scheme (Scheme 2-18)[26]:

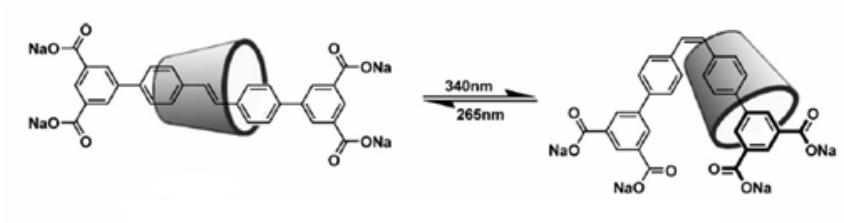

Scheme 2-18.- An example of a light-driven molecular shuttle.

We can show a stilbene-based rotaxane where isomerization of the –C=C- or –N=N- double bonds from the *trans* to *cis* form can take place. This change can be used to drive a molecular machine. Simply, by switching the wave lengh from 340 nm to 265 nm we can have reversible shuttling motions of the alfa-cyclodextrin as a result of the E/Z isomerization of the stilbene unit.

2.3.2.1.6 Multi-energy inputs

There are molecular machines which need the help of two or more energies to produce shuttle motions.[27] For example, in the following case, the switching of the molecular bead from one site to other was driven by pH value, but the reverse process requires a change in pH plus a thermal activation.[28] This example of rotaxane behaves as a kinetically controlled molecular switch- the new state induced by an external stimulus can be "locked in" after removal of the stimulus.

[26] Stainer, C. A.; Alderman, S. J.; Claridge, T. D. W.; Anderson, H. L.. *Angew. Chem. Int. Ed*., **2002**, *41*, 1769.

[27] Murakami, H.; Kawabuchi, A.; Matsumoto, R.; Ido, T.; Nakashima, N. *J. Am. Chem. Soc*., **2005**, *127*, 15891.

[28] Lee, J. W.; Kim, K.; Kim, K. *Chem. Commun*., **2001**, 1042.

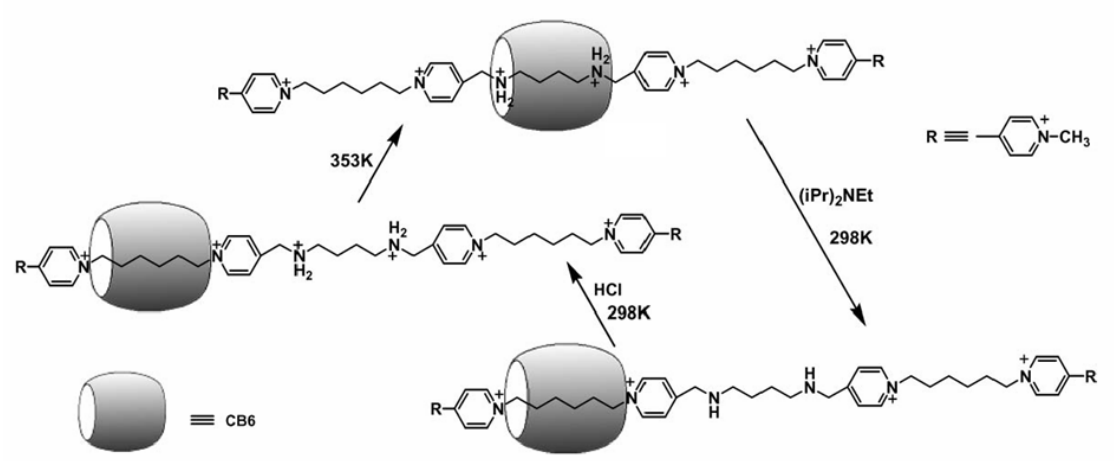

Scheme 2-19.-Multi-energy driven rotaxane.

2.3.2.1.7 Rotaxanes in this thesis

The [2]rotaxanes that we will study in this thesis have been synthesised and subsequently structurally and functionally characterized by Prof. Fitzmaurice's Group at the University College Dublin (UCD) in Ireland (see Scheme 2-20a).[29]

[29] a) Long, B.; Nikitin, K.; Fitzmaurice, D. *J.Am.Chem.Soc*., **2003**, *125(17)*, 5152. b) Long, B.; Nikitin, K.; Fitzmaurice, D. *J.Am.Chem.Soc*., **2003**, *125(50)*, 15490. c) Long, B.; Nikitin, K.; Fitzmaurice, D., *Chem.Comm*., **2003**, *(2),* 282. d) Nikitin, K.; Lestini, E.; Lazzari, M.; Altobello, S.; Fitzmaurice, D. Langmuir, **2007**, *23(24),* 12147. e) Nikitin, K.; Fitzmaurice, D. *J.Am.Chem.Soc.,* **2005**, *127(22),* 8067. f) Nikitin, K.; Lestini, E.; Stolarczyk, J. K.; Müller-Bunz, H.; Fitzmaurice, D. *Chem. Eur. J.* DOI: 10.1002/chem.200701384.

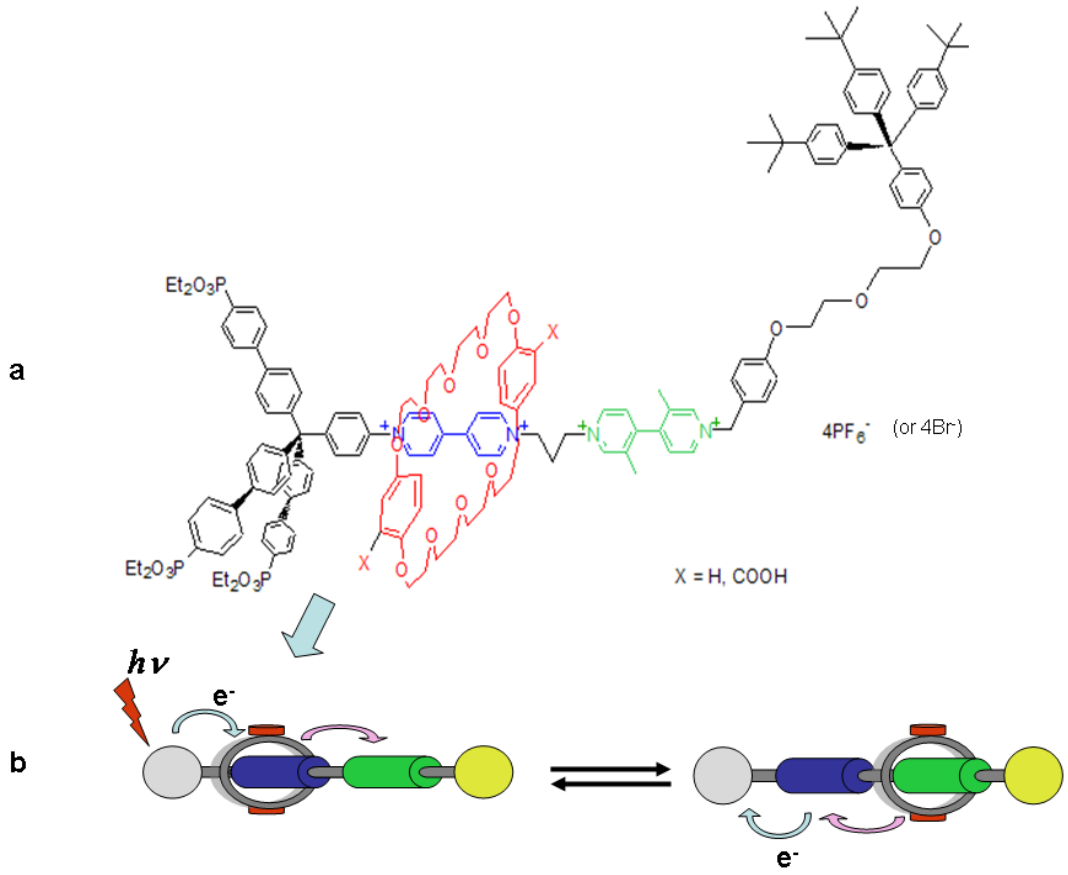

Scheme 2-20.- a) Representation of the [2]rotaxanes studied in this thesis. b) Shuttling process of light-controllable molecular shuttle based on a photoinduced electron-transfer process.

These rotaxanes are two-station photocontrollable which incorporate an electron-transfer photosensitizer unit, an electron-donor (acceptor) ring and two electron-acceptor (donor) stations. These stations have been designed to have different affinity towards the macrocycle, which should then reside on the station with the best receptor ability. Light irradiation of the photosensitizer results at an electron-transfer process which disables the best recognition site (or enables the worst one), leading to the inversion of the affinity of the two stations towards the macrocycle, which is then forced to move (see Scheme 2-20b).

The expected benefits are insights that will enable a rational approach to the design of [2]rotaxanes possessing the desired function and suitable for incorporation in

nanoscale electronic devices[30]. The investigation of a switching behaviour of the multiple-station rotaxanes is of particular importance because of their potential application in molecular switches and machines.

2.3.2.2 Identification of the co-conformations

The detection, characterization and monitoring of the co-conformational states and their changes is very important in order to detect all the changes that can occur during a molecular machine work. Generally, the stimulus-triggered relative positional changes were spectroscopically characterized in solution and some other spectra such as absorption, NMR, circular dichroism and fluorescence spectra, as well as cyclic voltametry, were also often used.

2.3.2.3 Applications of the switchable rotaxanes

Some of the applications of the molecular shuttles are the following: molecular machines, molecular switches, molecular transistors, molecular logic gates and memory devices.

2.3.2.3.1 Molecular machines

Switchable rotaxanes are able to perform relative inter-component positional changes in response to external stimuli. These potential applications attracted the attention of many chemists, physicists and materials scientists. One of these aplications

[30] Flood, A. H.; Ramirez, R. J. A.; Deng, W. Q.; Muller, R. P.; Goddard, W. A.; Stoddart, J. F.; *Australian J. Chem*., **2004**, *57(4)*, 301.

is related to the utilization of the rotaxanes for the construction of molecular devices and machines.[31]

These molecules are clever enough to move on command in solution. An organization of these shuttling molecules in bulky solution and their correct deposition onto a surface are needed if we want to obtain assemblies in the proper order. However, these processes are difficult because of the large number of existing molecules.

Some examples of molecular machines based on [2] rotaxanes can be found. One of them is a reversible molecular valve [32] created by I. Zink, J. Fraser Stoddart and their co-workers, as shown in the following scheme (Scheme 2-21):

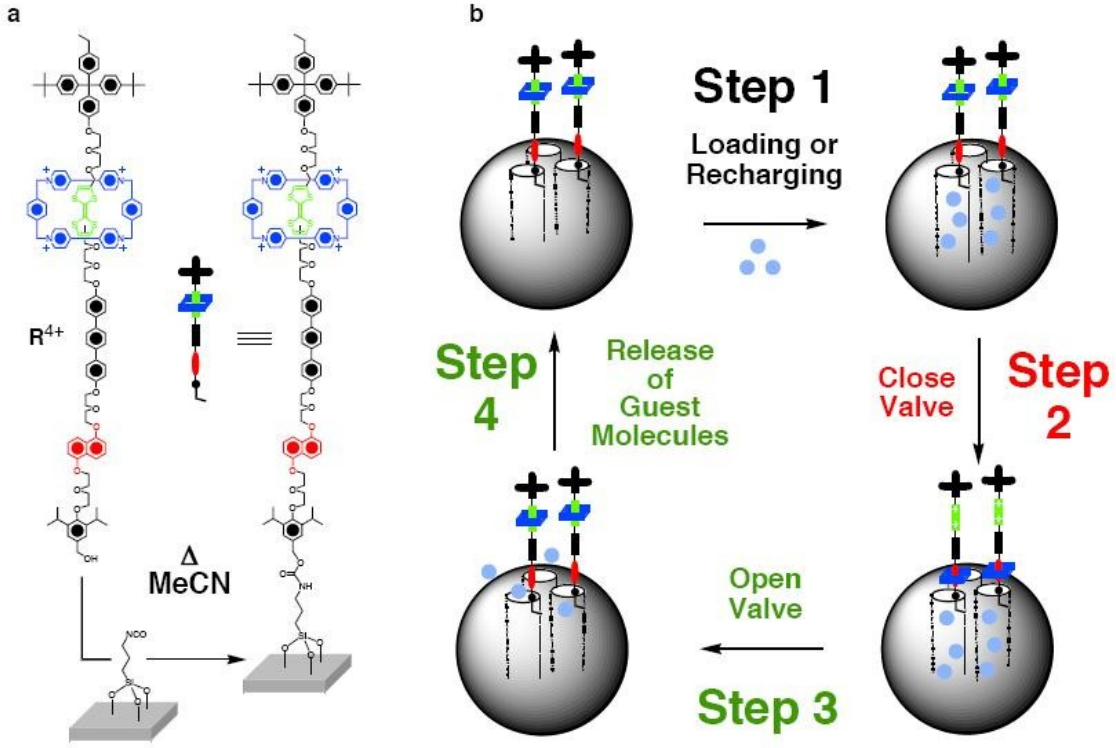

Scheme 2-21.- Schematic representation of the molecular valve. a) Representation of the bistable [2]rotaxane and the procedure for attaching it to a silica particle. b) Mechanism for the operation of the nanovalve.

[31] a) Balzani, V.; Gómez-López, M.; Stoddart, J. F. *Acc. Chem. Res.* **1998**, *31*, 405. b) Ozin, G. A.; Manners, I.; Fournier-Bidoz, S.; Arsenault, *A. Adv. Mater.*. **2005**, *17*, 3011. c) Browne, W. R.; Feringa, B. L. *Nature nanotechnology*, **2006**, *1*, 25.

[32] Nguyen, T. D.; Tseng, H.-R.; Celestre, P. C.; Flood, A. H.; Liu, Y.; Stoddart, J. F.; Zink, J. I. *Proc. Nat. Acad. Sciences*, **2005**, *102*, *29*, 10029.

Essentially, the nanovalve is based on a [2]rotaxane which contains a tetracationic cyclophane, cyclobis(paraquat-*p*-phenylene) ($CBPQT^{4+}$) (blue ring), a TTF station (green station) and a dioxynaphthalene (DNP) station (red station). The [2]rotaxane is supported in a silica gel, as shown in the Scheme 2-21a. The valve can be closed and opened reversibly following the next steps (see Scheme 2-21b):

First step: Loading of the guest molecules into the cylindrical pores on the silica. The blue ring is located on the green station.

Second step: The $CBPQT^{4+}$ ring is moved to the DNP station by oxidation of the TTF unit to its dication. It means that the valves are now closed.

Third step: The nanovalve can be opened after the blue ring shuttles from the red station to the TTF station. It can be done by adding ascorbic acid to reduce the TTF dication back to its neutral state.

Fourth step: The valve is open and the guest molecules can be released. The valve is ready for loading.

2.3.2.3.2 Molecular switch

A molecular switch is a nanoscale machine which switches reversibly between two or more positions. Molecular switches are needed to fabricate molecular electronic components. They must be controllable, reversible and readable at the molecular level. A molecular shuttle can serve as a molecular switch.

A molecular monolayer of the molecule (shown in the Scheme 2-22a) has been used for the fabrication of the nanoscale molecular-switch devices using imprint lithography and whose procedure is represented in the Scheme 2-22b.

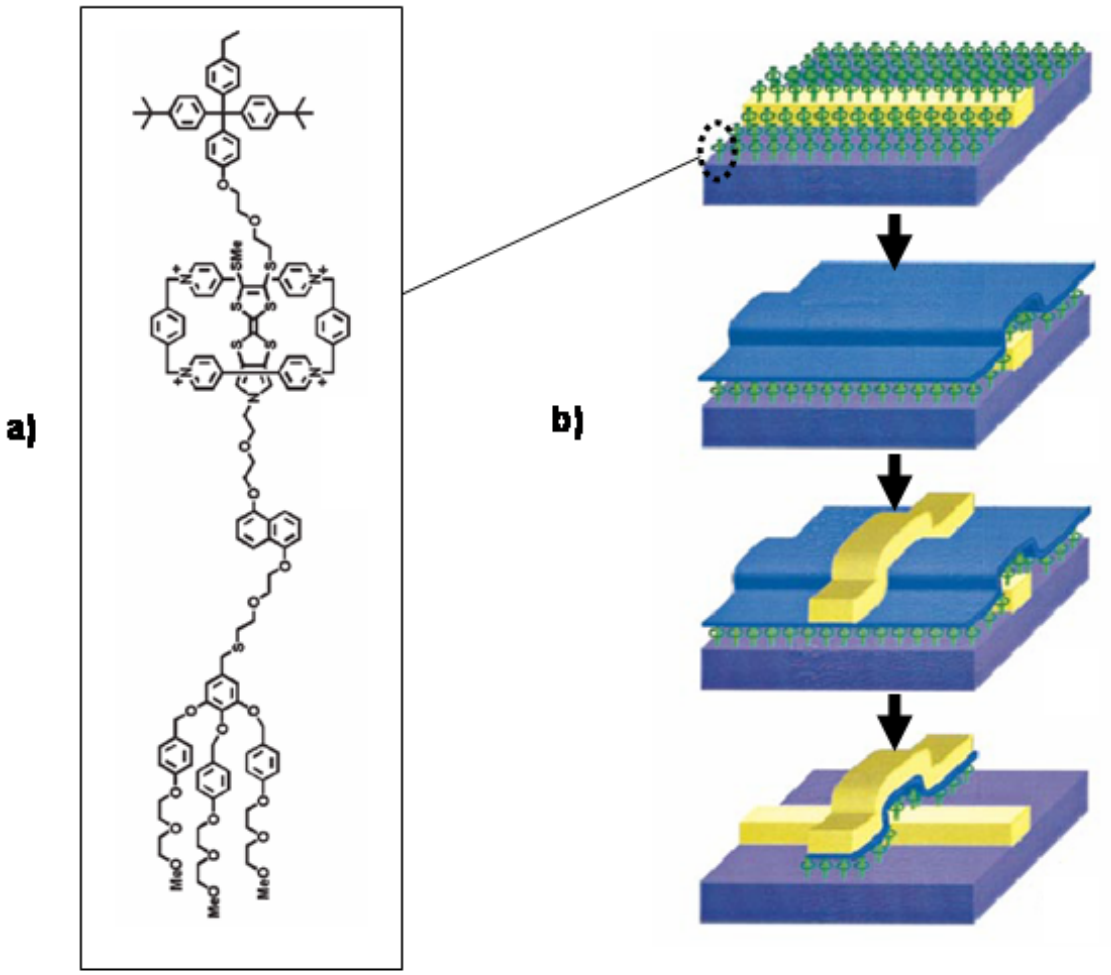

Scheme 2-22.- a) Schematic representation of the bistable [2]rotaxane used. b) Graphical Schematic of the procedure used for fabrication of nanoscale molecular-switch devices by imprint lithography.

The design, the development and the examination of this device has been done mostly at the Hewlett Packard laboratories in California.[33]

[33] a) Chen, Y.; Jung, G.-Y.; Ohlberg, D. A. A.; Li, X.; Stewart, D. R.; Jeppesen, J. O.; Nielsen, K. A.; Stoddart, J. F.; Williams, R. S.. *Nanotechnology*, **2003**, *14*, 462. b) Chen, Y.; Ohlberg, D. A. A.; Li, X.; Stewart, D. R.; Williams, R. S.; Jeppesen, J. O. ; Nielsen, K. A.; Stoddart, J. F.; Olynick, D.; Anderson, E.. *Appl. Phys. Lett*., **2003**, *82*, *10*, 1610.

2.3.2.3.3 Molecular transistor

Another use of the switchable rotaxanes is for the fabrication of molecular transistors. In the following scheme present an example of single-molecule devices (Scheme 2-23a) which contains molecular transistors[34] (Scheme 2-23c) based on a bistable [2]rotaxane (see Scheme 2-23d):

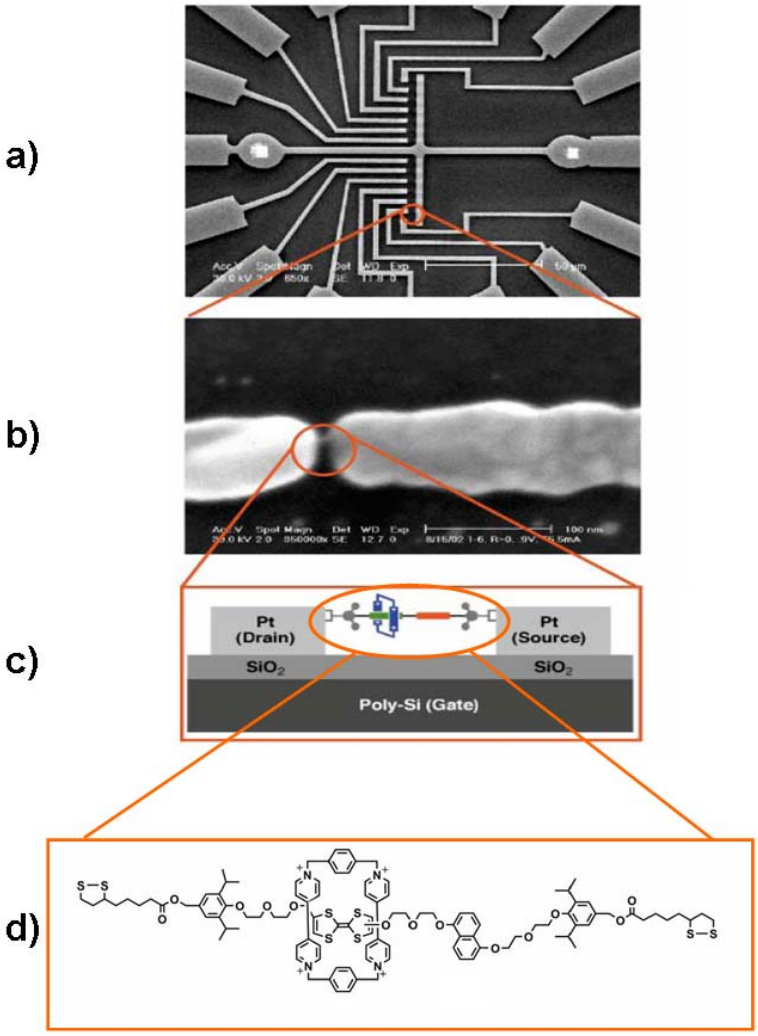

Scheme 2-23.- a) Scanning electron microscope (SEM) pictures of single-molecule devices fabricated on a Si substrate. The center metal electrode, where the break junction is made of 7 nm thick Pt, followed by 100 nm thick gold wires and pads for wire bonding. b) The SEM image after the break junction is made. The gap between the two metal electrodes is around 4 nm. c) A cross-section through a single-molecule transistor. d) [2]rotaxane which the molecular transistor is based on.

[34] Yu, H.; Luo, Y.; Beverly, K.; Stoddart, J. F.; Tseng, H.-R.; Health, J. R. *Angew. Chem. Int. Ed.* **2003**, *42*, 5706.

2.3.2.3.4 Molecular logic gates

Logic gates were fabricated from an array of switches based on a monolayer of rotaxanes driven electrochemically (see Scheme 2-24): [35]

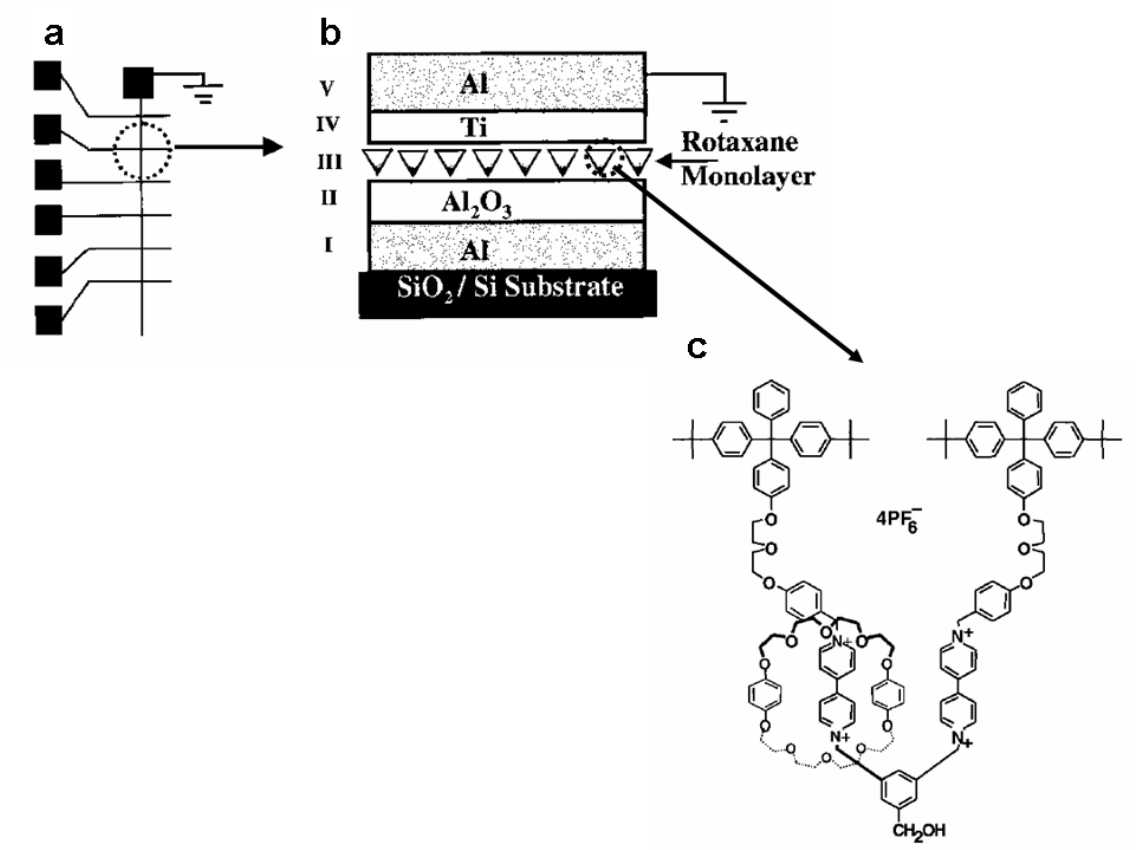

Scheme 2-24.- a) Top view of a linear array of six devices. b) Side view cross section of a single device junction. Each device is composed by a rotaxane monolayer located between two electrodes. c) Representation of the [2]rotaxane used.

The switches open and close merely by applying a voltage across the device.

[35] a) Luo, Y.; Collier, P.; Jappesen, J. O.; Nielsen, K. A.; Delonno, E.; Ho, G.; Perkins, J.; Tseng, H.-R.; Yamamoto, T.; Stoddart, J. F.; Health, J. R. *ChemPhysChem*. **2002**, *3*(6), 519. b) Leigh, D. A.; Morales, M. A. F.; Pérez, E. M.; Wong, J. K.Y.; Saiz, C. G.; Slawin, A. M. Z.; Carmichael, A. J.; Haddleton, D. M.; Brouwer, M.; Bruma, W. Jan; Wurpel, G. W. H.; León, S.; Zerbetto, F. *Angew. Chem. Int. Ed*. **2005**, *44*, 3062. c) Collier, C. P.; Wong, E. W.; Belohradsky, M.; Raymo, F. M.; Stoddart, J. F.; Kuekes, P. J.; Williams, R. S.; Heath, J. R. *Science*, **1999**, *285*, 391.

2.3.2.3.5 Memory devices

Rotaxanes are molecules in which a macrocycle is mechanically locked onto a thread by two bulky stoppers. Their architecture, analogous to that of an abacus, suggests that they could be used as switchable components for artificial machines that function through mechanical motion at the molecular level. Controlling such motion in the solid state could be used to store information (see Scheme 2-25) by encoding the two different states into binary digits.

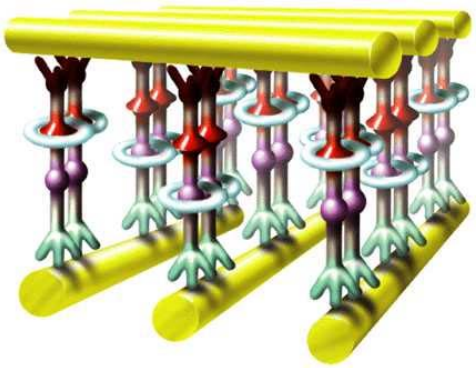

Scheme 2-25.- Graphical representation of a molecular memory based on [2]rotaxanes.

The following rotaxane has been used for the construction of a nanorecording (see Scheme 2-26) : [36]

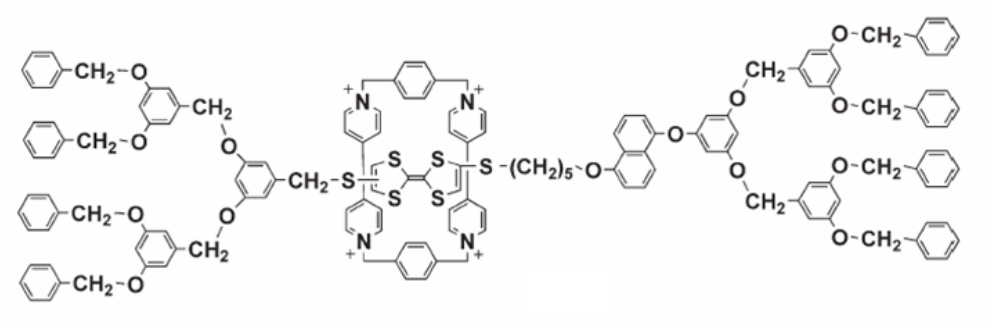

Scheme 2-26.- Molecular structure of the rotaxane. It contains a $CBPQT^{4+}$ (ring) and two stations (one TTF unit and one DNP unit). The movement of the ring from one station to the other is done by chemical stimuli.

[36] Feng, M.; Guo, X.; Lin, X.; He, X.; Ji, W.; Du, S.; Zhang, D.; Zhu, D.; Gao, H. *J. Am. Chem. Soc.*, **2005**, *127*, 15338.

Those devices that can compute and store information (molecular switches, logic gates and memory devices) can be used for the fabrication of Chemically Assembled Electronic Nanocomputers (CAEN's).[37]

2.3.2.3.6 Electrochromic devices

Knowing that an electrochemical redox reaction can also take place in polymeric electrolyte, J. Fraiser Stoddart, James R. Heath and their coworkers fabricated a solid-state electrochromic device by immobilizing the bistable [2]rotaxane shown in the Scheme 2-27 within a solid polymeric electrolyte, and three electrodes (working, counter and reference electrodes) were arranged. [38]

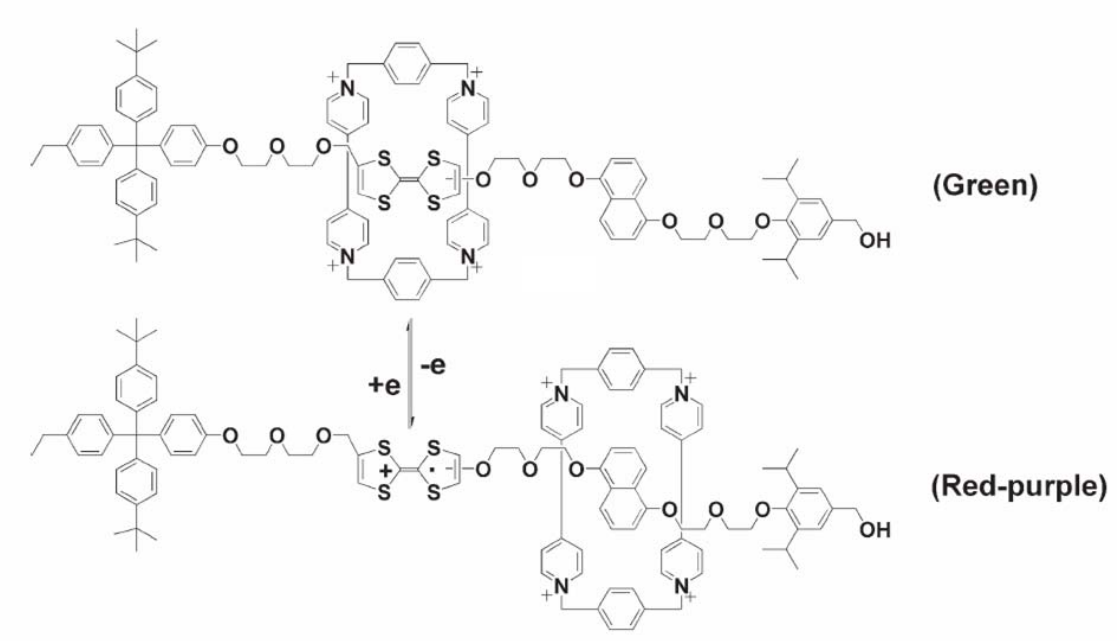

Scheme 2-27.- Schematic representation of the states of the rotaxane used to build up an electrochromic device.

[37] Health, J. R.. *Pure Appl. Chem*., **2000**, *72(1-2)*, 11.

[38] Steuerman, D. W.; Tseng, H.-R.; Peters, A. J.; Flood, A. H.; Jeppesen, J. O.; Nielsen, K. A.; Stoddart, J. F.; Heath, J. R. *Angew. Chem. Int. Ed.* **2004**, *43*, 6486.

When the ring is located on the TTF unit, the color of the device is green (see Scheme 2-28a). After applying a potential of +1 V on the working electrode, the ring moves to the DNP unit and the color of the device becomes red-purple (see Scheme 2-28b).

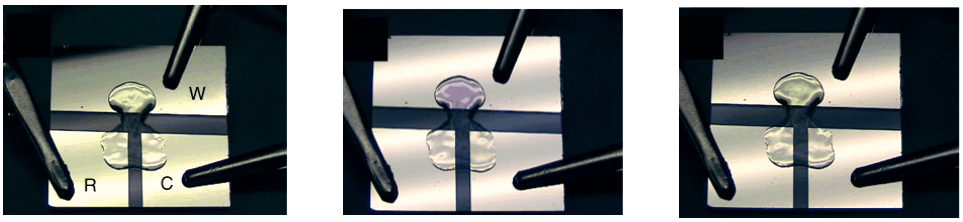

a) b) c)

Scheme 2-28.- Electrochromic response of the solid-state polymer devices. The working (W), counter (C) and reference (R) electrodes are indicated. a) The green color points out that the ring is on the TTF unit. b) After a +1V oxidizing potential is applied to the working electrode, the red-purple co-conformation is shown. c) When W is returned to 0 V, the ring goes back to TTF unit.

The green color of the device can be recovered only by removing the potential (Scheme 2-28c).

To sum up, the rotaxanes are an exciting and quickly developing area of supramolecular chemistry. They hold promise for a wide range of potential future applications, including molecular machines and nanoelectronic devices.

RESULTS

An old Irish recipe
for longevity:
'Leave the table hungry.
Leave the bed sleepy.
Leave the table thirsty.'

3 MODELLING OF PSEUDOROTAXANES

3.1 INTRODUCTION

As we have shown in Chapter 2, the [2]rotaxanes are molecular species with special interests for physicists, chemists, and Materials Science experts as well. One of the most interesting properties of these molecular species is that the relative positions of their components can be modified using an external stimuli. The ability to locate with precision the position of their components and to change it under control makes the [2]rotaxanes very interesting molecular species to be studied in the Nanochemistry field.

Our purpose was to study modifications of [2]rotaxanes, as such as that represented in the Scheme 3-1, to find their structural and dynamic properties and to compare the theoretical results with those experimentally obtained in collaboration with the professor D. Fitzmaurice's group at the UCD.

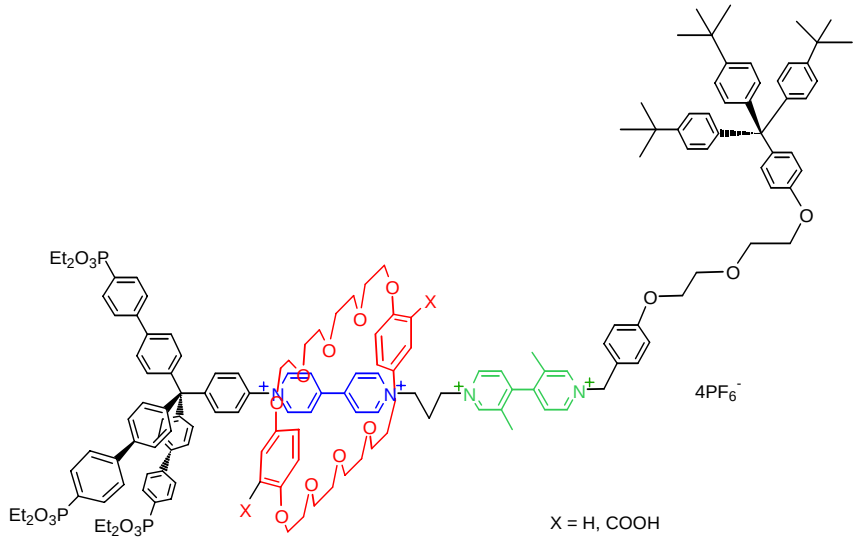

Scheme 3-1.- General scheme of the [2]rotaxanes studied

This sort of rotaxane has two different bipyridinyl stations and a crown ether that can be displaced from one station to the other.

As a first approach, [2]pseudorotaxanes, whose axles were composed by the bipyridinyl stations contained in the [2]rotaxane shown in the Scheme 3-1 were studied.

The main goal in this first step of the examination was to determine the dynamic structure of the pseudorotaxanes in acetonitrile and in methanol solutions and to understand how it varies depending on the counterions used. In our case, the ions used were the PF_6^- and Br^- .

The [2]pseudorotaxanes and their components studied in this chapter were those shown in the Scheme 3-2 and Scheme 3-3.

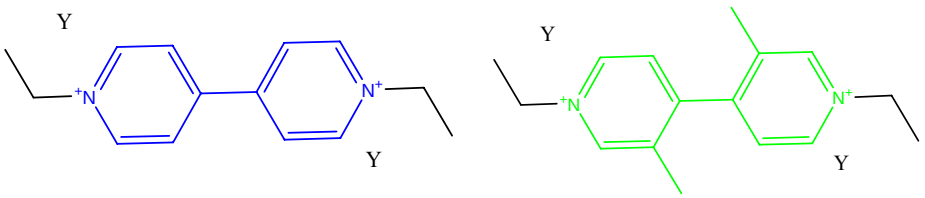

Y= PF_6^- or Br^-

a) ETH·2Y b) DIM·2Y

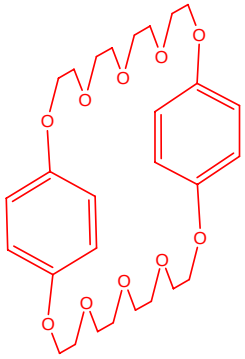

c) crown

Scheme 3-2.- Viologens and crown ether studied. a) 1,1'-diethyl-4,4'-bipyridinium bis(hexafluorophosphate) or dibromide. b) 1,1'-diethyl-3,3'-dimethyl-4,4'-bipyridinium bis(hexafluorophosphate) or dibromide. c) bis(*p*-phenylene)-34-crown-10.

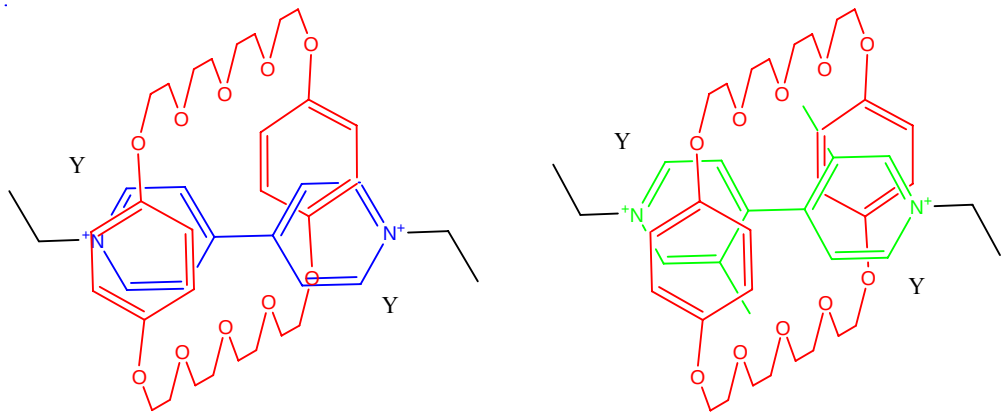

Y= PF_6^- or Br^-

a) ETH·2Y·crown b) DIM·2Y·crown

Scheme 3-3.- [2]pseudorotaxanes studied. a) 1,1'-diethyl-4,4'-bipyridinium bis(*p*-phenylene)-34-crown-10 bis(hexafluorophosphate) or dibromide. b) 1,1'-diethyl-3,3'-dimethyl-4,4'-bipyridinium bis(*p*-phenylene)-34-crown-10 bis(hexafluorophosphate) or dibromide.

These pseudorotaxanes were synthesized and experimentally studied in the Nanochemistry group at the UCD and they were theoretically studied in own group at the UAB using molecular dynamics.

Further goals were formulated to calculate the complexation energy for the pseudorotaxanes (viologen-crown complex) and to determine the energy profiles of the complexes by modifying the distances between its components (the crown ether and the axle). Finally, our results were compared with the experimental data.

3.2 DETERMINATION OF THE COMPLEXATION ENERGY FOR THE PSEUDOROTAXANES

The complexation energy (for more details, read Chapter 12) for the two pseudorotaxanes was determined in different solvents (acetonitrile and methanol) and different counterions (hexafluorophosphate ion and bromide ion) using molecular

dynamics simulations (see Chapter 7) and these results were compared with the complexation energies experimentally obtained (Table 3-1):

	Complexation Energy (kcal/mol)							
	Theoretical results (Molecular Dynamics)				Experimental results (UV-VIS Spectroscopy)			
Solvent	Acetonitrile		Methanol		Acetonitrile		Methanol	
Counterion	PF_6^-	Br^-	PF_6^-	Br^-	PF_6^-	Br^-	PF_6^-	Br^-
ETH·crown	-8.48	-8.67	-11.51	-6.11	-2.92	-----	-----	-3.56
DIM·crown	-2.63	-5.40	-2.68	-1.79	-0.96	-----	-----	-1.19

Table 3-1.- Complexation energies determined theoretically and experimentally.

It was proved experimentally that the pseudorotaxanes are not soluble when bromide is used in acetonitrile. The same happens when we used hexafluorophosphate as a counterion in methanol. For these reasons, only values of complexation energies for PF_6^- in acetonitrile and bromide in methanol (experimentally calculated) are included in Table 3-1.

A careful analysis of the experimental and theoretical results (Table 3-1), indicates that the values depend on the method used. In spite of the observed differences, we always obtained that the pseudorotaxane composed by the viologen ETH more stable under the conditions examined. Moreover, all values are negative. Consequently the complexation is always favoured.

3.3 STRUCTURAL ANALYSIS

3.3.1 Introduction

The results obtained from the molecular dynamics (MD) simulations (trajectories) for each pseudorotaxane in each of the different environments studied (different solvent and different counterion) were analysed. Essentially, the geometrical parameters analysed were those shown in Scheme 3-4:

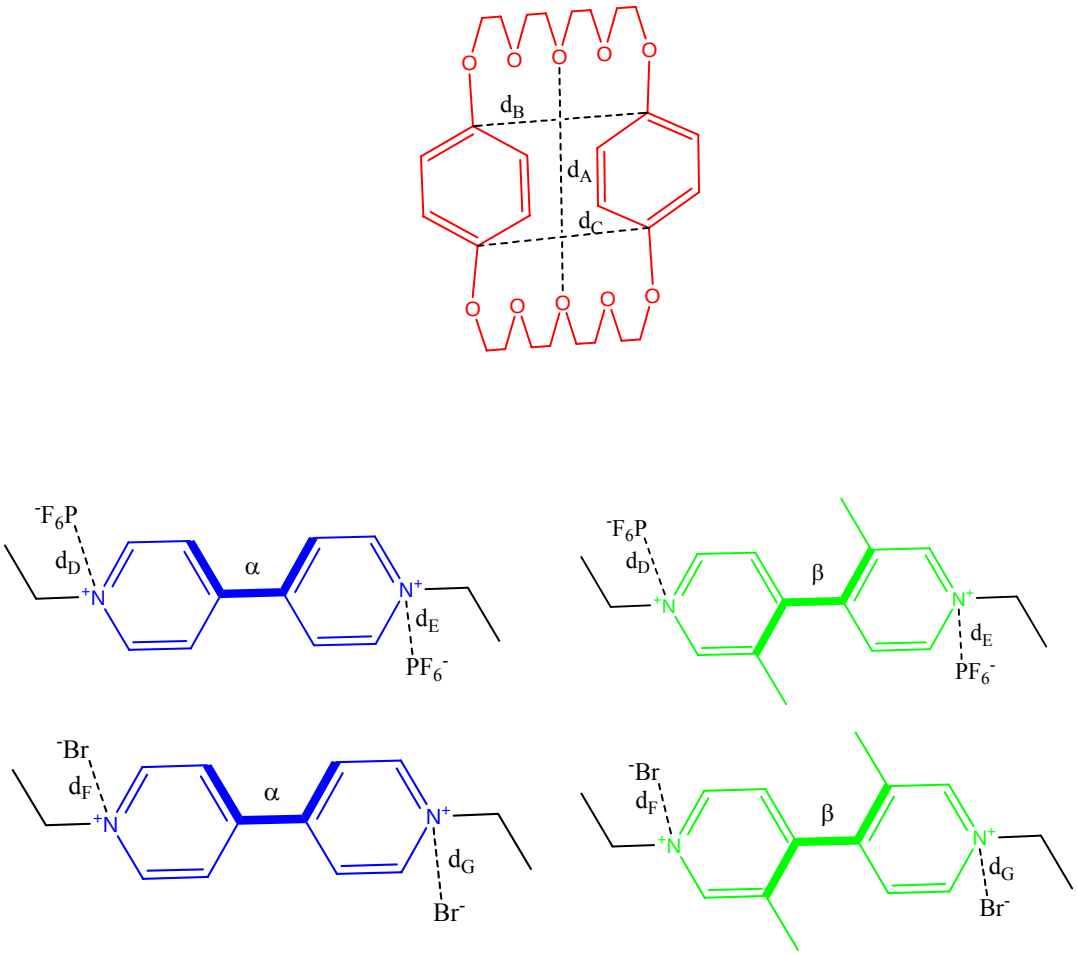

Scheme 3-4.- Distances and angles measured (distances are marked by dotted lines and identified by a "d" while angles are marked by thick lines and identified by greek letters).

Basically, the flatness of the viologens were monitored by measuring the torsional angle α in the ETH viologen (or β in the DIM viologen) as well as their changes when the crown ether is threaded and unthreaded. Moreover, the motion of the counterions and the variation of their distances to the nitrogen atoms of the axle were also monitored. Finally, the variations of the shape of the crown when complexed and uncomplexed were also examined.

3.3.2 Systems in acetonitrile

Table 3-2 and Table 3-3 contains the distances (in Å) and the angles (in degrees) measured for the systems which were run in acetonitrile as the solvent. The standard deviation are given in parenthesis.

3.3.2.1 Counterion used: PF_6^-

The results in acetonitrile and with hexafluorophosphate as counterion, are presented in Table 3-2:

PF_6^- + CH_3CN						
	α(β)	**d_A**	**d_B**	**d_C**	**d_D**	**d_E**
ETH	0.16 (64.26)				6.72 (1.72)	11.56 (4.65)
ETH·crown	3.05 (18.54)	13.74 (0.47)	7.14 (0.33)	7.09 (0.35)	5.65 (0.91)	14.15 (5.70)
DIM	98.70 (18.22)				7.22 (2.08)	7.93 (3.26)
DIM·crown	97.35 (18.57)	12.91 (1.11)	7.11 (1.11)	6.89 (1.12)	10.71 (6.59)	12.07 (4.03)
Crown		13.32 (1.17)	5.98 (0.99)	5.85 (1.09)		

Table 3-2.- MD results taken in acetonitrile as solvent and using hexafluorophosphate as ion.

The ETH viologen uncomplexed seems to be flat. However, the values of α are around ±30 º and for this reason, the average is almost zero, whereas the standard deviation is high. When ETH is complexed, the viologen becomes flatter.

The DIM viologen has the methyl groups almost perpendicular to each other. Another interesting observation is that the shape of the crown is modified when the viologen is threaded: the distances between the two phenyl groups from the crown (d_B, d_C) became larger, both for the ETH and the DIM complexes.

3.3.2.2 Counterion used:Br^-

Br^- + CH_3CN						
	α(β)	**d_A**	**d_B**	**d_C**	**d_F**	**d_G**
ETH	1.35 (110.64)				6.67 (2.16)	6.72 (2.03)
ETH·crown	-6.08 (17.54)	13.71 (0.39)	7.08 (0.32)	7.03 (0.33)	14.29 (6.57)	4.80 (0.57)
DIM	96.99 (18.91)				8.49 (1.97)	8.64 (1.90)
DIM·crown	103.76 (20.04)	13.65 (0.63)	7.63 (0.59)	7.69 (0.50)	4.87 (0.97)	5.00 (1.29)
Crown		13.32 (1.17)	5.98 (0.99)	5.85 (1.09)		

Table 3-3.- MD results using bromide and acetonitrile as a counterion and solvent respectively.

Table 3-3 contains the results about the systems studied using bromide in acetonitrile. The α and β values are similar to those in Table 3-2 (using hexafluorophosphate in acetonitrile). The standard deviation for α in free ETH viologen is also very high. In fact, the ETH viologen is not flat because the alpha values fluctuate around ±35º. The shape of the crown changes more in the system DIM·crown in the precense of bromide than using hexafluorophosphate (compare results in Table 3-2 and Table 3-3) making the crown larger. In the ETH·crown case, the distances measured in the crown (d_A, d_B and d_C) are not dependent on the ion used - analogous results when using Br^- and PF_6^- were obtained.

3.3.3 Systems in methanol

The following tables present the results related to the systems when methanol was used as a solvent.

3.3.3.1 Counterion used: PF_6^-

PF_6^- + MeOH						
	α(β)	**d_A**	**d_B**	**d_C**	**d_D**	**d_E**
ETH	4.23 (44.01)				11.23 (1.68)	7.62 (1.75)
ETH·crown	3.72 (19.55)	13.74 (0.45)	7.09 (0.36)	7.15 (0.35)	7.66 (2.67)	10.53 (2.80)
DIM	97.09 (19.07)				13.59 (4.63)	9.33 (3.06)
DIM·crown	96.82 (19.62)	13.04 (0.96)	7.29 (0.90)	7.17 (0.92)	11.01 (4.75)	15.79 (6.36)
Crown		13.21 (1.03)	6.10 (1.20)	6.11 (1.04)		

Table 3-4.- MD results for the systems with hexafluorophosphate as counterion and solvated in methanol.

The α and β values obtained are similar to those in Table 3-2 and Table 3-3. Free ETH viologen has α values that are around ±20º and for that reason, a high standard deviation for α is stimated. The distances d_B and d_C in ETH·crown are shorter than in the DIM·crown. However, these distances (d_B and d_C) are larger in the complexes than when the crown is uncomplexed (Table 3-5).

Besides, the d_A values vary depending on the type of complexation of the crown. The distance d_A in the free crown is larger than in the DIM·crown, whereas d_A acquires the largest value in the ETH·crown.

3.3.3.2 Counterion used: Br^-

The data in Table 3-5 show that the aromatic area, when the ETH is complexed, is almost flat. However, the free ETH viologen has α values about ±25º. The average value is around zero and the standard deviation is high.

In the DIM viologen, the methyl groups of the bipyridinyl system are situated almost perpendicular to each other. The distances d_B and d_C follow the same tendency as the one displayed in Table 3-4. The distance d_A is increased when the crown is complexed with the ETH viologen. However, the same distance remains almost unchanged when the crown is free or forms a complex with the DIM viologen (see Table 3-5).

Br^- + MeOH						
System	**α(β)**	**d_A**	**d_B**	**d_C**	**d_F**	**d_G**
ETH	1.16 (55.60)				8.30 (3.63)	9.38 (4.23)
ETH·crown	2.06 (19.37)	13.80 (0.39)	6.99 (0.35)	7.06 (0.33)	6.02 (1.93)	8.50 (2.31)
DIM	96.55 (19.45)				7.85 (2.89)	11.11 (3.66)
DIM·crown	97.42 (19.62)	13.23 (0.52)	7.70 (0.50)	7.70 (0.41)	8.15 (3.96)	12.12 (4.03)
Crown		13.21 (1.03)	6.10 (1.20)	6.11 (1.04)		

Table 3-5.- MD results obtained in methanol as solvent using bromide as counterion.

The distance d_A in all the cases studied for the ETH·crown systems is larger than in DIM·crown by 0.5-0.7 Å. In the opposite, the distance between the two aromatic rings in the crown (d_B and d_C) in the DIM·crown pseudorotaxanes are larger than in the ETH·crown systems by 0.1-0.7 Å, indicating a change from an extended shape to a round shape.

3.3.4 Conclusions

As expected, the geometry of the components of the pseudorotaxanes changes depending on if they are free or a complex is formed. Moreover, the crown ether structure varies significantly with the type of the station. In fact, distances related to the crown in the DIM·crown complexes are much larger than in the ETH·crown pseudorotaxanes and, as a consequence, the complexation energies for the DIM·crown are more positive than in ETH·crown systems.

Except for the ETH·crown pseudorotaxanes, the results depend also on the solvent used. The ETH·crown pseudorotaxanes are also not dependent upon variation of the counterions.

3.3.5 Structures of the complexes in acetonitrile and with PF_6^- as counterion: comparison between experimental and theoretical results.

Different views of the superimposed structures of the pseudorotaxanes solvated in acetonitrile and using hexafluorophosphate as counterion are shown in Scheme 3-5, Scheme 3-6 and Scheme 3-7.

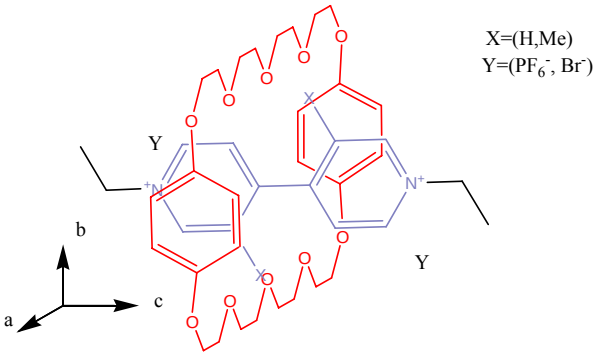

Scheme 3-5.- General representation of the pseudorotaxanes studied and the axis used.

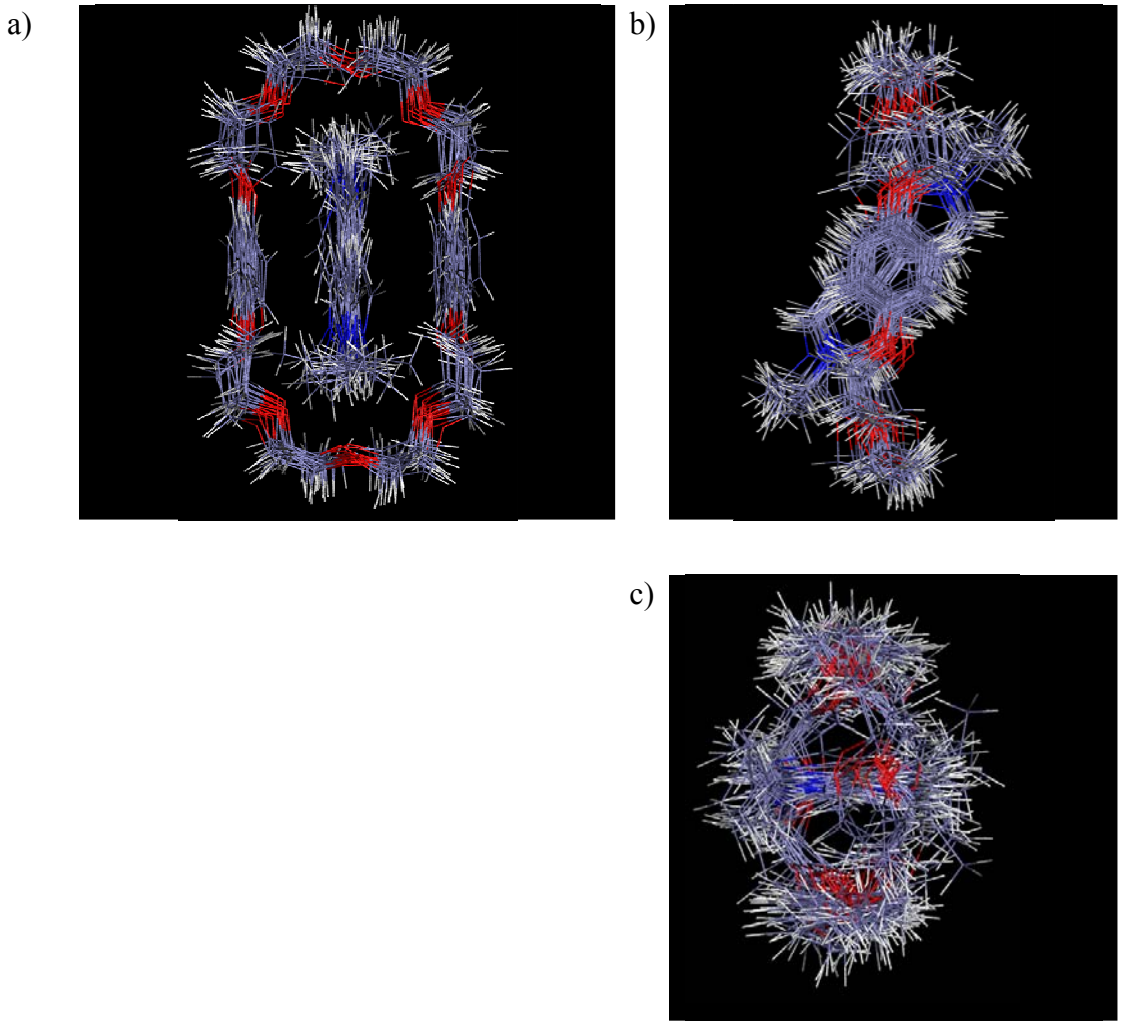

Scheme 3-6.- Superimposed structures from ETH·crown·2PF_6^- in acetonitrile. a) Side view (ab plane) . b) front view (bc plane). c) Top view (ac plane).

Pseudorotaxane ETH·crown·2PF_6^- presents a structure where the viologen is located in the center of the crown ether and its aromatic rings are parallel with respect to the phenyl rings from the macrocycle (see Scheme 3-6a). Moreover, the diethyl groups from the viologen stick out slightly from the cavity of the crown ether (see Scheme 3-6b and Scheme 3-6c) . The viologen remains almost in the same position inside the macrocycle. The structure of the crown ether is very symmetric and the phenyl rings are arranged parallel to the viologen.

a)

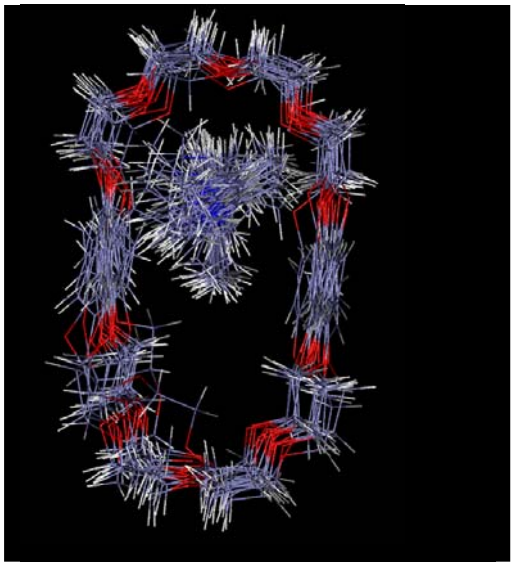

b)

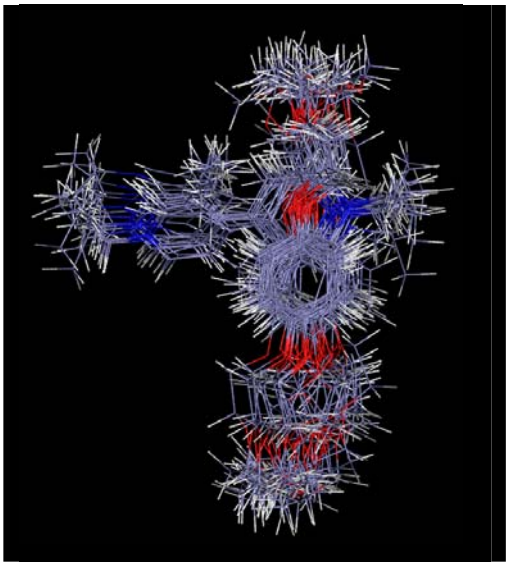

c)

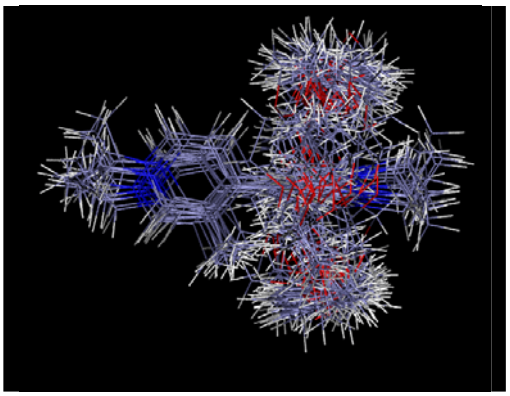

Scheme 3-7.- Superimposed structures from DIM·crown·2PF_6^- in acetonitrile. a) Side view (ab plane) . b) front view (bc plane). c) Top view (ac plane).

Superimposed structures from DIM·crown·2PF_6^- in acetonitrile are shown in the Scheme 3-7. In contrary to the analogous ETH system, at least half part of the DIM viologen remains outside of the cavity of the macrocycle (see Scheme 3-7b and Scheme 3-7c).

The distance between the phenyl groups (d_B and/or d_C) with DIM are larger than when using ETH. Moreover, the distance between the two ether chains from the crown ether in DIM complex are shorter than in the case of the ETH complex. For these reasons, the crown ether shape in the ETH complex more elongated than in the DIM complex.

Experimentally,[39] and after the completion of this part of the study, it was possible to analyse the ETH·crown·PF_6^- system by X-Ray crystallography (Scheme 3-8):

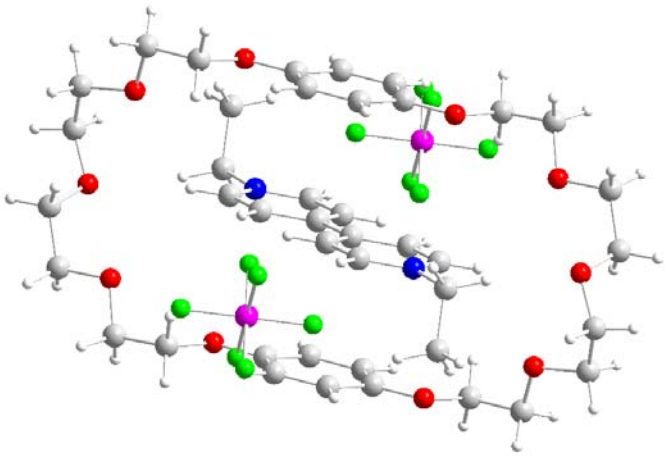

Scheme 3-8.- X-Ray structure of the ETH·crown·2PF_6 (CCDC 64823).

The crystallographic data for the ETH·crown·2PF_6^- are collected in Table 3-6.

Empirical formula	$C_{48}H_{70}F_{12}N_2O_{12}P_2$
Formula weight	1157 g/mol
Crystal system	Triclinic
Space group	P-1(2)
Cell parameters	a=8.2205(7) Å, b=12.3809(11) Å, c=13.5071(12) Å, α=80.37(0)°, β=83.89(0)°, γ=88.11(0)°
Cell ratio	a/b=0.6640 b/c=0.9166 c/a=1.6431
Cell volume	1347.48(34) $Å^3$
Z	1
Calc. density	1.42572 g/cm^3

Table 3-6.- Crystallographic information for the ETH·crown·PF_6^-

[39] Altobello, S.; Nikitin, K.; Stolarczyk, J. K.; Lestini, E.; Fitzmaurice, D. *Chem. Eur. J.* DOI: 10.1002/chem.200700898.

Table 3-7 contains the experimental (X-Ray) and the computed (MD) values for selected angles and distances. [40]

Angle (º) and distances (Å)	X-Ray	MD
α	0.1	3.05 (18.54)
d_A	13.3	13.74 (0.47)
d_B	6.9	7.14 (0.33)
d_C	6.9	7.09 (0.35)
d_D	5.0	5.65 (0.91)
d_E	8.5	14.15 (5.70)

Table 3-7.- Comparison of the X-Ray and Molecular Dynamics results. X-Ray values are taken from CIF file. Standard deviation values are for the MD results are given in parenthesis.

The structures obtained from the molecular dynamic simulations are in good agreement with the X-Ray structure except for d_E (the distance between one PF_6^- and the nearest nitrogen atom from the viologen). The bipyridinium area from the ETH viologen is almost flat and the crown shape is more open when complexed than for the free crown. Besides, the hexafluorophosphate anions are moving around the nitrogen atoms from the viologen and as a result the distances d_D and d_E fluctuate significantly. The differences in d_E can originate from the starting structure of the system used for the molecular dynamic simulations. X-Ray information was not available at the time the modelling of the system was carried out - other values for the unknown distances were adopted.

Unfortunately, it was not posssible to obtain the crystallographic data for the DIM·crown·$2PF_6^-$ due to the difficulty of determining its structure with reasonable accuracy.

[40] Geometric parameters studied for crown and ETH·PF_6^-, see Scheme 3-4

3.4 ENERGY PROFILE FOR THE COMPLEXATION PROCESS

3.4.1 Introduction

The energy profile for the complexation process of pseudorotaxanes ETH·crown·$2PF_6^-$ and DIM·crown·$2PF_6^-$ in acetonitrile was obtained following the methodology described in Chapter 13. In summary, the methodology consists of approaching the centers of mass of the host (crown) and guest (viologen) after appropriately orienting the structures (Scheme 3-9 and Scheme 3-10).

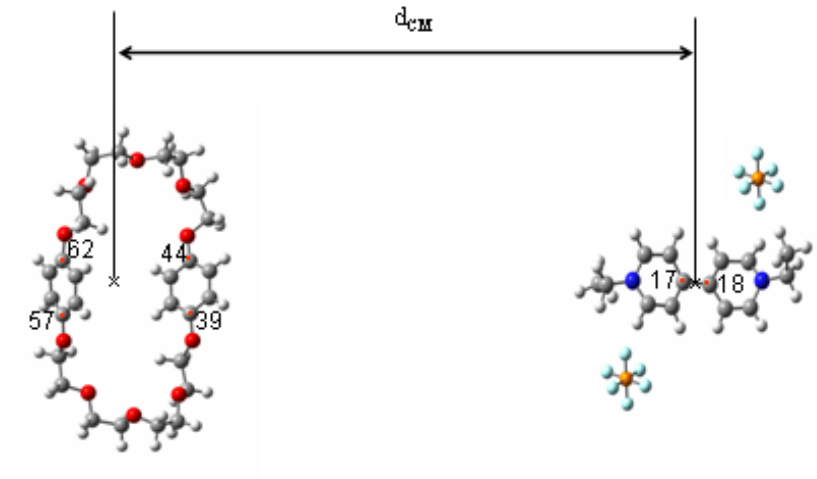

Scheme 3-9.- Distance between the center-of-masses of the crown and the viologen ETH.

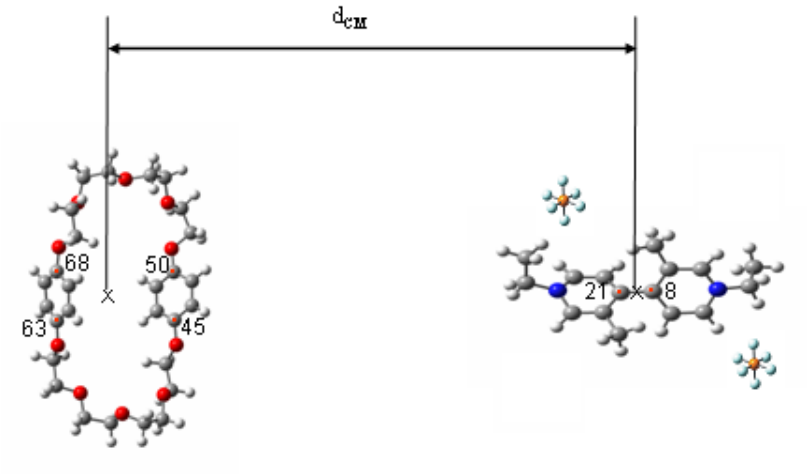

Scheme 3-10.- Distance between the center-of-masses of the crown and the viologen DIM.

In the definition of the atoms used for searching the reference points for each pseudorotaxane, we have keept the absolute atom numbering used in AMBER. For each system, it is necessary to define two atom groups whose center-of-mass averaged positions will be two points (X points). The distance between the X points (termed d_{CM}) will be constrained. Later we found that it is possible to use up to 200 atoms to define each center-of-mass group. However, this possibility not available to us at the moment of the calculation and for that reason, only a few atoms were used for the definition of the center-of-mass groups.

For the system ETH·crown·$2PF_6^-$ (Scheme 3-9), the center-of-mass averaging for the crown (see the X marked) was defined by the carbon atoms 39, 44, 57 and 62. The carbon atoms 17 and 18 of the viologen were used for calculating its center-of-mass. In case of the pseudorotaxane DIM·crown·$2PF_6^-$ (Scheme 3-10), a center-of-mass for the crown was defined using the carbon atoms 45, 50, 63 and 68. The atoms 8 and 21 were used to calculate the center-of-mass for the viologen.

3.4.2 Results

Scheme 3-11 and Scheme 3-12 display graphical representation of the energy changes during the complexation process as a function of the distance between the center-of-masses of the two manin components for each [2]pseudorotaxane.

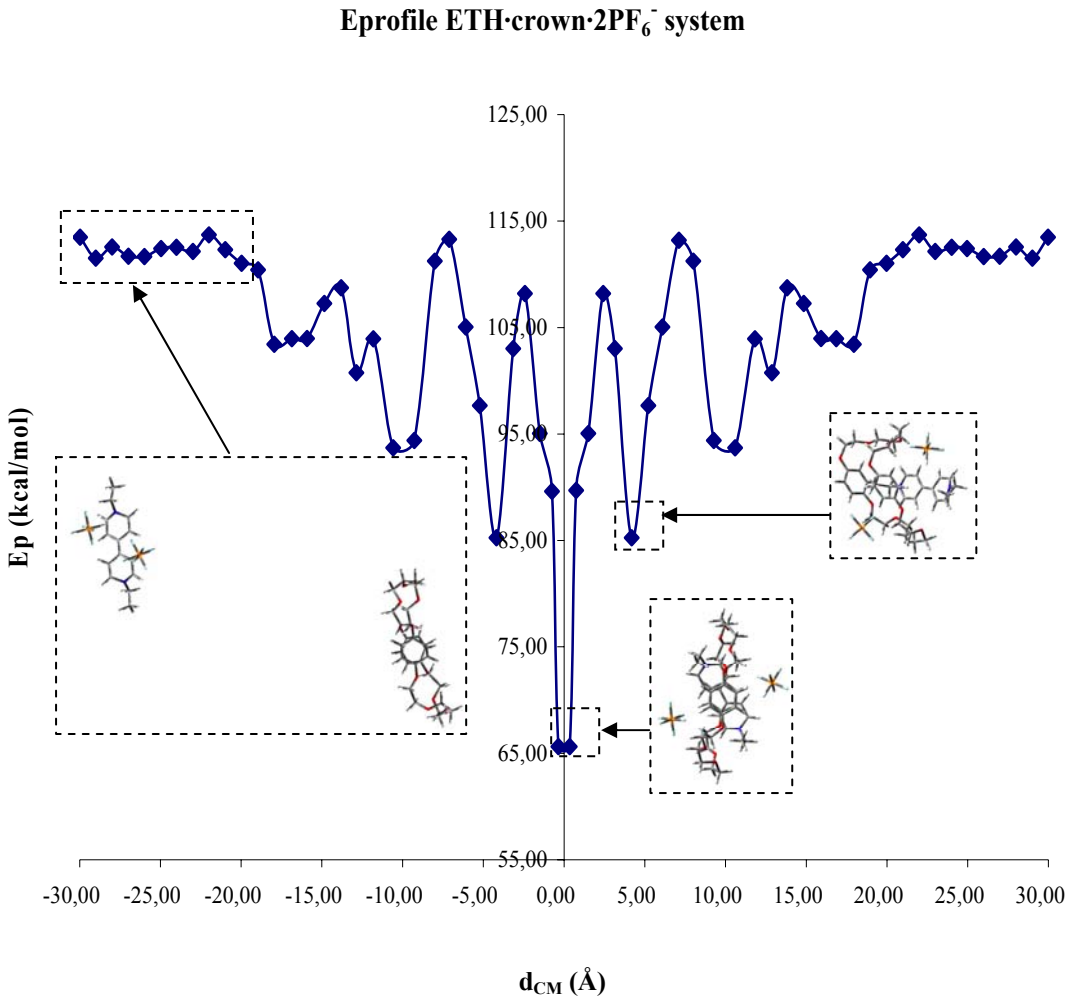

Scheme 3-11.- Energy profile for the system ETH·crown·2PF_6^- as obtained with AMBER.

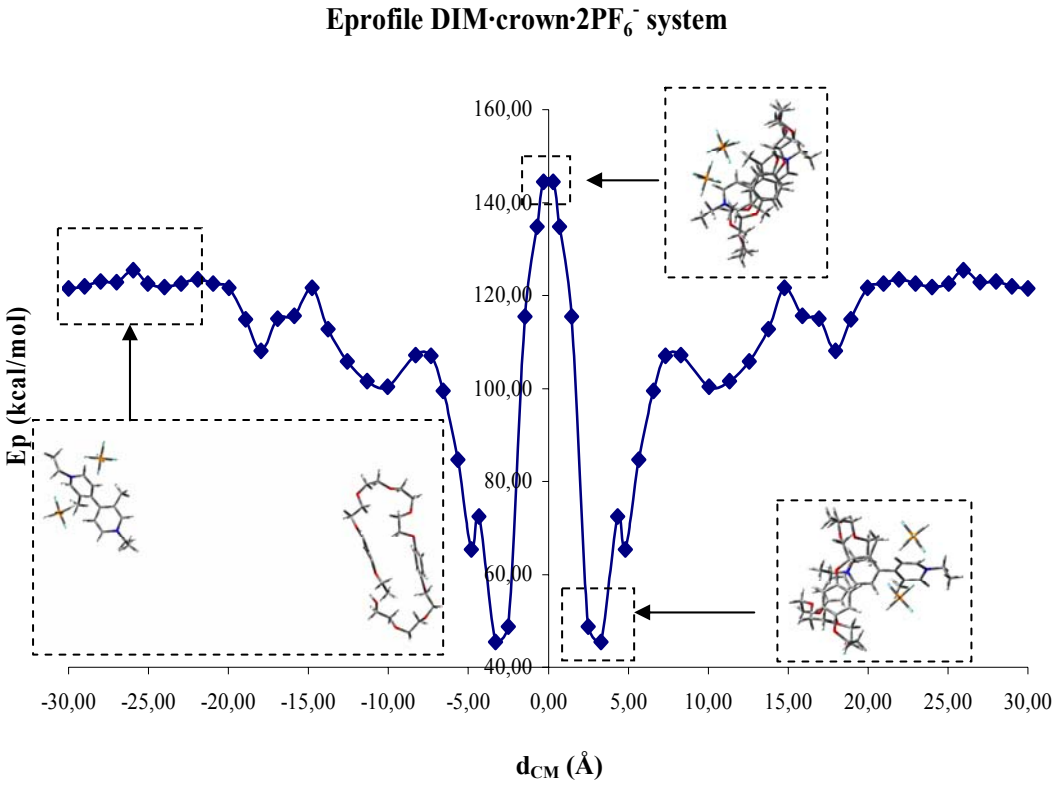

Scheme 3-12.- Energy profile for the system DIM·crown·PF_6^- as obtained with AMBER.

Two plots were obtained and they are shown in Scheme 3-11 and Scheme 3-12. In the first case, the complex exists when the distance between the ring and the viologen ETH is 0 Å.When both components are far away and the complex does not exist, the energy is higher. The complexation energy is about -47 kcal/mol. There is another local minimum at 4.19 Å (Ep = 85.25kcal/mol). In this case, the viologen is almost outside the cavity of the crown. The π-π stacking interaction between both components is small and, therefore, the complex is close to start to be unthreaded.

In the case of DIM, when the viologen is located at 0 Å from the crown, the energy of the system is 144 kcal/mol, but when the complex is completely unthreaded, the energy of the system is about 122 kcal/mol. In this case, the complexation energy is +20 kcal/mol. As can be seen from Scheme 3-12, another arrangement exists when the distance between the ring and the viologen is 3.30 Å, its energy being 45 kcal/mol, much lower than in the previous case. However, it was observed that both components were oriented perpendicularly to each other and the viologen is almost outside from the cavity of the crown. So, this is an association complex whose complexation energy is

equal to -77 kcal/mol. In summary, the complexation is energetically more favorable for the DIM·crown association complex than for the ETH·crown inclusion complex.

3.4.3 Conclusions

The energy profile nicely illustrates how the complexation changes over the distance between its components. Moreover, it permits us to identify the main conformations of the system analysed. In this thesis, the energy profile for the complexation of two pseudorotaxanes were studied and both showed that the inclusion complexation with viologen ETH is more favorable than when using DIM. For threading the viologen DIM into the crown, a more opened macrocycle is needed because of the methyl groups from the viologen. Consequently, the distance between the phenyl groups from the crown increases when the π-π stacking interaction between the host and the guest is reduced.

3.5 Π-Π STACKING INTERACTIONS IN PSEUDOROTAXANES

In order to show the π-π stacking interaction differences between the DIM·crown and ETH·crown pseudorotaxanes, HOMO for each pseudorotaxane were calculated. For more details about the calculations, see Chapter 14.

HOMO for the pseudorotaxanes are shown in Scheme 3-13 and Scheme 3-14:

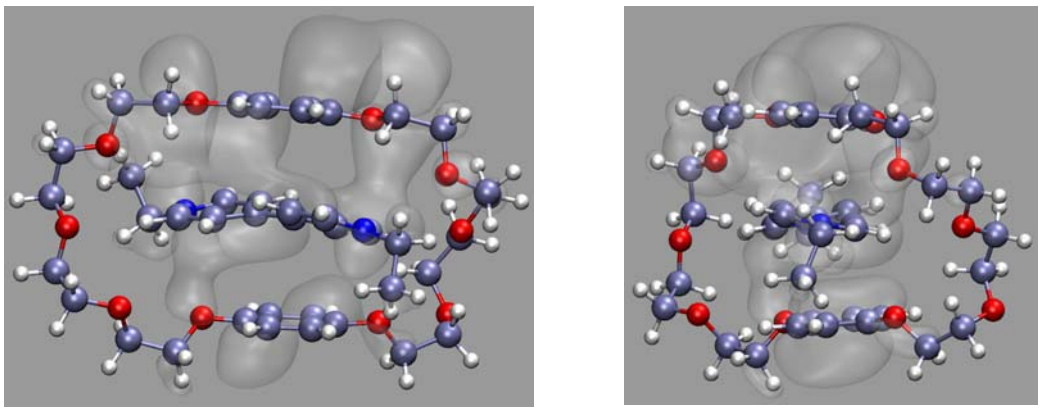

Scheme 3-13.- Different views for the HOMO orbitals (painted in grey) from the ETH·crown

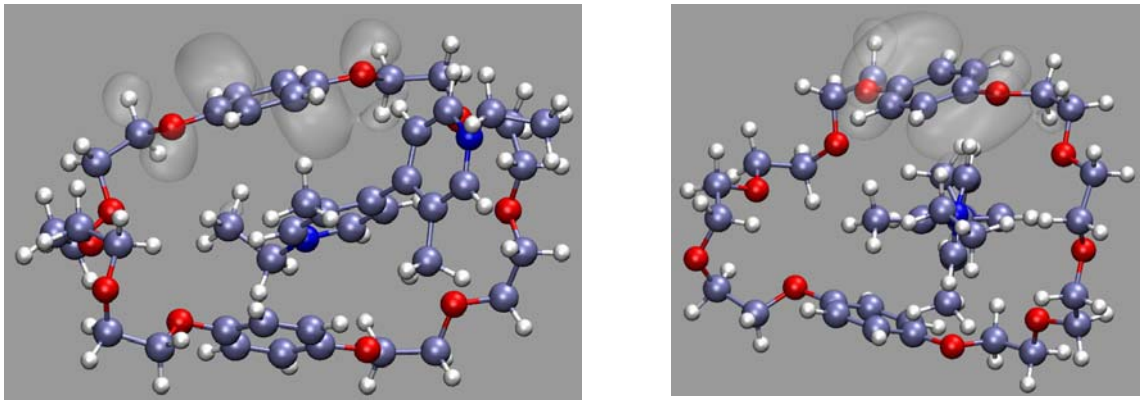

Scheme 3-14.- Different views for the HOMO orbitals (painted in grey) from the DIM·crown

It is seen from Scheme 3-13 that there is a high π-π stacking interaction around the aromatic rings from the macrocycle and the viologen ETH. However, no electron density appears around viologen DIM in its HOMO. The aromatic interaction present in the ETH·crown pseudorotaxane does not exist in the case of the DIM·crown pseudorotaxane (Scheme 3-14).

3.6 CONCLUSIONS

One of the purposes of this thesis was to study each pseudorotaxane. After all analyses were done, it became clear that crown complexes better with the ETH viologen than with the DIM viologen. Thus, it can be easily deduced that in case a rotaxane contains the two stations seen in this chapter was built, the crown would be around the station related to the ETH viologen. Moreover, the best conditions for a good complexation using these systems are with hexafluorophosphate in acetonitrile.

'May the luck of the Irish be always at hand,
And good friends always near you.
May each and every coming day
Bring some special joy to cheer you.'

Irish blessing

4 MODELLING OF [2]ROTAXANES

4.1 INTRODUCTION

In this chapter, the study of the [2]rotaxane[41] shown in Scheme 1-2 will be performed. It contains two viologen stations (V1 and V2) which exhibit different levels of affinity towards the crown ether, two bulky stoppers (including one which could be used to attach the rotaxane to the surface of an electrode or semiconductor nanoparticle), and a crown ether. The two viologen stations are connected through a flexible aliphatic linker.

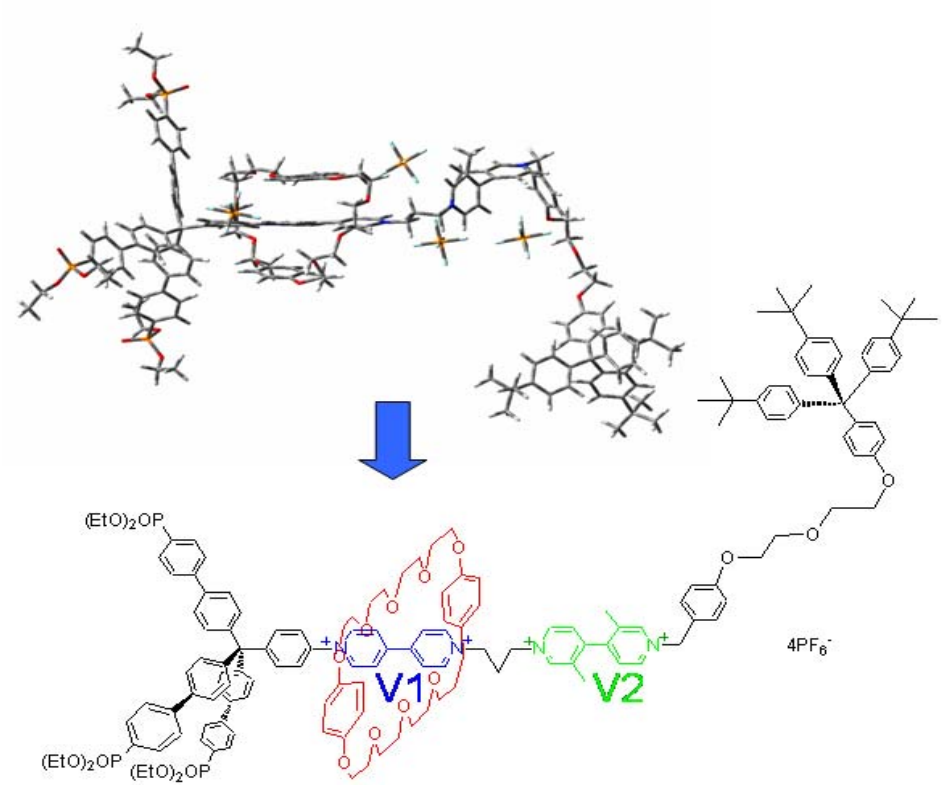

Scheme 4-1.- General scheme of the [2]rotaxane studied

[41] The IUPAC name for the rotaxane shown in the Scheme 4-1 is as follows: 1-{4-[Tris{4-(4-dihydrophosphonophenyl)-phenyl}-methyl]phenyl}-1'-(3-[3,3'-dimethyl-1'-(4-[bis{4-*tert*-butylphenyl}-4-ethylphenylmethyl]phenoxyethoxyethoxyphenylmethyl)-4,4'-bipyrid-1-yl]propyl)-4,4'-bipyridinium 34-crown-10 tetra(hexafluorophosphate).

Modelling the structural and dynamical properties of such [2]rotaxane was the final goal of the study, as well as to compare the results with experimentally determined solution structures. The experimental results were obtained using NMR, optical absorption spectroscopy and cyclic voltammetry.

The structure and energy for the axle (termed Axle A, the axle with stations V1 and V2 unreduced) and for the full rotaxane taking into account the two possibilities of location of the crown on the axle (Scheme 4-2 and Scheme 4-3), are studied in this chapter.

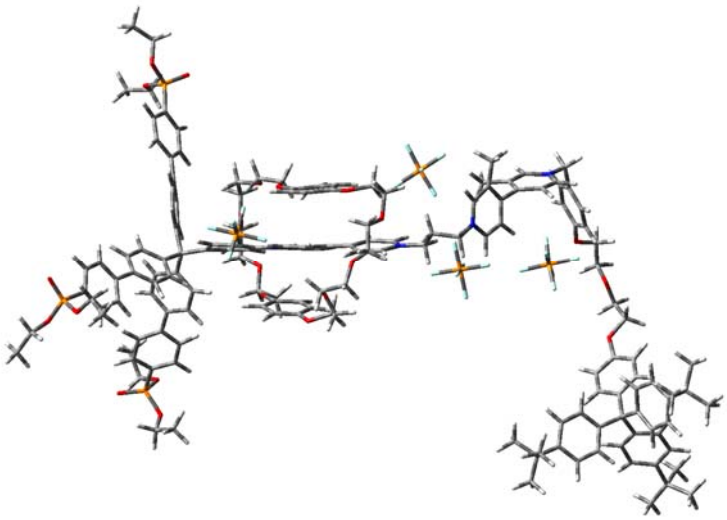

Scheme 4-2.- AxleA·4PF_6^-·crown V1. [2]rotaxane with axle A where the crown is located on the first station (V1).

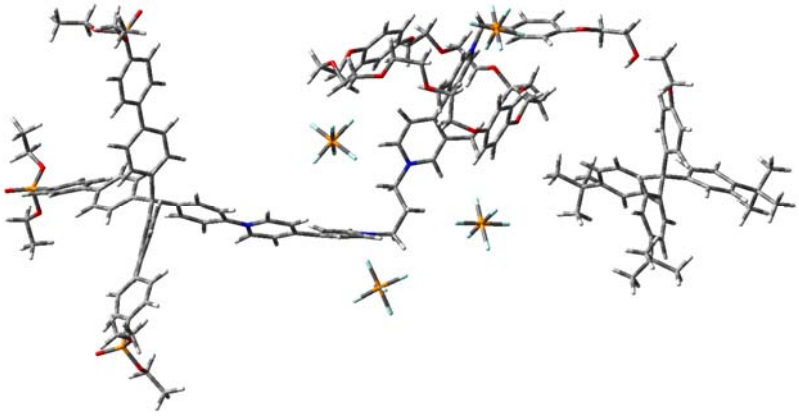

Scheme 4-3.- AxleA·4PF_6^-·crown V2. In this rotaxane, the crown is located on V2.

The study of these two translational conformations were performed in acetonitrile as solvent (cubic box of size 16 Å) and with hexafluorophosphate as counterions using AMBER (for more details, see Chapter 7).

4.2 STRUCTURAL STUDY

The changes of the structure of the system, as a function of the location of the crown, were studied. Different shape of the crown in each situation was expected as well. Moreover, the behaviour of the counterions around the stations was also examined. Finally, the macromolecule size variations, when shuttling the crown from one station to the other, were also monitored. The distances and angles studied were d_H (indicates the total lenght of the axle), d_A, d_B and d_C (inner dimensions of the crown), d_D, d_E, d_F and d_G (distances from the N^+ to the corresponding counterion), and α, β and γ (dihedral angles between aromatic rings of the axle).

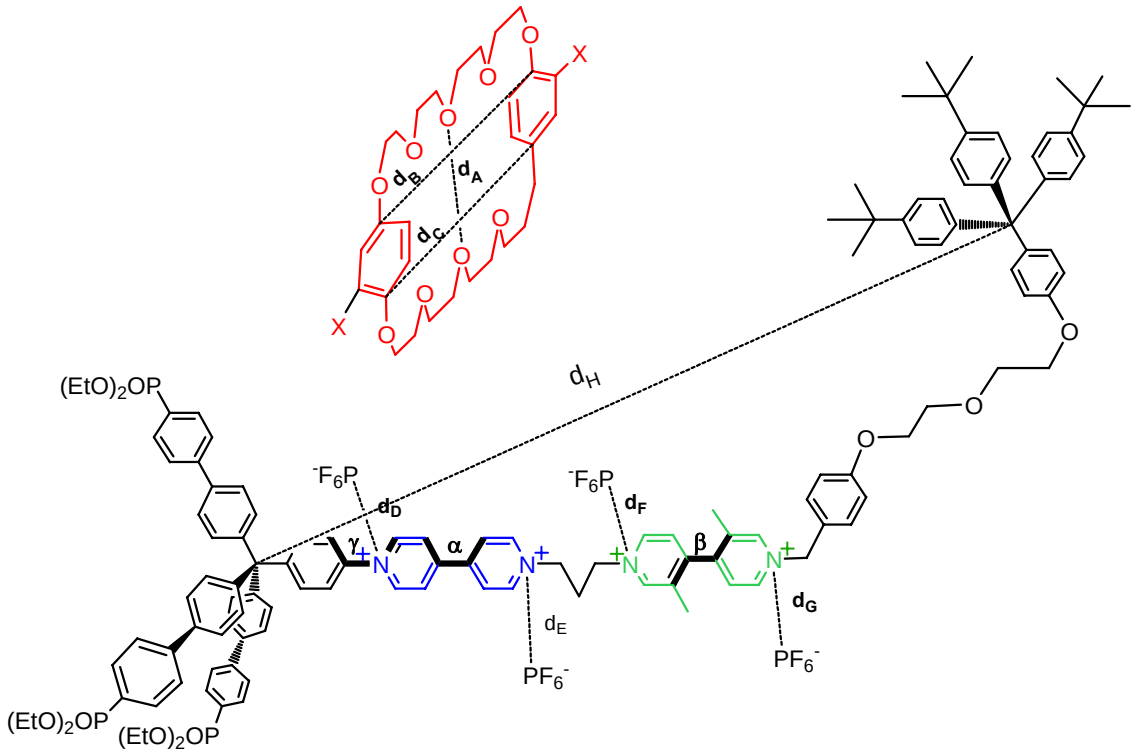

Scheme 4-4.- Distances and angles measured for the rotaxane and its components.

All the data related to the distances (Å) and angles (º) monitored are gathered in Table 4-1:

system	α	β	γ	d_A	d_B	d_C	d_D	d_E	d_F	d_G	d_H
crown				13.32 (1.17)	5.98 (0.99)	5.85 (1.09)					
AxleA·4PF_6^-	10.22 (27.67)	-101.45 (19.28)	2.83 (14.70)				8.94 (2.78)	7.84 (2.47)	10.48 (5.90)	16.67 (9.75)	22.98 (3.70)
AxleA·4PF_6^- ·crown V1	11.28 (19.90)	-100.74 (19.03)	12.12 (13.58)	13.48 (0.49)	7.03 (0.34)	7.02 (0.33)	5.53 (0.37)	7.19 (1.19)	5.11 (0.42)	8.64 (2.60)	22.86 (1.92)
AxleA·4PF_6^- ·crown V2	13.72 (25.48)	-110.67 (21.17)	-0.15 (15.58)	12.59 (0.84)	8.08 (0.78)	7.87 (0.55)	12.07 (3.33)	4.96 (0.35)	5.12 (0.75)	5.21 (0.31)	33.24 (2.97)

Table 4-1.- Distances (in Å) and angles (in degrees) monitored in the rotaxane structural study. Standard deviation is given in brackets.

The shape of the crown depends on its position in the axle. Distances d_B and d_C in AxleA·4PF_6^-·crown V2 are larger than in AxleA·4PF_6^-·crown V1. However, d_A is shorter when the crown in located at V2, than when the macrocycle is at V1. The d_B and d_C distances from the complexed crown are much larger than when it is uncomplexed. When crown is free, d_A becomes larger compared to the state when it is located in V2 from the axle. However, d_A in AxleA·4PF_6^-·crown V1 is larger than in AxleA·4PF_6^- ·crown V2 and when the crown is uncomplexed. These results are analogous to those observed in pseudorotaxanes using acetonitrile as solvent and PF_6^- as counterion (see Table 3-2).

The value of d_H changes depending on the crown position in the axle as well. Distance d_H when crown is on V2 is larger than when it is located on V1. However, when crown is on V1, d_H is similar to value from the uncomplexed axle.

Another interesting observation from Table 4-1 is that the dihedral values for α and γ increase, whereas β keeps its value when crown is located on viologen V1. However, when crown is on V2, α and γ remain almost constant, while β increases.

The values for d_D , d_E, d_F and d_G that measure the distances between counterion and the N^+ atoms decrease when crown is on the axle.

4.3 DETERMINATION OF THE COMPLEXATION ENERGY FOR THE [2]ROTAXANE

In order to know where the crown is located on the rotaxane, the complexation energies with the crown on each station wer calculated using molecular dynamics simulations (for details, see Chapter 7 and Chapter 12).

The complexation energy of the rotaxane when the crown is located on the V1 viologen is -5.95 kcal/mol. However, when the crown is on the other station (V2), the complexation energy is 0.01 kcal/mol. The energy difference (about 6 kcal/mol) clearly favours the crown to be located on the first station (V1).

The fact that the crown prefers to be located at V1 is in agreement with the experimental data taken from the experimental studies done by Fitzmaurice's group at the UCD.[42]

[42] Nikitin, K.; Lestini, E.; Stolarczyk, J. K.; Müller-Bunz, H.; Fitzmaurice, D. *Chem. Eur. J.* DOI: 10.1002/chem.200701384.

4.4 CONCLUSIONS

The [2]rotaxane was modelled and its two translational conformations were structurally and energetically studied. It is concluded on the basis of the results discussed in this chapter that the position of the crown ether on the first station (V1) is the most favourable of all situations studied when hexafluorophosphate and acetonitrile are used, as a counterion and solvent, respectively (in agreement with experiments).

'There is nothing so bad
that it could not be worse'

Irish Proverb

5 MODELLING OF SHUTTLING PHENOMENON UNDER REDUCTION

5.1 INTRODUCTION

One of the most interesting goals of this thesis was the study of the shuttling process of the [2]rotaxane induced by stepwise reduction of the viologen stations. It is observed experimentally, that after a single reduction of the stations V1 and V2, crown does not move to the second station. However, when the viologen V1 gains one more electron, the shuttling occurs and the crown moves to the V2 station.

The structure and energy of singly and doubly reduced pseudorotaxanes were calculated and studied to visualize what happened when pseudorotaxanes are reduced.

The energy and geometry changes of the [2]rotaxane after the complete reduction processes was studied in detail.

5.2 SINGLY AND DOUBLY REDUCED PSEUDOROTAXANES

As given in the introduction Chapter, there are many types of interactions in chemistry. However, non-covalent interactions play an important role in the stability of macromolecules. In our case, the pseudorotaxane stability can be modified varying the interaction between the viologen and the crown. For example, a way to unthread a pseudorotaxane is by reducing the dication viologen to radical cation viologen or to neutral viologen. Working in this way, we decided to study in this chapter the singly and doubly reduced pseudorotaxanes.

5.2.1 Complexation Energy

The complexation energy for each radical pseudorotaxane was calculated following the methodology explained in Chapter 12, and the computed data are presented in Table 5-1. The designations CRE, CRD and NET are defined in Scheme 5-1.

System	Complexation Energy (kcal/mol)
CRE·crown·PF_6^-	-4.84
CRD·crown· PF_6^-	-1.31
NET·crown	-0.88

Table 5-1.- Complexation energy for CRE, CRD and NET complexes.

It is observed that complexation with CRE is more favourable than with CRD. However, both energies are negative, which means that the two complexes can exist. Moreover, if we compare these results with the complexation energies for ETH and DIM complexes in acetonitrile given in Table 3-1 [$\Delta G_{(ETH\cdot crown\cdot 2PF6-)}$ =-8.48 kcal/mol, $\Delta G_{(DIM\cdot crown\cdot 2PF6-)}$ =-2.63 kcal/mol], it appears that complexes with CRE and CRD are less favorable than complexes with dication viologens (ETH and DIM). The complexation energy for NET·crown is negative as well, however, this is the least favorable complex among all complexes (see Table 5-1).

These results are in agreement with the experimental stimates obtained recently.[43]

It can be concluded on the basis of the results discussed above that it would be possible to design a switchable rotaxane with stations analogous to ETH and DIM viologen and afterwards, by selectively reducing each station, to force the switching of the crown from one station to the other.

[43] Stolarczyk, J.; Pérez-Mirón, J.; Nikitin, K.; Altobello, S.; Jaime, C.; Fitzmaurice, D. *Comparative Experimental and Computational Studies of [2]pseudorotaxanes in Solution.* Manuscript in preparation.

5.2.2 Structural study

Molecular dynamics simulations (for details, see Chapter 7) were used for the calculation of the complexation energy of CRE (ETH viologen singly reduced), CRD (DIM violgen singly reduced) and NET (ETH viologen doubly reduced) complexes and to study the structure of each complex. The distances and angles mesured are shown in the following scheme:

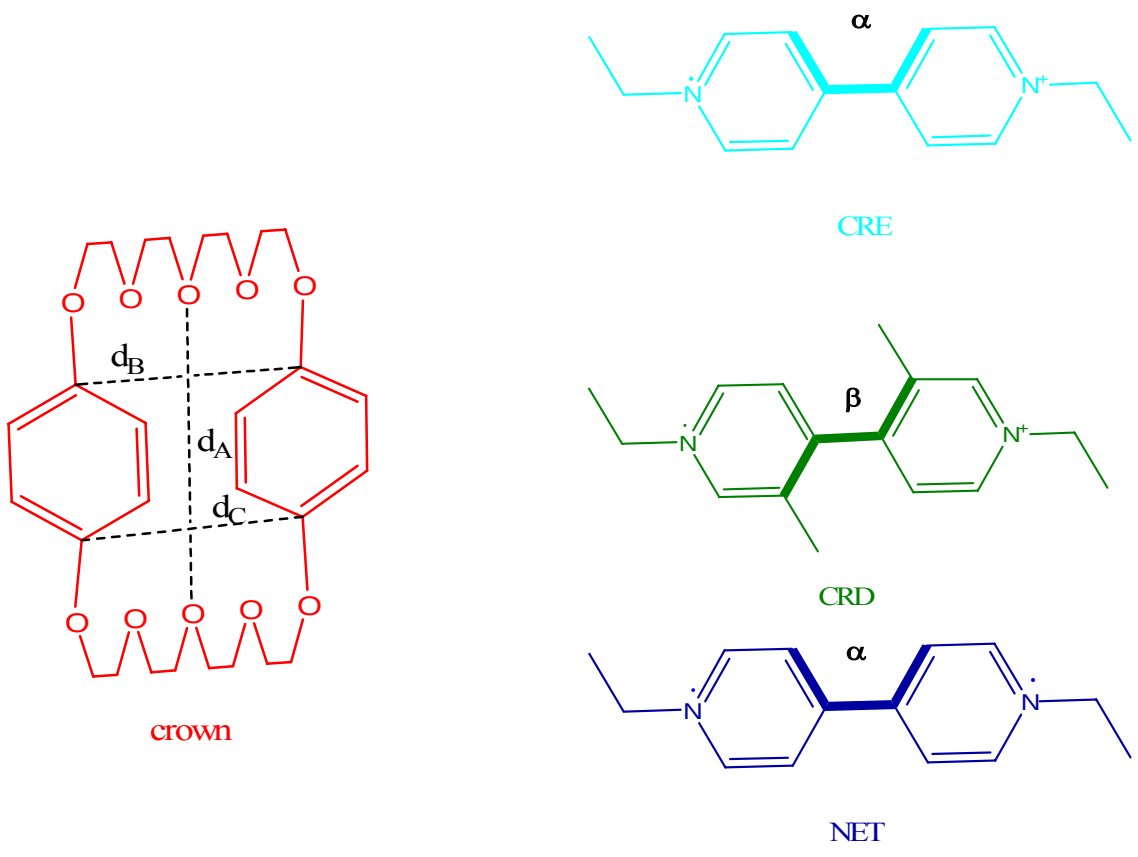

Scheme 5-1.- Geometry parameters analysed in CRE, CRD, NET viologens and in their complexes with crown.

The average values with the standard deviations for each geometrical parameter mesured are presented in Table 5-2.

System	α (β)	d_A	d_B	d_C
CRE·PF_6^-	-0.27 (10.84)			
CRE·crown· PF_6^-	0.37 (10.39)	13.71 (0.47)	7.28 (0.46)	7.38 (0.45)
CRD·PF_6^-	141.86 (7.71)			
CRD·crown· PF_6^-	143.72 (7.64)	13.04 (0.88)	7.79 (1.42)	7.80 (1.07)
NET	-0.30 (11.77)			
NET·crown	-0.17 (11.82)	13.31 (1.11)	6.32 (1.20)	6.18 (1.18)

Table 5-2.- Average values of the dihedral angles α and β, and the distances d_A, d_B and d_C. Standard deviation are given in parentheses.

The viologens CRE and NET are very flat (α is about 0º) in all the cases studied (Table 5-2; when they remain inside the crown and when they are unthreaded as well). However, α is around 142º in the case of the cation viologen CRD complexed with crown and free (in agreement with Gaussian calculations).[44]

About the crown size in CRE and NET complexes, the macrocycle presents a shape similar to the ETH complex (d_A is increased and d_B and d_C become shorter with respect to the values in free crown). However, the crown becomes more rounded when its guest is the CRD viologen (d_A becomes shorter and d_B and d_C are larger with respect to the crown unthreaded). The crown shape in the CRD complex is similar to the complex formed by the DIM viologen.

[44] Geometry optimization calculations with the hybrid functionals BHandHLYP and a basis function set 6-311++G(d,p) were computed for the cation radical viologens CRE and CRD. The method MP2 and a basis function set 6-31G were used to perform geometry optimization calculations for the neutral viologen NET.

5.2.3 Spin delocalisation calculation

In order to understand how the electrons were distributed along the structure of the radical viologens, spin delocalisation calculations with Gaussian were done (see Chapter 14).

In the following schemes (Scheme 5-2 and Scheme 5-3), spin delocalisations (unpaired spin) for cation radical viologens 1,1'-diethyl-4,4'-bipyridinium monocation (CRE) and 1,1'-diethyl-3,3'-dimethyl-4,4'-bipyridinium monocation (CRD) are shown:

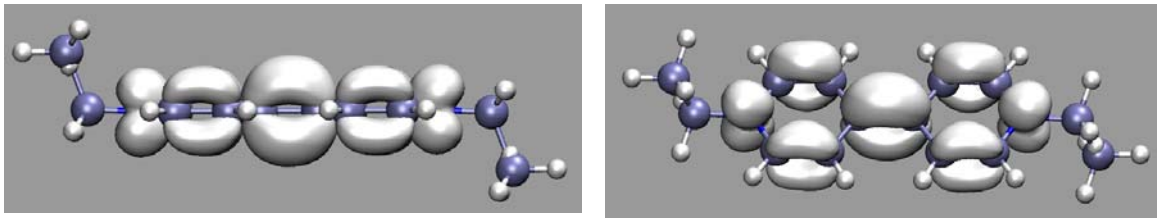

Scheme 5-2.- Spin delocalisation for CRE viologen (α≈0º)

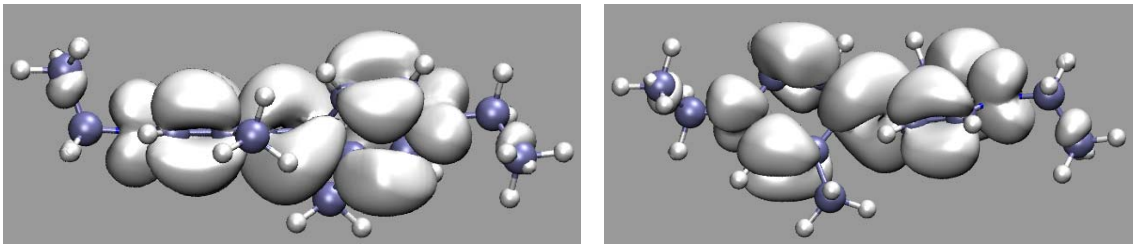

Scheme 5-3.- Spin delocalisation for CRD viologen (β≈38º)

It is evident from Scheme 5-2 and Scheme 5-3 that the radical cation viologens CRE and CRD have the unpaired electron very well delocalised.

Due to the existence of two electrons more in the structure of the NET viologen , two spin delocalisation calculations were necessary to be executed (Scheme 5-4).

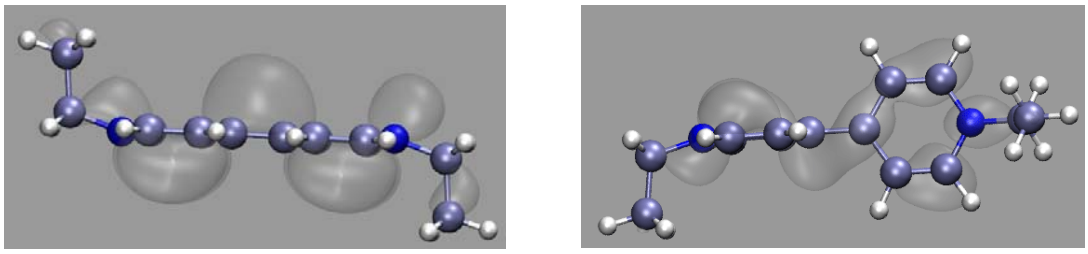

a) b)

Scheme 5-4.- Doubly reduced viologen NET, 1,1'-diethyl-4,4'-bipyridinium. a) singlet state, α≈0º . b) triplet state, α≈90º .

A singlet state of the NET viologen is shown in Scheme 5-4a. The viologen is flat and the electrons are well delocalised. In the other case (triplet state), the electrons are also delocalised. However, the two aromatic rings of the structure are perpendicular. Experimentally, only the structure of the singlet state is observed for NET viologen.[45]

5.3 SHUTTLING PHENOMENON UNDER REDUCTION IN A [2]ROTAXANE

5.3.1 Introduction

It is known that there are some [2]rotaxanes with interesting properties and useful applications that makes this kind of compounds intensively studied nowadays. The most important property of the [2]rotaxane studied in this thesis is that this macromolecule can be used as a switch by moving its crown ether from one station to the other using an external stimuli. It is important to know more about this shuttling phenomenon induced

[45] Stolarczyk, J.; Pérez-Mirón, J.; Nikitin, K.; Altobello, S.; Jaime, C.; Fitzmaurice, D. *Comparative Experimental and Computational Studies of [2]pseudorotaxanes in Solution.* Manuscript in preparation.

by stepwise reduction of the viologen stations in order to design other switchable [2]rotaxanes which can be used in the fabrication of molecular electronic devices.

Working along this line, we studied the reduction processes of the [2]rotaxane by performing Free Energy Perturbation (FEP) calculations using the Gibbs module of AMBER 7.

In order to know if the shuttling of the crown is favourable after the first, the second or third reduction, we decided to build the following energy cycles:

a)

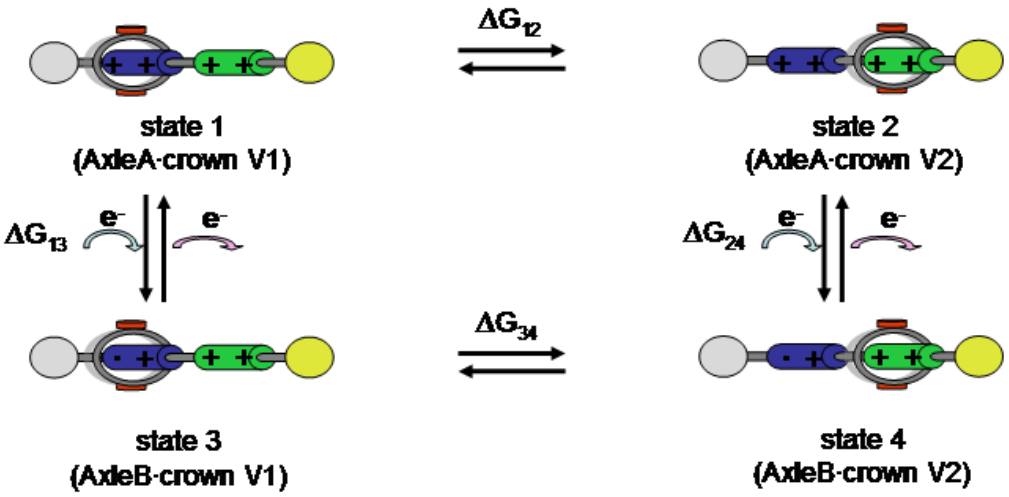

Single reduction of viologen V1

b)

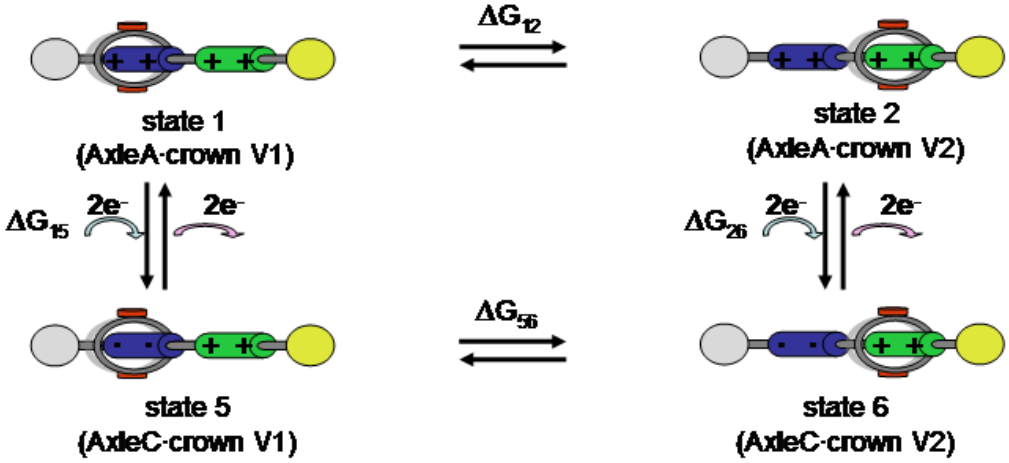

Double reduction of viologen V1

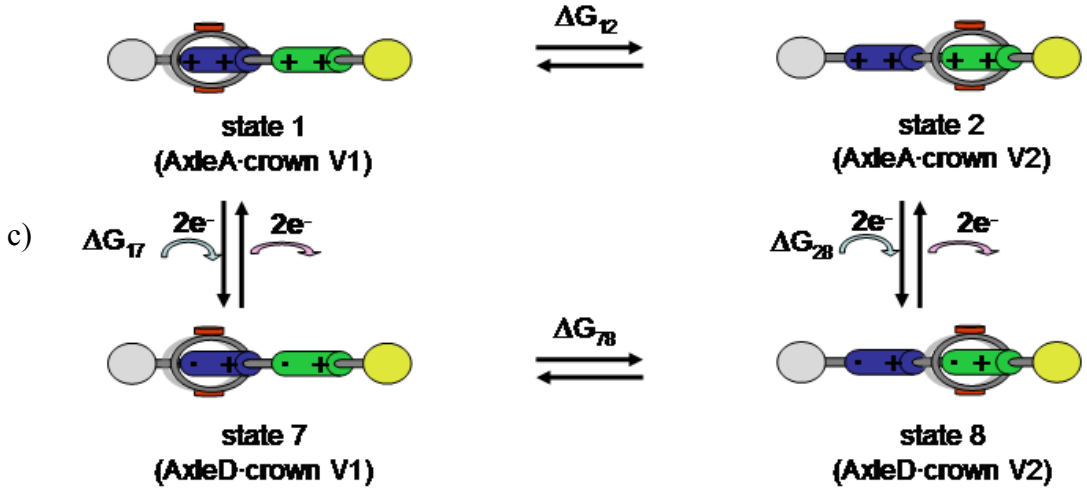

Double reduction process (both viologens are singly reduced)

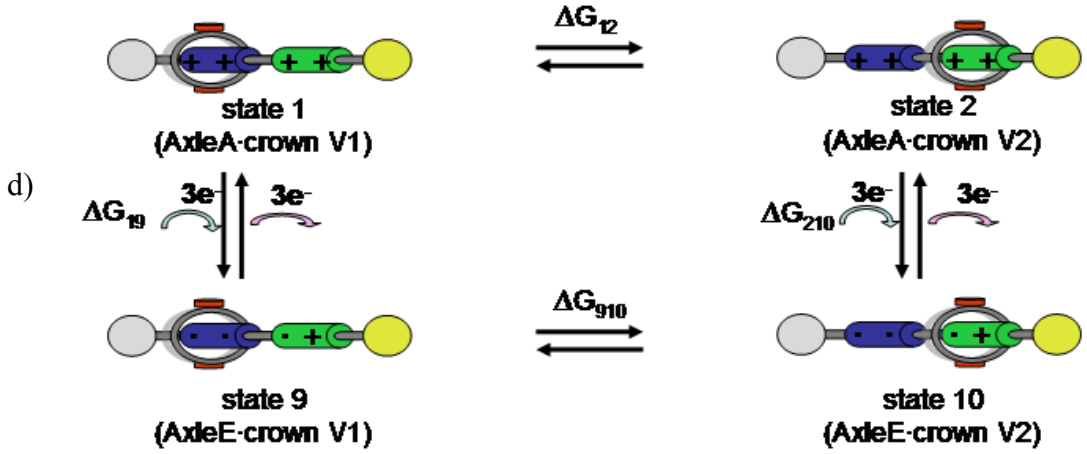

Triple reduction process (viologen V1 is doubly reduced and V2 is singly reduced)

Scheme 5-5.- Energy cycles for the different reduction processes. The crown is located on the station V1 in odd states, however, for even states, the crown is on the second station, V2. a) First reduction process, where V1 is singly reduced. b) Viologen V1 is doubly reduced. c) V1 and V2 are singly reduced. d)The rotaxane is doubly reduced on V1 and singly reduced on V2.

It is known experimentally that, after the first reduction, station V1 is singly reduced (Scheme 5-5a). There are two possibilities for the second reduction. One of

them is to have both stations singly reduced (Scheme 5-5c), whereas the other possibility is to have only station V1 doubly reduced (Scheme 5-5b). Both possibilities were examined. Only the first case however was experimentally observed. Finally, third reduction was carried out by reducing twice the station V1 and remaining V2 singly reduced. [46]

5.3.2 FEP calculations

All the rotaxanes represented in Scheme 5-5 were built in AMBER using the axles and crown which are shown in Chapter 9. Afterwards, FEP methodology (see Chapter 7 for more details) was used to calculate the energy involved in all the processes where no shuttling is produced, see Scheme 5-5.

5.3.2.1 Single reduction of viologen V1 on the rotaxane

FEP calculations were used to calculate the energies ΔG_{13} and ΔG_{24} which are gathered in the following table:

	$\Delta G_{forward}$	$-\Delta G_{reverse}$	$/\Delta G_{forward}+\Delta G_{reverse}/$	$\Delta G_{average}$
ΔG_{13}	-10.4	-8.5	1.9	-9.5
ΔG_{24}	-16.4	-17.1	0.7	-16.8

Table 5-3.- FEP results for single reduction of viologen V1 on the rotaxane.

It can be concluded from the data in Table 5-3 that single reduction without translation can be carried out (ΔG_{13} and ΔG_{24} are negative). In fact, the final states are more stable than the starting states. Moreover, taking into account the thermodynamic cycle shown in Scheme 5-5a, the energy differences between the shuttling processes from state 3 to state 4 (ΔG_{34}) and from state 1 to state2 (ΔG_{12}) gives as a result that the

[46] Nikitin, K.; Lestini, E.; Stolarczyk, J. K.; Müller-Bunz, H.; Fitzmaurice, D. *Chem. Eur. J.* DOI: 10.1002/chem.200701384.

shuttling process after the first reduction is favorable ($\Delta G_{34} - \Delta G_{12} = \Delta G_{24} - \Delta G_{13} =$ -7.3 kcal/mol).

5.3.2.2 Double reduction of viologen V1 on the rotaxane

The energies related to the reduction processes from state 1 to state 5 and from state 2 to state 6 were calculated and are presented in Table 5-4:

	$\Delta G_{forward}$	$-\Delta G_{reverse}$	$/\Delta G_{forward}+\Delta G_{reverse}/$	$\Delta G_{average}$
ΔG_{15}	43.2	45.3	2.1	44.3
ΔG_{26}	1.7	4.7	3.0	3.2

Table 5-4.- FEP results for doubly reduction of viologen V1 on the rotaxane.

Using the energy values from Table 5-4 and taking into account the cycle shown in Scheme 5-5b, the difference between ΔG_{56} and ΔG_{12} will be equal to -41.1 kcal/mol ($\Delta G_{56} - \Delta G_{12} = \Delta G_{26} - \Delta G_{15}$). This result indicates that after a double reduction of viologen V1, the crown shuttles from station V1 to station V2.

5.3.2.3 Double reduction of the rotaxane (both stations are singly reduced)

FEP calculations were used to calculate the energies ΔG_{17} and ΔG_{28} which are included in Table 5-5:

	$\Delta G_{forward}$	$-\Delta G_{reverse}$	$/\Delta G_{forward}+\Delta G_{reverse}/$	$\Delta G_{average}$
ΔG_{17}	12.6	11.6	1.0	12.1
ΔG_{28}	-53.5	-54.2	0.7	-53.9

Table 5-5.- FEP results for the double reduction of the rotaxane (V1 and V2 are singly reduced).

Using the energies from Table 5-5, it is possible to understand if the shuttling process after the double reduction of the rotaxane (V1 and V2 singly reduced) is favorable. In the present case, the difference between ΔG_{78} and ΔG_{12} is equal to ΔG_{28} - ΔG_{17} and this amounts to -66.0 kcal/mol. Consequently, the shuttling process is possible.

5.3.2.4 Triple reduction (viologen V1 is doubly reduced and V2 is singly reduced)

Triple reduction of the rotaxane (Scheme 5-5d) was evaluated using FEP calculations and the energies involved in the process are presented in Table 5-6.

	$\Delta G_{forward}$	$-\Delta G_{reverse}$	$/\Delta G_{forward}+\Delta G_{reverse}/$	$\Delta G_{average}$
ΔG_{19}	-26.7	-23.5	3.2	-25.1
ΔG_{210}	-54.0	-50.8	3.2	-52.4

Table 5-6.- FEP results for the triple reduction (V1 is doubly reduced and V2 is singly reduced).

The results from Table 5-6 suggest that the reduction process, while keeping the crown in the same position (no shuttling), can be carried out because the ΔG values for the reductions (ΔG_{19} and ΔG_{210}) are negative.

Moreover, shuttling process after triple reduction occurs due to the difference between ΔG_{910} and ΔG_{12} (ΔG_{910} - ΔG_{12} = -27.3 kcal/mol, calculated through the difference between ΔG_{210} and ΔG_{19}), indicating that the shuttling process from V1 to V2 is more favourable after the triple reduction of the axle (Scheme 5-5d).

5.3.3 Structural study of the different states of the rotaxane

The axles of the different rotaxane states were structurally analysed. The following scheme shows the dihedral angles and the distance monitored.

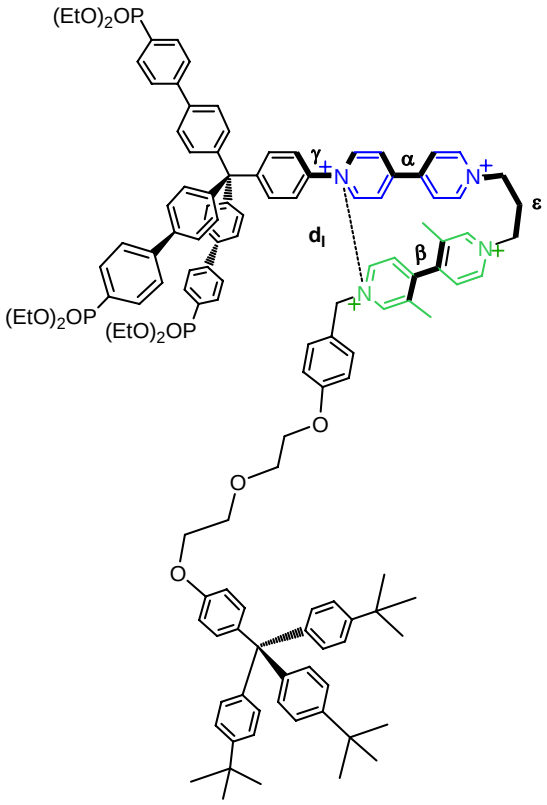

Scheme 5-6.- Dihedral angles (α, β, γ, ε) and distance (d_l) monitored for all the studied states.

The structural analysis of each state was carried out using 2000 structures taken from the molecular dynamics simulation (1 structure/picosecond of simulation was taken). Frequency of dihedral angle (or distance) values monitored were normalized by the number of structures taken from the trajectory file. This normalization will appear, in schemes, named as “normalized probability”.

5.3.3.1 Dihedral angle α

Scheme 5-7 represents the normalized probability for the dihedral α of all odd states (states which contain the crown on V1).

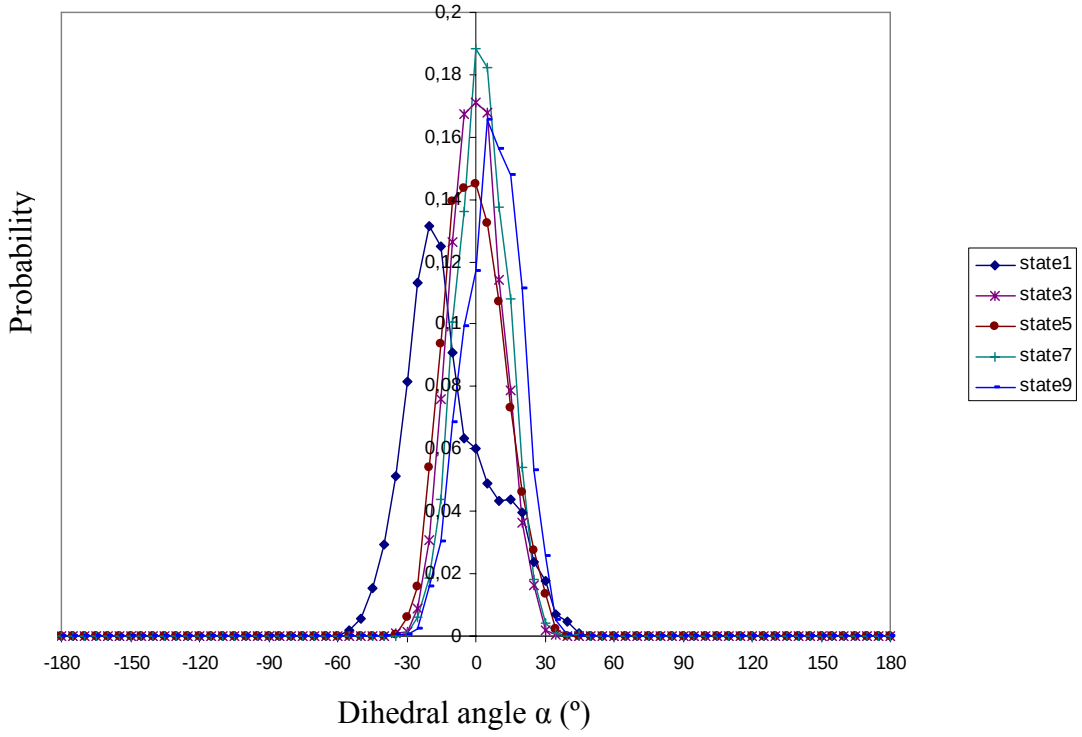

Scheme 5-7.- Normalized probability of values of the dihedral angle α for states that contain the crown ether on the viologen V1.

The values of α are close to 0º for all the states of the rotaxane. For state 1 (the parent state), the curve presents a high peak around -20º, but there are also structures for which the value of α is around +10º. This finding points to the existence of a conformational preference when the crown is located on V1, which will produce the presence of a new chirality element (chiral axis) on V1. This chiral element clearly indicates that the simulation time was too short.

In Scheme 5-8, the normalized probability for the dihedral angle α of the states which contain the crown on V2 (with even numbers) is given.

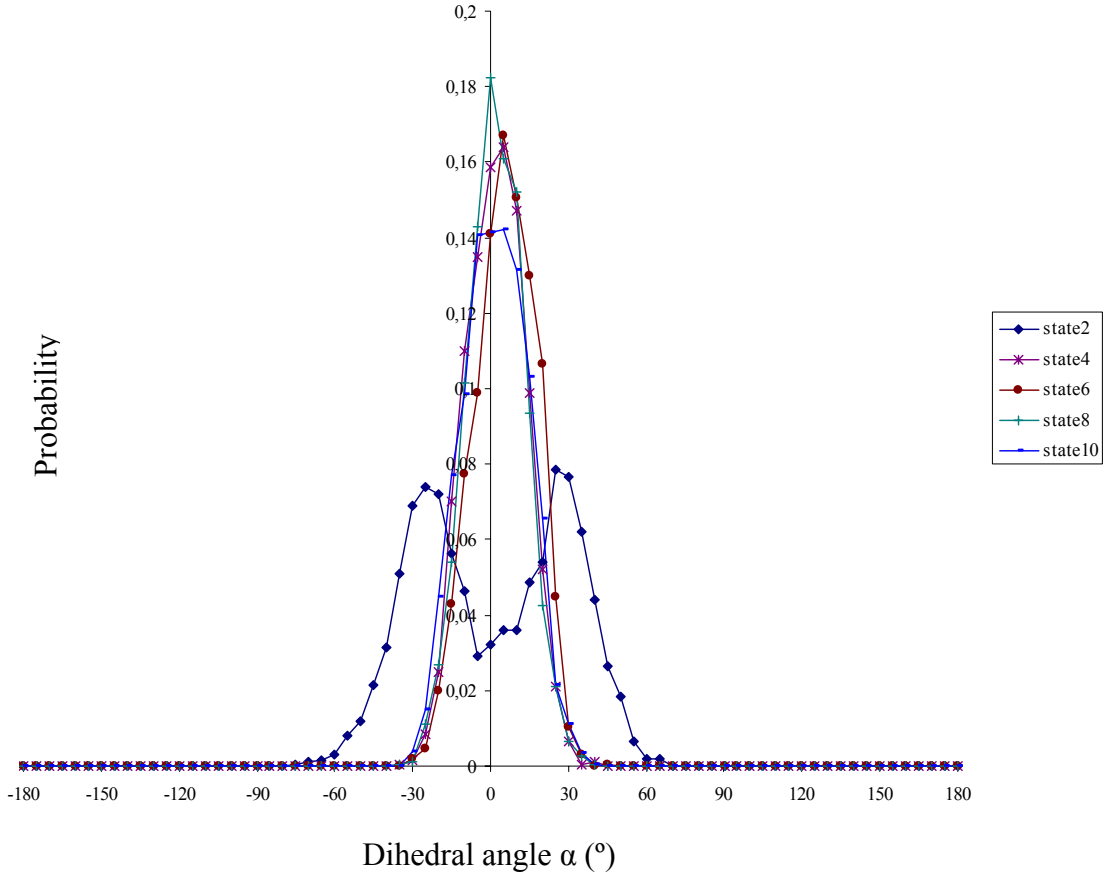

Scheme 5-8.- Normalized probability of the α values for the rotaxane states whose crown ether is located on the viologen V2.

In this case (Scheme 5-8), two phenomena are present. The dihedral angle α is acquires values around ±30º for the parent state when the crown is on the second station, V2. However, for the reduced states, the dihedral angle α remains close to 0º and, consequently, station V1 is almost flat due to a higher electron delocalization (in agreement with Gaussian calculations).

The two symmetrical peaks in state 2 (α is ±30º) point to the absence of chirality on viologen V1 when crown is localized on V2 (see Scheme 5-8, state2).

5.3.3.2 Dihedral angle β

In Scheme 5-9 is represented the normalized probability for the dihedral angle β of odd states (states which contain the crown on V1).

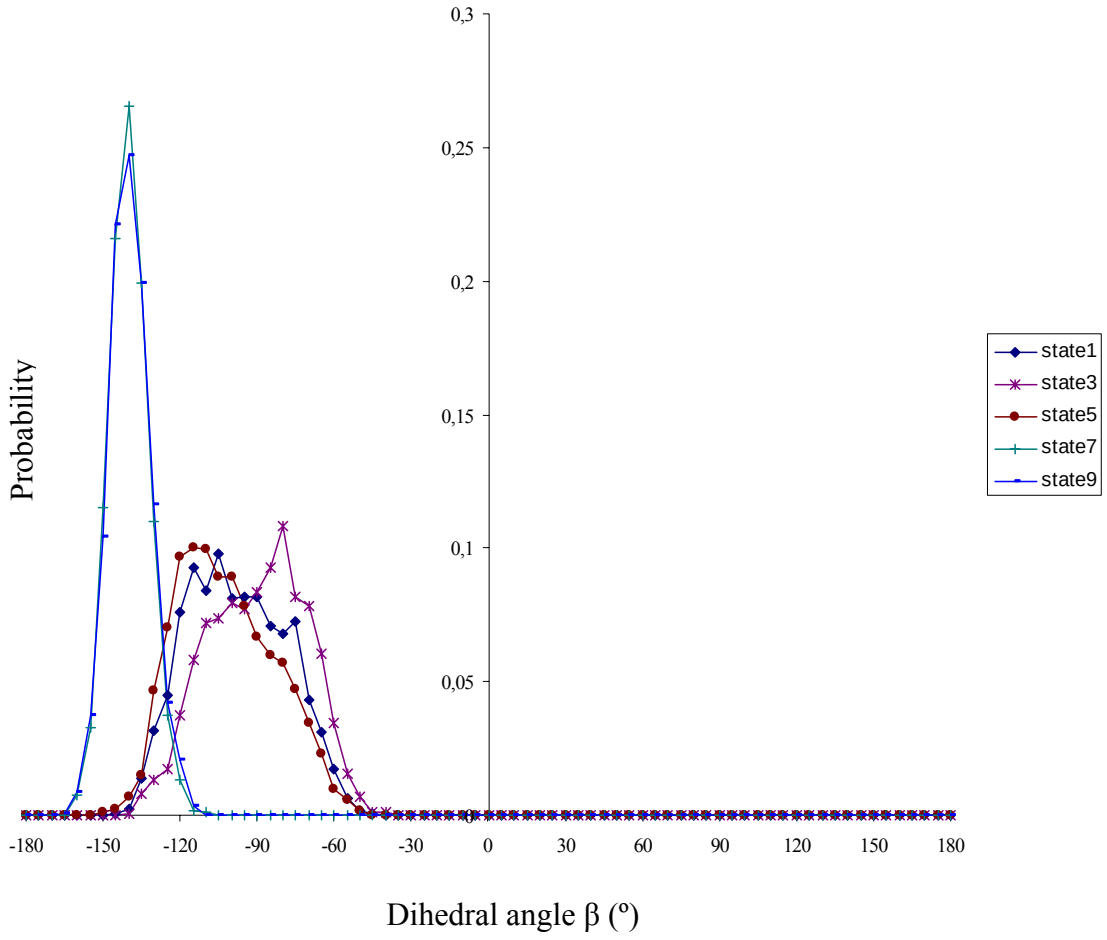

Scheme 5-9.- Normalized probability of dihedral angle β for odd states.

The values for the dihedral angle β are around 90º for states 1, 3 and 5. However, β is around -145º (see states 7 and 9) when the rotaxane is singly reduced on V2 (in agreement with quantum mechanics calculations with Gaussian).

The normalized probability for the dihedral angle β of even states is given (states which contain the crown on V2) in Scheme 5-10.

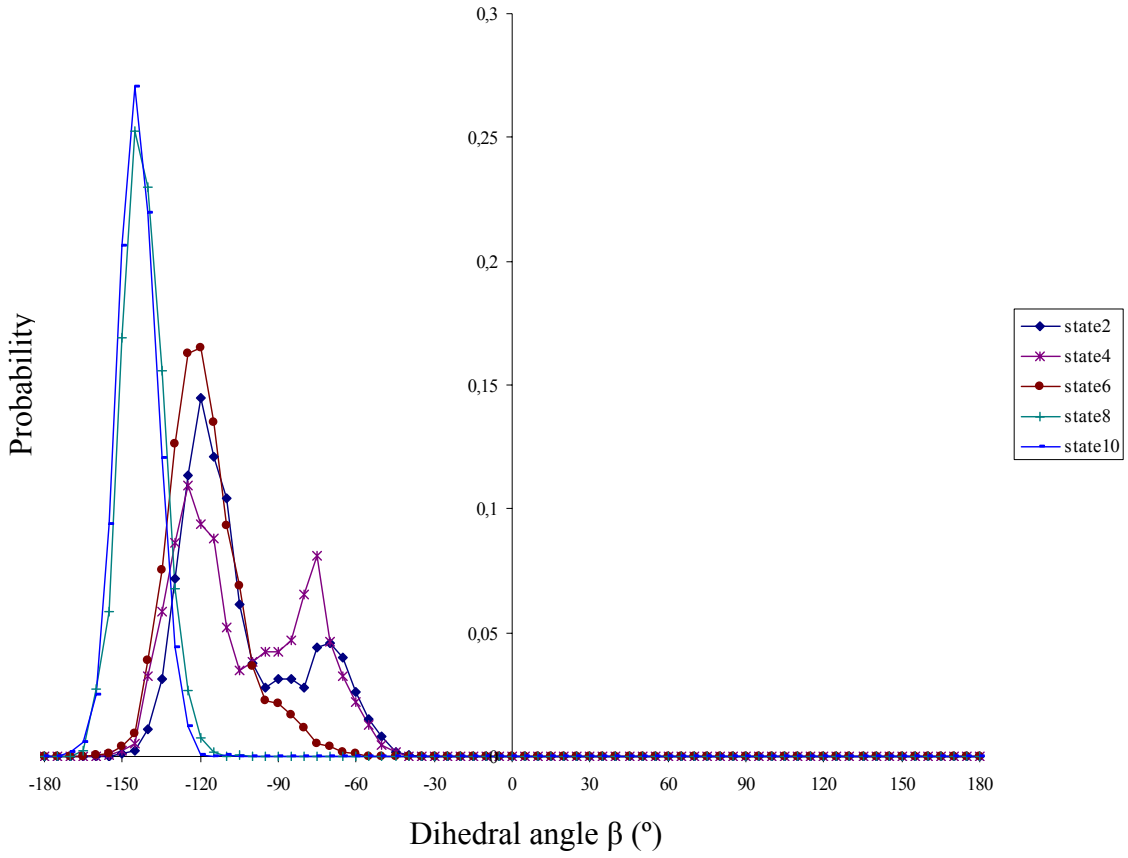

Scheme 5-10.- Normalized probability of dihedral angle β for even states .

In this case, β has values around -75º and -120º (the station V2 is not reduced). However, for states 8 and 10, β is around -145º.

5.3.3.3 Dihedral angle γ

In Scheme 5-11, the normalized probability for the γ dihedral angle of odd states is represented(states which contain the crown on V1).

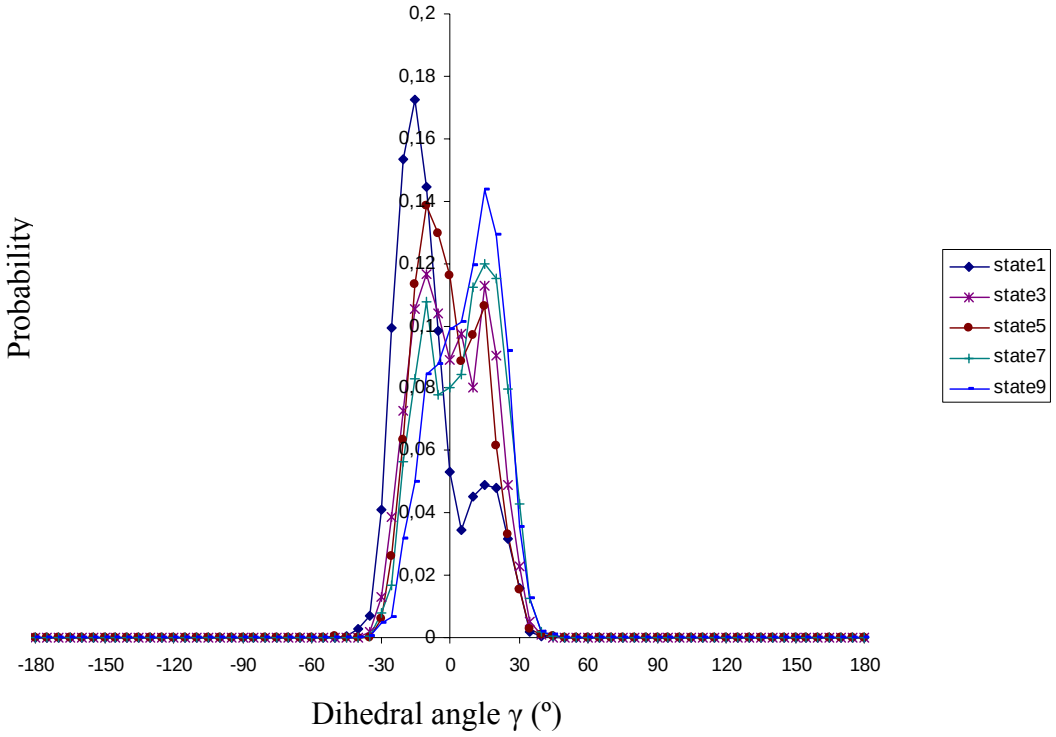

Scheme 5-11.- Normalized probability of dihedral angle γ for odd states.

It was found that the probability of having more structures with γ values around 0º is higher in the reduced states than in the state1. The states which have the station V1 doubly reduced (states 5 and 9) present more structures with γ around 0º. The values for which the probability is maximum are when γ is close ±15º.

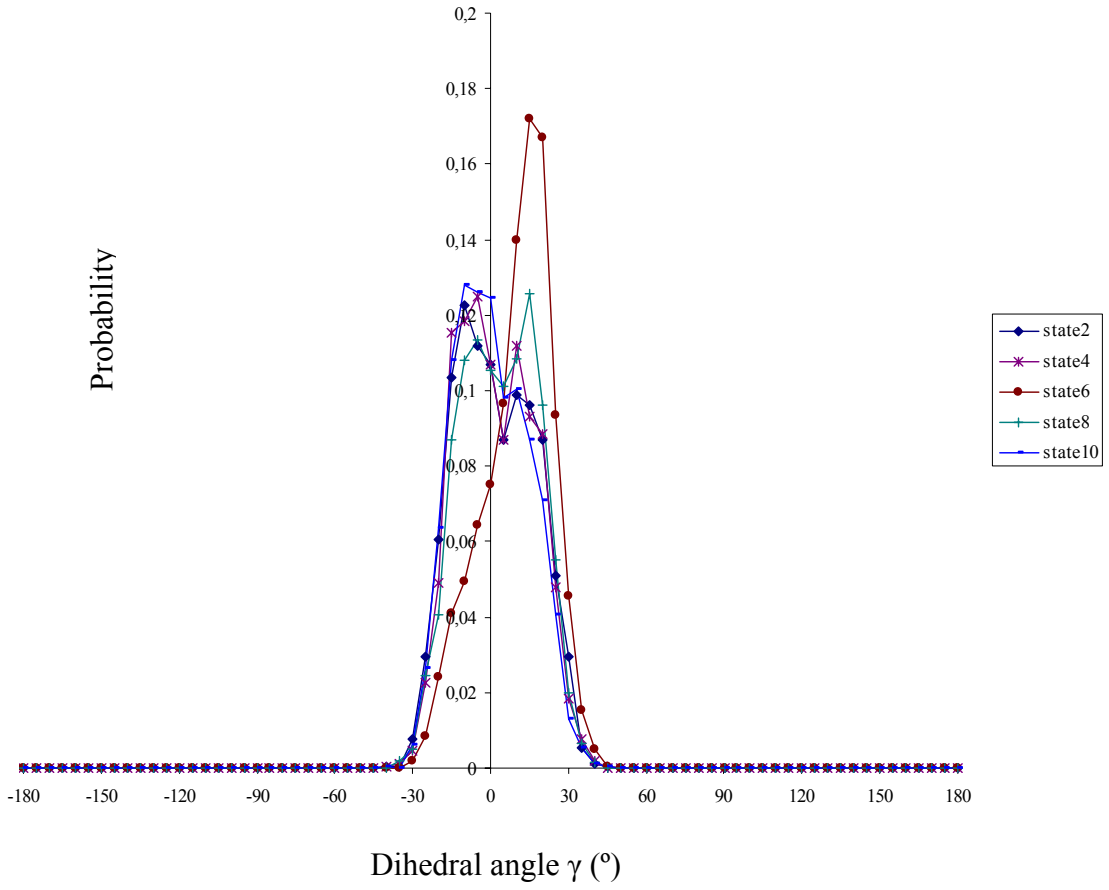

Scheme 5-12.- Normalized probability of the dihedral γ for even states.

When crown is located on the second viologen (V2), the values of γ are around 0º (Scheme 5-12). The maxima of the curves corresponding to each state are close to ±15º. These results for γ in this case are similar to those obtained when crown is on the first station (V1).

5.3.3.4 Dihedral angle ε

Dihedral angle ε was monitored and its normalized probability for states which contain the crown on V1 is given.

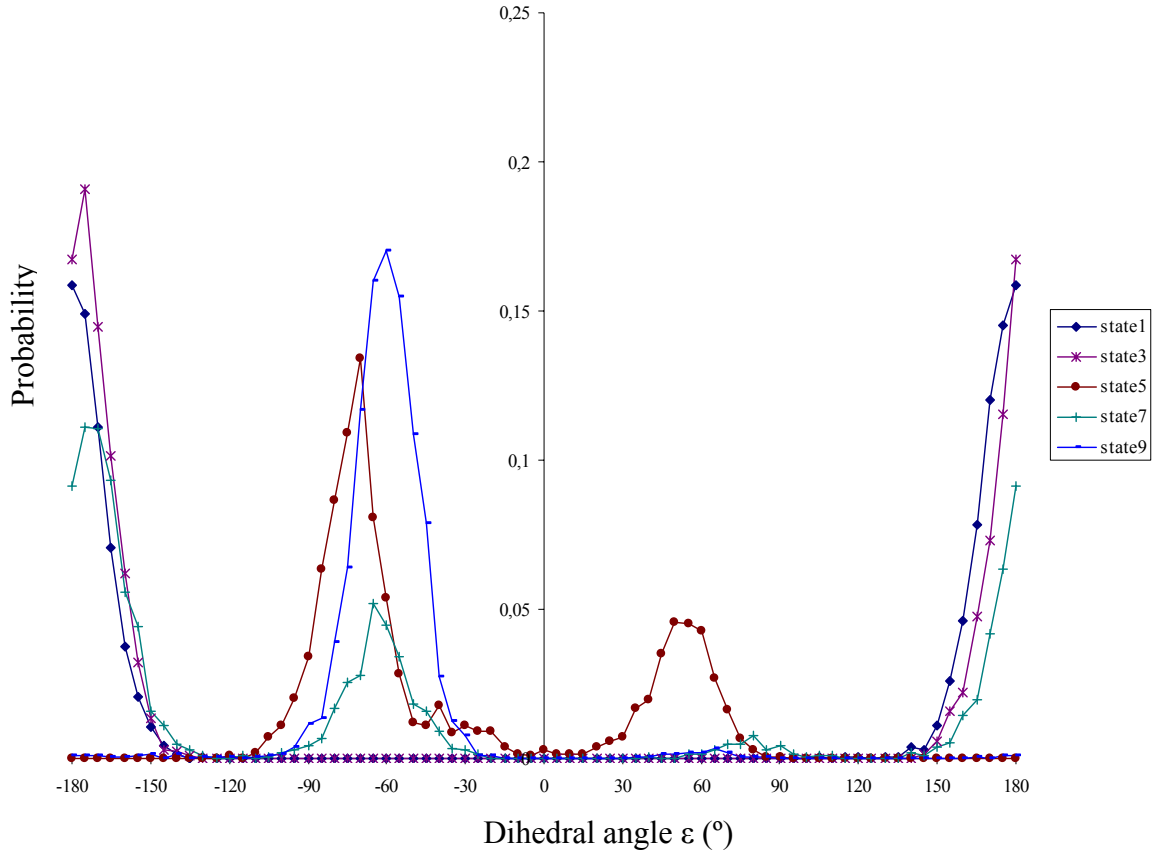

Scheme 5-13.- Normalized probability of dihedral angle ε for states whose crown ether is located on the viologen V1.

It is observed that dihedral ε goes around 180º for the states where V1 is not doubly reduced (linear structure). In the case of state 7 (rotaxane with both stations singly reduced), it presents an important percentage (27 %) of structures with the dihedral ε around -65 º. On the other hand, the two states with viologen V1 doubly reduced (state 5 and state 8) do not present dihedral ε values close to 180º. The state 5 (rotaxane with double reduction on V1) has ε values around -75º (72% of structures) and 60º (28 % of structures). For state 9, ε is close to -60º almost in all structures.

In the following, the normalized probability of the dihedral ε for even states is given (states which contain the crown on V2).

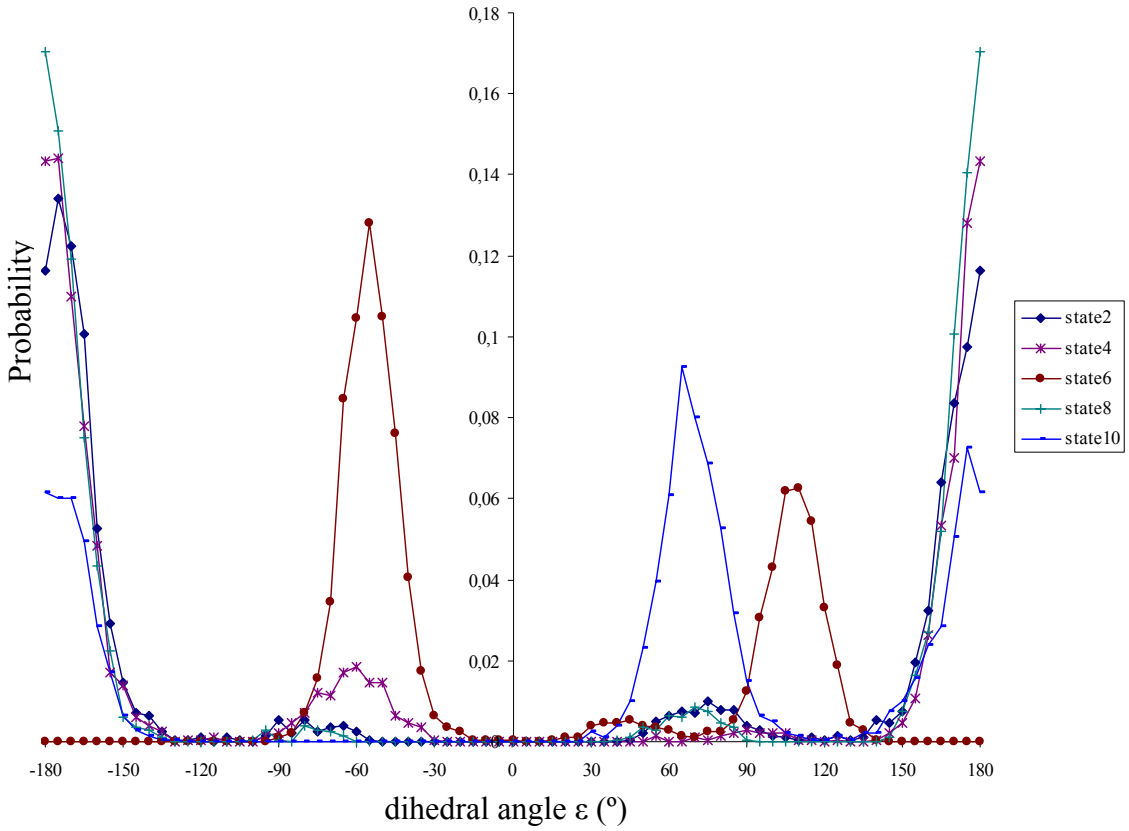

Scheme 5-14.- Normalized probability of the values of dihedral ε for even states.

Scheme 5-14 clearly shows that for states 2, 4 and 8 (rotaxanes which do not contain the station V1 doubly reduced), the values of ε are preferentially around 180º (linear structure). For state 2, 7 % of the structures are with a dihedral ε 75º. Moreover, for state 4, 12 % of the structures have a dihedral ε of -60º and for state 8, ε is around 75º for 5% of the structures. These results indicate a high flexibility of the axle which adopts preferentially a linear structure.

For state 6 (rotaxane with double reduction of V1), the dihedral ε presents differents values: 63% of the structures have ε value of -60º, 33%-110º, and 4%-45º (partially folded structures).

Finally, for state 10, we estimated that 50% of the structures have ε angle of 180º, and 50% have an angle of 65º.

5.3.3.5 Distance I

In the following scheme, the normalized probability for the distance I of odd states is given(states which contain the crown on V1).

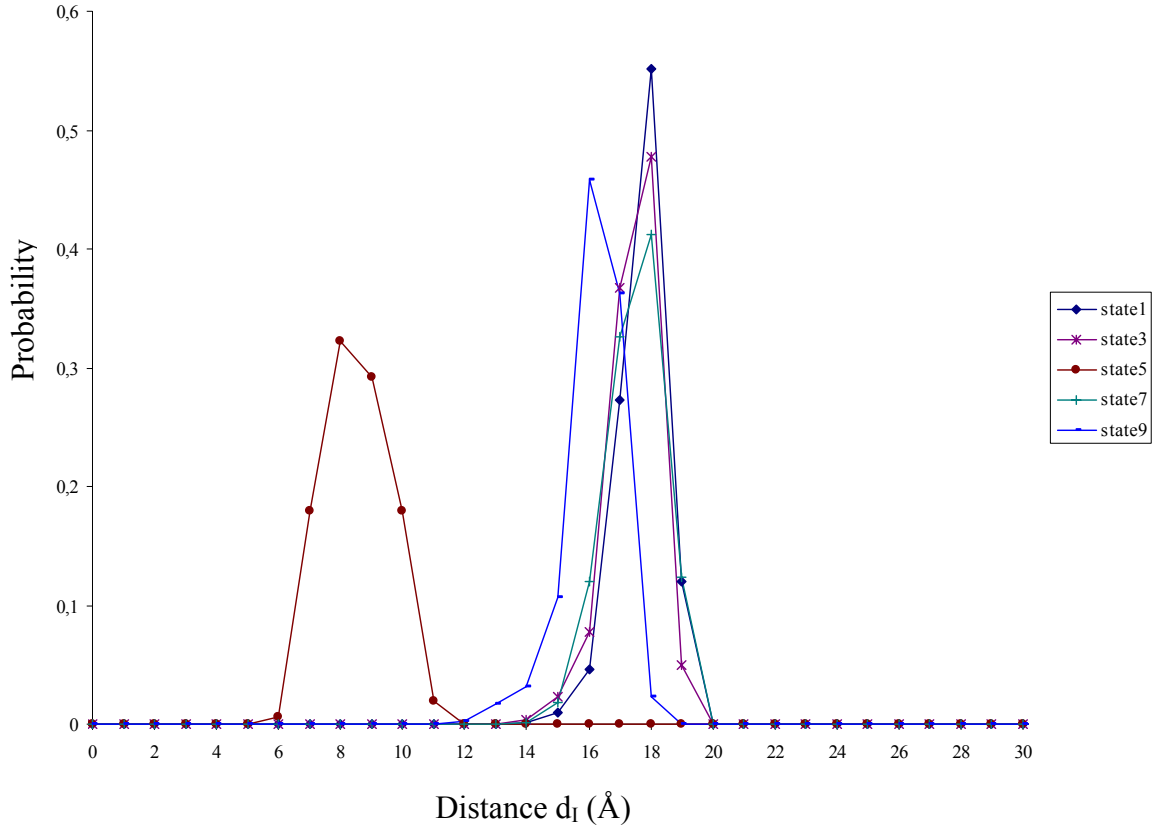

Scheme 5-15.- Normalized probability of distance d_I for states where the crown ether is on the station V1.

Distance I is around 18 Å for states with viologen V1 not doubly reduced. However, for state 5, that distance drops to 8 Å. In the case of state 9, distance d_I is around 16 Å. These results indicate that the rotaxane adopts a linear conformation except in case of having only the station V1 doubly reduced, where the rotaxane is partially folded.

Finally, in Scheme 5-16, the normalized probability of the distance I for even states is given (states which contain the crown on V2).

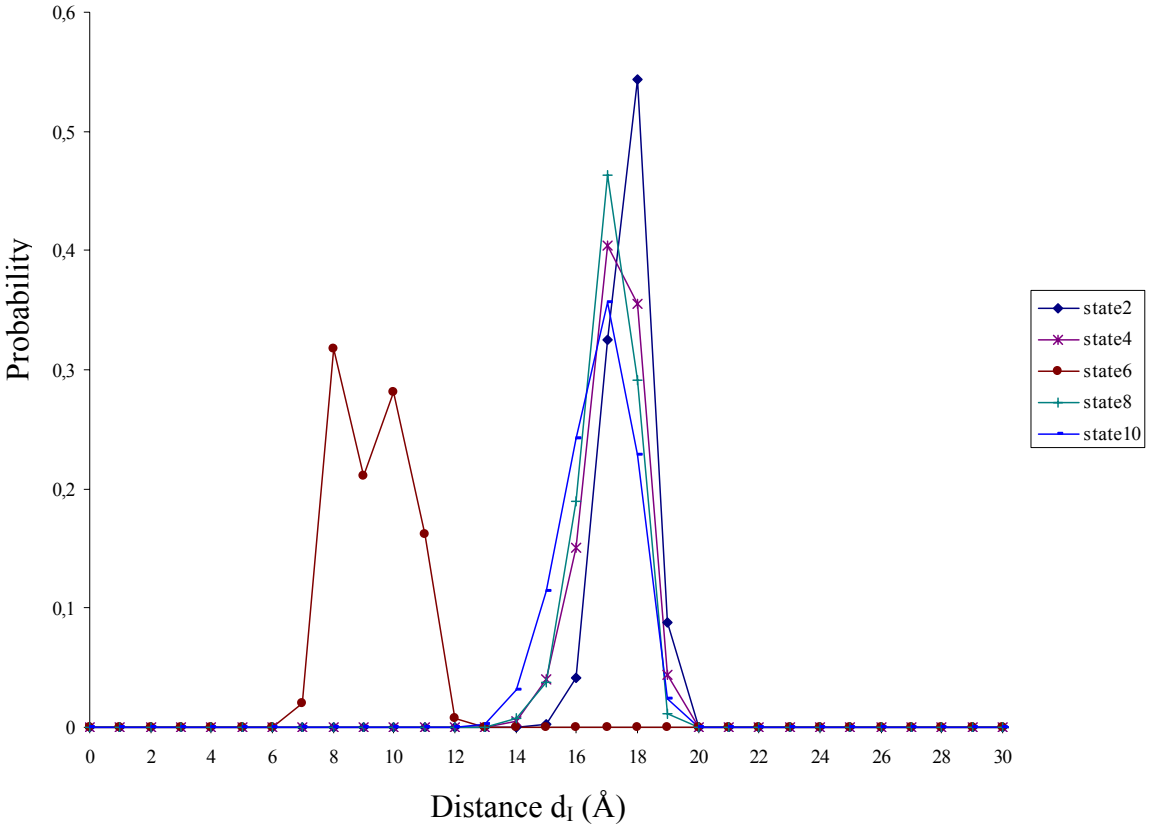

Scheme 5-16.- Normalized representation of distance d_I for even states.

In this last representation, it is observed that for state 2, distance d_I is around 18 Å and for states 4, 6, 8 and 10, d_I is a bit shorter (around 17 Å). In all these cases, the axle remains unfolded. However, that distance decreases for state 6 and fluctuates around 8-10 Å which means that the rotaxane adopts a partially folded conformation (in agreement with the dihedral angle ε analysis).

The data taken from each histogram were analysed in order to search for the most representative structures of each state.

Scheme 5-17 displays the main conformation of the rotaxane when no stations are reduced (parent states).

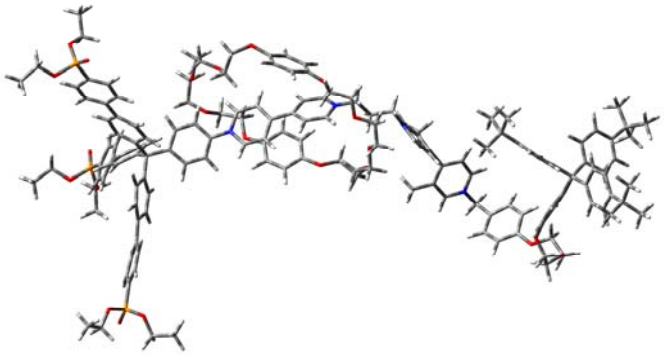

state 1

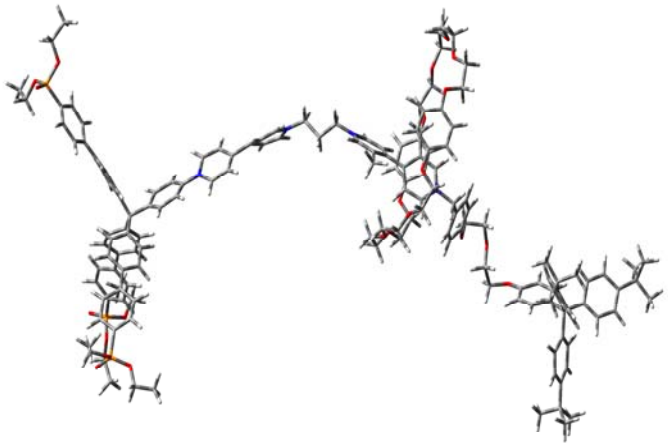

state 2

Scheme 5-17.-Structure of the parent states of the rotaxane

The rotaxane adopts a linear conformation which is preserved irrespective of the position of the macrocycle ($\varepsilon \approx 180^{o}$ and $d_I \approx 18$Å in both states).

Rotaxane remains unfolded after singly reducing selectively V1, such as shown in Scheme 5-18:

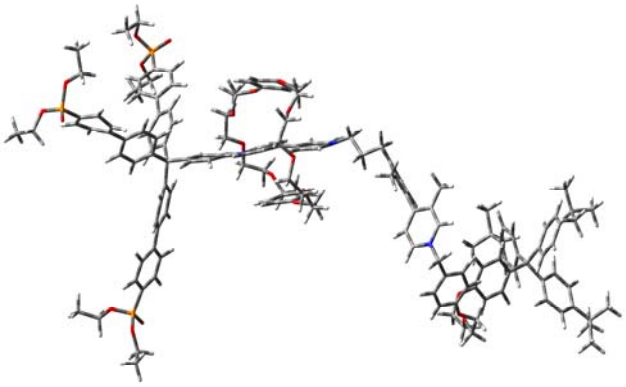

state 3

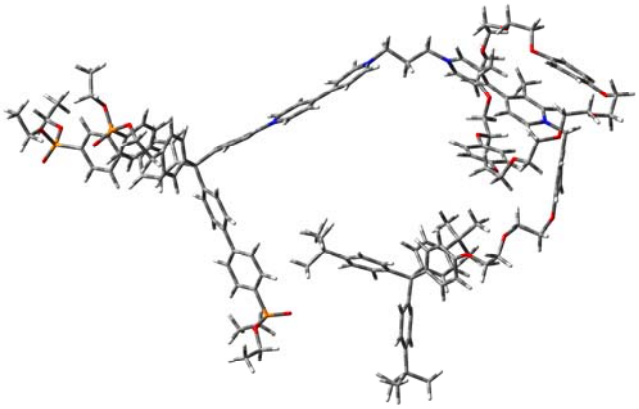

State 4

Scheme 5-18.- Structure of the singly reduced states of the rotaxane.

Angle ε and distance d_I get values 180º and 18 Å, respectively, when the crown is on V1. Distance d_I decreases 1 Å when the macrocycle is switched from V1 to V2. Viologen V1 becomes flat (α≈0º) when it is singly reduced.

The axle becomes partially folded when viologen V1 is doubly reduced and V2 remains doubly charged. The most representative structures for the states 5 and 6 are shown in the following scheme:

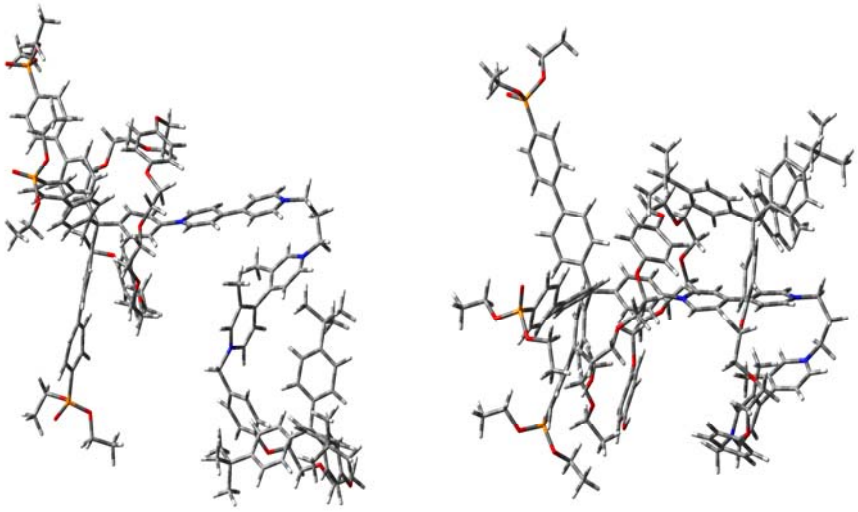

(72%) (28%)

state 5

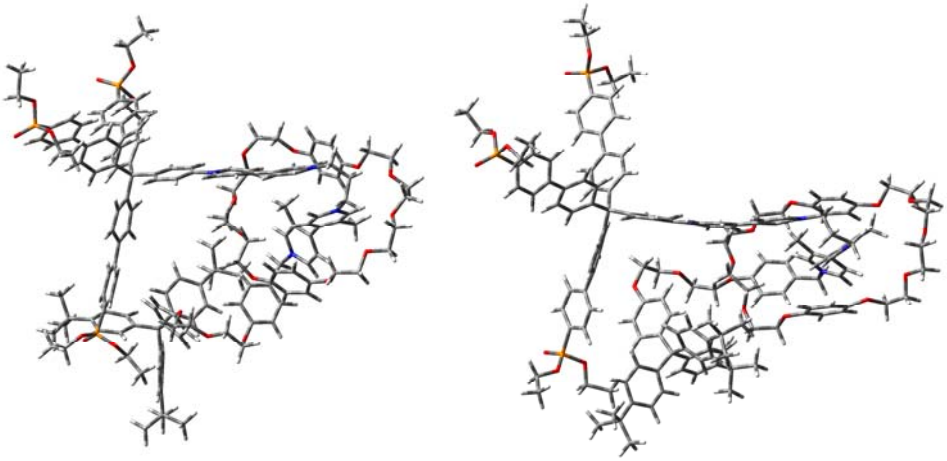

(63%) (33%)

state 6

Scheme 5-19.- Structrures of the states which contain the viologen V1 doubly reduced.

Most of the structures (72%) in state 5 have ε values of -75º and the other 28% of the structures have ε of 60º. In both cases, d_I, α and β fluctuate around 8 Å, 0º and -110º, respectively.

The translational isomer for state 5 (state 6) presents two representative conformations. The most important conformation (63 % structures) has ε values around

-60º and d_I similar to the structures of state 5. However, ε gets values of 110º and the distance d_I increases up to 10 Å for the second more representative conformation (33 % of the structures).

In the case of singly reducing both stations, the axle remains unfolded (Scheme 5-20).

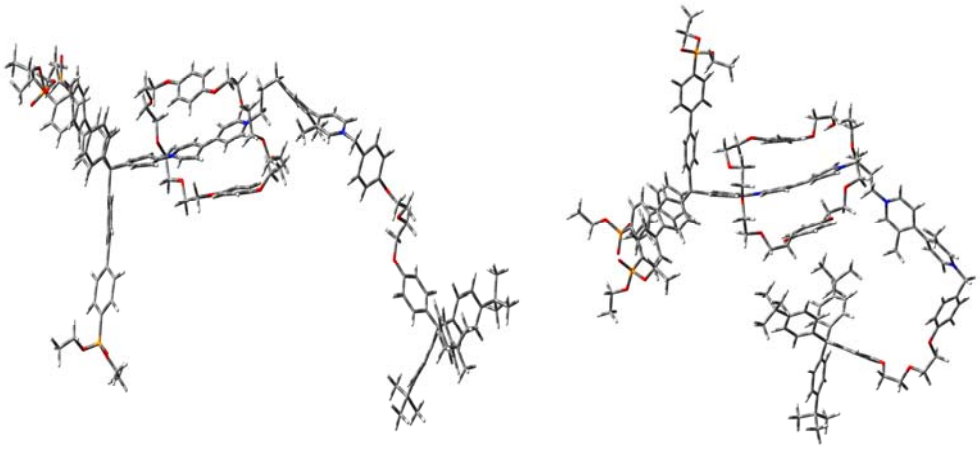

(73%) (27%)

state 7

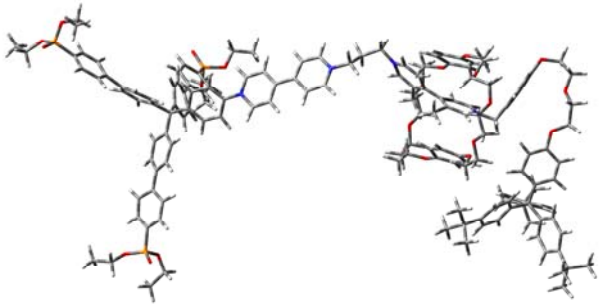

state 8

Scheme 5-20.- Structures of the states which contain both stations singly reduced.

The rotaxane with the crown located on the first station (V1) have values of α, β and d_I around 0º, -140º and 18 Å, respectively. The 73% of the structures present a straight dihedral angle ε. However, the other 27% of the structures contain values of ε around -65º. With respect to state 8, d_I is 1 Å shorter (17 Å) and ε is 180º. Dihedral angle β becomes flatter (β around -145º) when V2 is singly reduced.

The most representative structures for the rotaxane when it is triply reduced are shown in the following scheme:

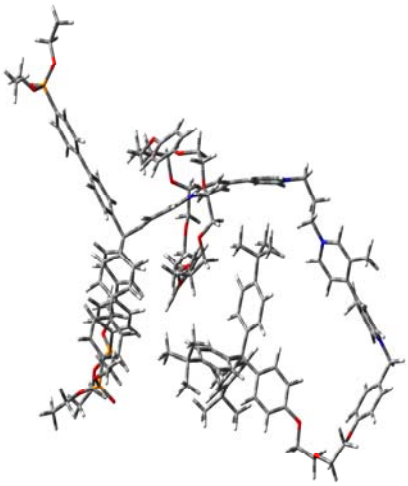

state 9

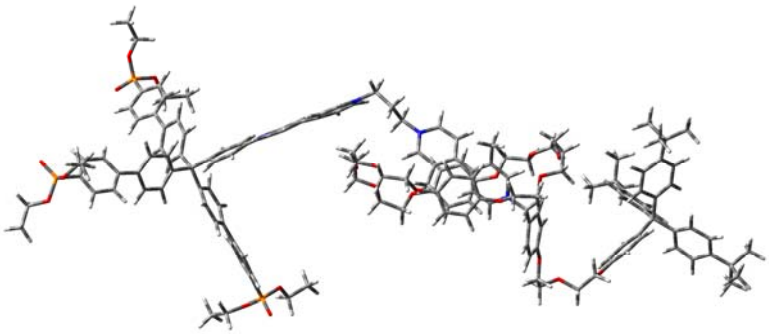

(50%)

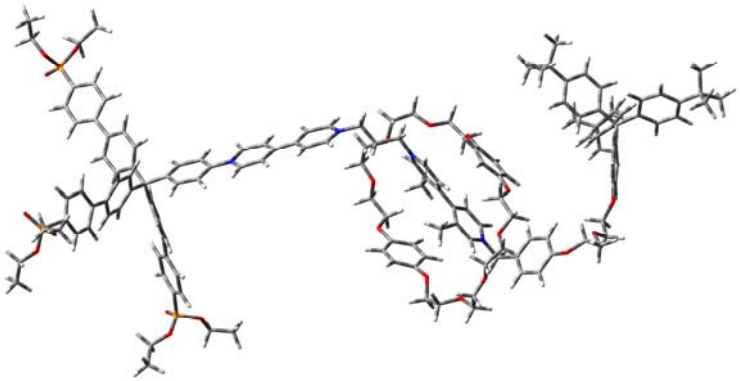

(50%)

state 10

Scheme 5-21.- Structure of the triply reduced states.

Scheme 5-21 shows that the rotaxane after triple reduction (V1 doubly reduced and V2 singly reduced) contains the axle unfolded. The state 9 has an ε value of -60º and the distance d_I is 16 Å. However, distance d_I is 1 Å larger in state 10. Moreover, two values of dihedral angle ε (65 and 175º) are observed when the crown is located on the second viologen (state 10).

It can be concluded from the analysis of the structural data related to the different states of the rotaxane that two main forms are present in the reduction process. One of these conformations has the extrems of the stations very far (d_I fluctuates from 16 to 18 Å), whereas in the other case, the conformation contains the two stations almost parallel – the ε value is small and the distance d_I is very short (8-10 Å).

5.3.4 Conclusions

In view of the results from the energy and the structural studies, the conformation of the rotaxane after each reduction step can be represented in the following way (Scheme 5-22):

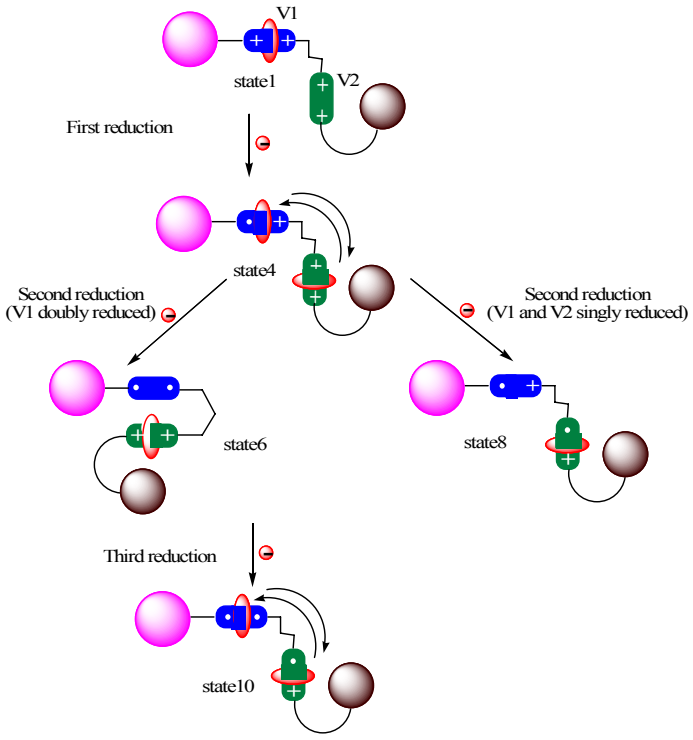

Scheme 5-22.- Representation of the different reduction steps of the rotaxane.

The rotaxane contains the crown preferentially on the first station V1 and its structure is not folded, such as it is observed experimentally.

After the first reduction, the rotaxane remains unfolded and the shuttling process from V1 to V2 can occur. However, after the single reduction of the viologen V1, the crown can be located on V1 as well. This result is in agreement with the experimental data obtained recently. [47]

When station V1 is doubly reduced, our results indicate that the rotaxane is folded and the crown is located preferentially on the second station V2. In the case of a single reduction of both stations, the structure of the rotaxane remains unfolded; however, the macrocycle moves to the second station V2. Experimentally, it is shown that V1 and V2 are singly reduced and that the rotaxane is folded. Moreover, shuttling process from V1 to V2 does not occur.

Finally, after the third reduction, the theoretical results show that the crown can be found on both stations and the rotaxane is not folded. However, it is experimentally observed that the macrocycle is located preferentially on the station V2 and the structure of the rotaxane is folded.

[47] Nikitin, K.; Lestini, E.; Stolarczyk, J. K.; Müller-Bunz, H.; Fitzmaurice, D. *Chem. Eur. J.* DOI: 10.1002/chem.200701384.

CONCLUSIONS

'There is light
at the end
of the tunnel.'

Irish proverb

6 CONCLUSIONS

The key conclusions that emerge from the work presented in this thesis can be summarised as follows:

Firstly, different pseudorotaxanes synthesized have been modelled and studied using molecular dynamics. One of the conclusions of this work is that the complexation with crown depends on the type of viologen and it becomes more unfavorable when reducing the viologen. Moreover, the complexation is more favorable with the ETH viologen or with its singly reduced state (CRE viologen) than with the DIM viologen. However, complexation is less favorable with the NET viologen (ETH doubly reduced) than with DIM or with its singly reduced form (CRD). All these conclusions are in agreement with the experimental data.

These pseudorotaxanes have been used as simpler systems to approach the modelling a [2]rotaxane. The [2]rotaxane was studied using molecular dynamics and FEP calculations in order to predict energy differences and conformational changes in a shuttling process under reduction. An important conclusion is that the crown is located preferentially on the V1 station (viologen analogous to ETH) in the parent state and that the rotaxane structure is not folded, which is in agreement with the experimental data. Moreover, shuttling phenomenon and conformational changes have been shown to be possible by reducing the stations. In case of singly reducing the V1 station, crown can be located on both stations because reduction process with translation and without shuttling is both favorable and, moreover, the rotaxane remains unfolded. The same results have been observed experimentally. In the case of reducing the station V1 doubly, crown is preferentially located on V2 station and the axle of the rotaxane becomes folded. If both stations are singly reduced, shuttling process from V1 to V2 occurs but the axle remains unfolded. Experimentally, V1 and V2 are singly reduced and it is observed that crown is preferentially on V2 station. In this case, an important conformational change occurs and the axle becomes folded. Finally, after reducing doubly the V1 station and singly the V2 station, the macrocycle can be found on both stations and unfolded structure is retained. However, the experimental results show that crown is located preferentially on the station V2 and the axle of the rotaxane is folded.

With respect to the software used, it is concluded that AMBER is very useful for our goals. However, there are some modules that should be improved, as for example RESP. The atomic charge calculation using RESP has been checked and it has been demonstrated that the derivation of atomic charges by taking into account different conformations is not very well optimised.

To sum up, pseudorotaxanes have been used as an approach for modelling and understanding a [2]rotaxane and that approach can be an useful way to model other pseudorotaxanes and to use them in the design of new [2]rotaxanes.

METHODOLOGY

'May your blessings
outnumber
the shamrocks
that grow,
and may trouble
avoid you
wherever you go.'

Irish blessing

7 INTRODUCTION TO METHODOLOGY

7.1 COMPUTATIONAL METHODS

There are four kinds of calculation methods that are very used in computational chemistry: *ab initio* methods, methods that are based in Density Function Theory (DFT) [48], semiempirical methods, and the empirical or molecular mechanics methods. [49] The first three groups are based in quantum mechanics; meanwhile, last group is based in classical mechanics.

Nowadays, there are programs that contain different methodologies, for example, those called QM/MM, a hybrid method that uses quantum chemistry to study the reactive zone, or that zone that contains important electronic effects, and molecular mechanics to study the rest of the system.

7.1.1 *Ab initio* methods

Those methods consider the nucleus and the electrons of the system and solve the Schrödinger equation (Equation 7-1) using the Born-Oppenheimer approach (see Equation 7-2).

$$\hat{H}\Psi = E\Psi$$

Equation 7-1

$$\hat{H} = \hat{T}_n + \hat{T}_e + \hat{V}_{nn} + \hat{V}_{ne} + \hat{V}_{ee}$$

Equation 7-2

[48] Levine, I.N., *Química Cuántica*. Editorial AC: Madrid, **1977**.

[49] Leach, A.R., *Molecular Modelling: Principles and applications.* Pearson: Harlow, **2002**.

Using these methods, some useful and exact information about reactivity and geometry of the molecules studied can be obtained. The main disadvantage of *ab initio* methods is the high computational cost, which produces this kind of methods be used in problems where only a few dozens of heavy atoms are treated.

7.1.2 Methods based in Density Functional Theory (DFT)

According to the Hohenberg-Kohn theorem, the energy of the fundamental electronic state of one system can be calculated if the electronic density $\rho(r)$ is known. So, the energy is a function of electronic density.

The difference with other Quantum Methods is that DFT-based methods introduce electronic correlation spending less computational time. Nevertheless, these methods cannot be used in macromolecules because the computational time is still very important. Moreover, the reliability of these methods is low because the shape of the functional is unknown and we must model it.

7.1.3 Semiempirical Methods

Methods also based in Quantum Mechanics. The main difference with the *ab initio* methods is that some integrals are not computed to reduce the computational time. The error introduced is balanced adding a few number of empirical parameters. The information obtained with these methods is similar to that obtained using *ab initio* methods, but much less reliable. Those methods can already treat problems of systems with a few hundreds of heavy atoms.

7.1.4 Empirical or molecular mechanics methods

Many problems that we would like to treat with molecular modelling are just too big to be considered for Quantum Mechanics methods. The Quantum Mechanics takes

into account the electrons of the system, and even although some electrons are ignored (like in semiempirical methods) a high number of particles and the calculations require long computational time.

The empirical or molecular mechanics methods are used to treat a high number of atoms, and these methods have been chosen to do this research work. In some cases, the molecular mechanics methods give as good answers as the highest levels of Quantum Mechanics in only a fraction of computational time. We have to take into account that molecular mechanics cannot provide us with properties that depend of electronic distribution of a molecule. Molecular mechanics, thanks to Bohr-Oppenheimer approximation, can describe the energy of a molecule as a function of the nuclear coordinates.

Molecular mechanics is based in a mechanical model. It is considered that the atoms are mass of certain size and hardness (deformability), and the bonds are springs of different force that unite those mass (see Scheme 7-1 and Equation 7-3).

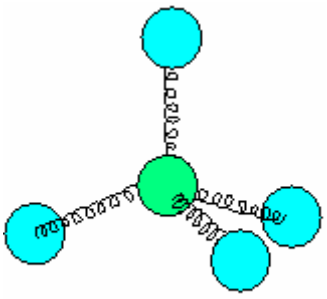

Scheme 7-1.- Schematic representation of methane in molecular mechanics.

$$F_{r_i} = m_i \frac{\partial^2 r_i}{\partial^2 t}$$

Equation 7-3.- Equation of the second law of Newton, basis of classical mechanics. It describes the movement of a mass particle m_i along the coordinate r_i, with a aplicated F_{r_i} on the particle in this direction.

The obtained energies are relative to an ideal situation, where all distances and angles coincide with the parameterized values, each deviation from this ideal situation produces an increase in Energy.

7.1.4.1 Force Field

The set of equations and parameters with which the energy will be calculated compose the Force Field. The energy of a system is the sum of a number of energetic terms between which the following ones can be found (see Equation 7-4):

Stretching (E_s)	Van der Waals interaccions (E_{vdw})
Bending (E_b)	Hydrogen bond (E_H)
Torsions (E_t)	Cross terms (E_{tc})
Electrostatic interactions (E_e)	Solvation (E_{solv})

$$E = E_s + E_b + E_t + E_e + E_{vdw} + E_H + E_{tc} + E_{solv}$$

Equation 7-4

We can find a great variety of force fields to treate different systems, as examples:[50]

MM2[51], MM3[52], MM4[53]: organic molecules.

[50] Names for set of parameters are in brackets.

[51] Allinger, N.L., *J. Am. Chem. Soc.* **1977**, *99(25)*, 8127.

[52] Allinger, N.L.; Yuh, Y.H.; Lii, J-H. *J. Am. Chem. Soc*. **1989**, *111(23)*, 8551.

[53] a) Allinger, N. L.; Chen, K.; Lii, J-H. *J. Comp. Chem.* **1996**, *5 & 6*, 642. b) Nevins, N.; Chen, K.; Allinger, N. L. *J. Comp. Chem*. **1996,** *5 &6*, 669. c) Nevins, N.; Lii, J-H, Allinger, N-L. *J. Comp. Chem.* **1996**, *5 & 6*, 695. d) Nevins, N.; Allinger, N. L. *J. Comp. Chem*. **1996,** *5 &6*, 730. e) Allinger, N. L.; Chen, K. *J. Comp. Chem*. **1996,** *5 &6*, 747.

amber: proteins and other biomolecules (parm94[54] and parm99[55]),
organic molecules (gaff[56]), glycosides (glycam[57]).

CHARMM[58]: proteins

The parameters of those forces come from experimental values (Vibrational spectroscopy, X Ray diffraction) or values that has obtained by *ab initio* methods.

The transferability of the force field parameters is decisive, because allows that a set of developed and tested parameters in a few number of molecules can be applied in a wide range of problems. Moreover, the developed parameters starting from the data of small molecules can be used to study molecules with much larger number of atoms. [59]

In this study, the AMBER force field was used with the gaff parameters implemented inside of the AMBER 7.0 version of the program.

7.2 METHODOLOGIES IN MOLECULAR MECHANICS

Some of the methodologies based in molecular mechanics (most of them have been used in this thesis) are as follows: minimisation methods, molecular dynamics, Monte Carlo methods and free energy perturbation methods.

[54] Cornell, W. D.; Cieplak, P.; Bayly, C. I.; Gould, I. R.; Merz, K. M.; Ferguson, D. M.; Spellmeyer, D. C.; Fox, T.; Caldwell, J. W.; Kollman, P. A. *J. Am. Chem. Soc*. **1995**, *117*, 5179.

[55] Wang, J.; Cieplak, C.; Kollman, P. A. *J. Comp. Chem*. **2000**, *21*, 1049.

[56] Wang, J.; Wolf, R. M.; Caldwell, J. W.; Kollman, P. A.; Case, D. A. *J. Comp. Chem*. **2004**, *25(9)*, 1157.

[57] Woods, R. J.; Dwek, R. A.; Edge, C. J.; Fraser-Reid, B. *J. Phys. Chem*. **1995**, *99(11)*, 3823.

[58] Brooks, B.R.; Bruccoleri, R.E.; Olasfon, B.D.; States, D.J.; Swaminathan, S.; Karplus, M., *J. Comput. Chem.* **1983**, *4(2)*, 217.

[59] Ivanov, P., *Lecture Notes in Molecular Mechanics*. Universitat Autònoma de Barcelona: Barcelona **1996**.

7.2.1 Minimisation methods

As starting point, a known structure with an initial conformation obtained experimentally (X-ray, NMR) is used. Alternatively a modelling program is used and an iterative mathematic method is applied until the energy minimum closest to initial coordinates is found.

There are many methods, but all of them are applied over the potential hypersurface generated by the force field equations. The main problems of this methodology are: computational time, time step and the convergence criteria, the convergence speed, and strength of the method and the possibility to arrive at a relative minimum of the system. To correct these problems and better explore the conformational space other methodologies exists as for example: Molecular dynamics and Monte Carlo methods.

In this thesis, all the systems were minimised before running a molecular dynamics simulation using the Newton-Raphson method.[60]

7.2.2 Molecular Dynamics

The molecular dynamics simulates the movement of a molecule at a fixed temperature. Kinetic energy is given to the system using a thermostatic bath, and it will be used to raise the potential barrier. This energy is distributed in the system as random velocities on the atoms and follows the next equation (see Equation 7-5):

$$E = \left(\frac{3N - 6}{2} \right) k_B T$$

Equation 7-5.- N **is the number of atoms of the system,** T **is the temperature of the system and** k_b **is the Boltzmann constant.**

[60] Leach, A.R., *Molecular Modelling: Principles and applications.* Pearson: Harlow, **2002.**

After supplying initial velocities to atoms and obtaining the forces that act on each atom from the force field, the calculation of the positions of each atom through time is calculated using a classical mechanics equation, the Newton's second law equation (see Equation 7-3). If that equation is integrated, we obtain a trajectory that simulates how the position and velocity vary through time. [61]

To solve the equation systems in problems with a lot of atoms and to obtain the trajectory, methods of finite differences must be used (in molecular mechanics, it is frequently used).

The sampling frequency (the size of Δt used) must be at least one order of magnitude smaller than the highest vibrational frequencies (3000 cm^{-1}, stretching C-H). For this reason, the time step (*ts*) is in the scale of femtoseconds. Depending on the temperature used in the simulation, the molecule will have enough energy to raise the potential energy barriers and it will change its conformation, finding different minima and remaining longer time in the most stable. The time that molecule is in each minimum is equivalent to the number of times that the structure appears through the simulation and follows the Boltzmann equation (see Equation 7-6):

$$\frac{t_i}{t_0} = \frac{N_i}{N_0} = e^{-\frac{\Delta E}{k_B T}}$$

Equation 7-6.- t_i **is the time that the molecule remains in a conformation** i**.** t_0 **is the time that the molecule is in the most stable conformation.**

The main limitation of Molecular Dynamics is the high computational cost per unit of simulation time (10^6 calculations of the positions of all the atoms are necessary for only one nanosecond of simulation, assuming that the time step (*ts)* is one

[61] Peña, M.D., *Termodinámica Estadística*. Editorial Alambra: Madrid, 1979.

femtosecond). Shorter simulations are easier and faster. However, the system could not be equilibrated, therefore, the molecule will not explore all the conformational space (it could be that we do not find the absolute minimum or other local minima).

The main advantage of Molecular Dynamics from Molecular Mechanics is the independence of the results from the starting structure. Giving energy to the system and with enough time, it is possibly to overcome the low potential barriers and, therefore, to explore better the potential hypersurface.

A Molecular Dynamics simulation can be divided in three steps (see Scheme 7-2):

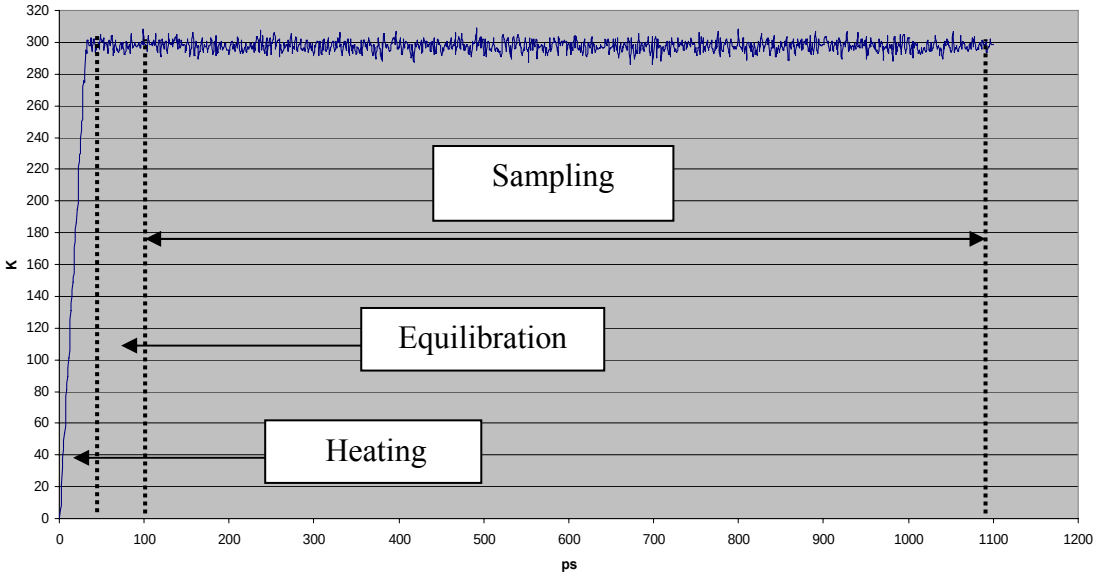

Scheme 7-2.- Typical representation of the temperature along time in a Molecular Dynamics simulation. The three typical steps of a Molecular Dynamics are shown.

Heating of the system: The system is heated from 1 K to the desired temperature. The heating is done at constant volume conditions. In this thesis, all the systems were heated from 1 K to 298 K during 70 ps and then the conditions are kept during 30 ps to get a better system equilibration.

Equilibration: First, the system is equilibrated at constant volume; later on, it is equilibrated at constant pressure. At the end of this step, the density and the

temperature should be constant. In our case, 100 ps were spent to equilibrate each system. Depending on the sytem studied, this time will be increased to have the system properly equilibrated.

Sampling: This is the most important step and it will be used to analyse the energy, geometric parameters, ... This step is done at constant pressure and temperature. All the molecular dynamics simulations related to pseudorotaxanes were run using a sampling step of 1ns. However, for the studies related to the rotaxane the sampling step was increased to 2 ns.

7.2.3 Monte Carlo Methods

The Monte Carlo method is a conformational searching method of one given system that randomly generates a large number of structures from a given structure by modifying different structural parameters.

One of the advantages of Monte Carlo methods in comparison with molecular dynamics is that in less simulation time we can obtain a better exploration of the conformational space. Obtaining the new structures is easier and faster because we do not need to integrate the Force Field equations.

Unlike Monte Carlo method, the Metropolis Monte Carlo method can rationalize the number of structures and store them using a selection criterion. Using this method, we can ensure a good scan of the conformational space, it spends less computational time and the set of stored structures follow a Maxwell- Boltzmann distribution.

7.2.4 Free Energy Perturbation methods

The free energy is often considered to be the most important quantity in thermodynamics. Unfortunately, the free energy is a difficult quantity to obtain for systems such as liquids or flexible macromolecules that have many minimum energy

configurations separated by low-energy barriers. Associated quantities such as the entropy and the chemical potential are also difficult to calculate. The free energy cannot be accurately determined from a "standard" molecular dynamics or Monte Carlo simulation, because such simulations do not adequately sample from those regions of phase space that make important contributions to the free energy. Simulation using either Monte Carlo or molecular dynamics sampling seeks out the lower-energy regions of phase space. Such simulations will never adequately sample the important high-energy regions and so to calculate the free energy using a conventional simulation will lead to poorly converged and inaccurate values.

Due to all these problems, three methods for computing free energy differences have been developed: free energy perturbation window growth, thermodynamic integration and slow growth.

7.2.4.1 Free energy perturbation (FEP) window growth

Free energy perturbation (FEP) theory, introduced by R.W. Zwanzig in 1954, is a method based on statistical mechanics that is used in computational chemistry for computing free energy differences from molecular dynamics or Metropolis Monte Carlo simulations. [62]

According to FEP theory, the free energy difference between two states A and B is expressed by the following equation, known as the Zwanzig eaquation (Equation 7-7):

$$\Delta G = G_B - G_A = -RT \ln \left\langle e^{-\left(\frac{V_B - V_A}{RT}\right)} \right\rangle_A$$

Equation 7-7

[62] Zwanzig, R. W. J. *Chem. Phys*. **1954**, *22*, 1420.

where R is the universal gas constant, T is the temperature, and the triangular brackets denote an average over a simulation run for state A. State B should not be too different from state A, so that the differences between the two states may be considered as a perturbation. These differences may also be in the atom types involved (in this case, the ΔG obtained is for transforming one molecule onto another) or it may be a difference of geometry. Note we use the potential energy V_x in place of the more general Hamiltonian H(x, p), considering that the momentum contribution to the free energy difference is zero.

FEP calculations only converge properly when the difference between the two states is small enough. Therefore it is usually needed to divide a perturbation into a series of smaller "windows", which are computed independently.

In AMBER, the free energy is calculated using FEP theory at discrete and uniformly spaced intervals of using the following equations (Equation 7-8 and Equation 7-9):

$$G_{\lambda(i+1)} - G_{\lambda(i)} = -RT \ln \left\langle e^{-\frac{(V_{\lambda(i+1)} - V_{\lambda(i)})}{RT}} \right\rangle_{\lambda(i)}$$

Equation 7-8

$$\Delta G = G_1 - G_0 = \sum_{i=1}^{n} (G_{\lambda(i+1)} - G_{\lambda(i)})$$

Equation 7-9

where G_1 and G_0 are the free energies of states 1 (final state) and 0 (initial state), respectively. The relationship between the initial, final and intermediate states is

described in terms of the parameter λ, which changes from 0 to 1. $V_{\lambda(i)}$ is the potential energy function representative of state $\lambda(i)$, and $\langle\ \rangle_{\lambda(i)}$ means the ensemble average of the enclosed quantity, representative of state $\lambda(i)$. The ensemble is evaluated from a molecular dynamics trajectory run with $V = V_{\lambda(i)}$. Numbers of equilibration and data collection steps for each $\lambda(i) \rightarrow \lambda(i+1)$ "window" must be specified.

The FEP equations are exact, and when computer resources are enough to perform sufficient sampling, very accurate results can be obtained. However, some difficulties should take into account when window growth is used. The first problem is that it is not possible to know if we sample to convergence because no reliable test to prove convergence has been developed. Another problem is that the quality of the results depends on the reversibility condition for each one of the transformations done. A way to assure that the perturbations are reversible in each step, is to calculate FEP in two directions [$0 \rightarrow 1$ (forward) and $1 \rightarrow 0$ (reverse)]. If the perturbation is reversible, the free energy difference in both ways should have the same value, but opposite in sign (see Scheme 7-3).

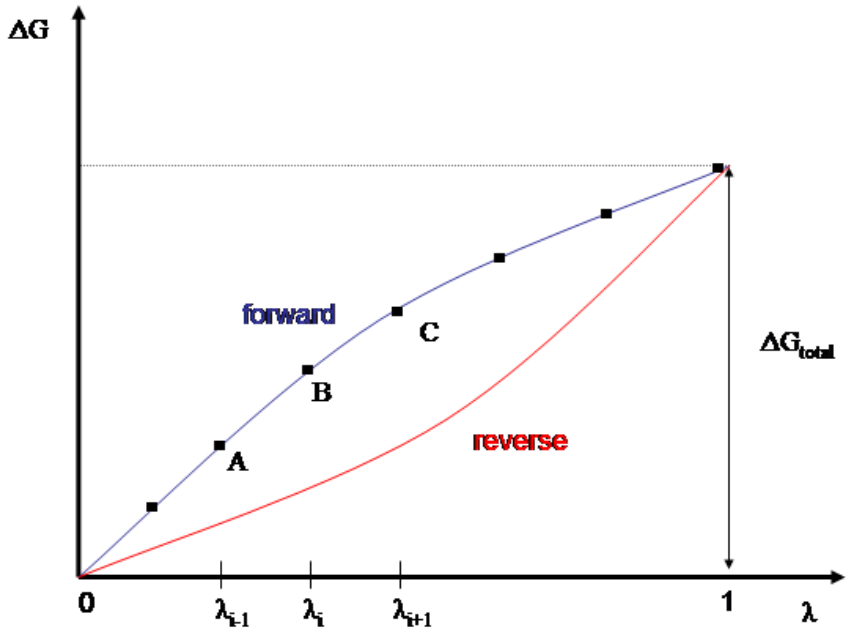

Scheme 7-3

Some uses for the FEP calculations are the followings: pKa predictions, solvent effects on reactions, enzymatic reactions and host-guest binding energetics.

This is the method used in Chapter 5 for calculating free energies. A molecular dynamics simulation of 2 ns was carried out for each system before starting running FEP in gibbs. Each free energy perturbation calculation was divided in 100 windows ($d\lambda$=0.01). Each window had a first equilibration step of 200 ps and then, a sampling step of 300 ps (in total, 50 ns).

7.2.4.2 Termodynamic integration

Another approach to calculate a free energy difference is using thermodynamic integration (TI).[63] This method is based on the integral shown in the Equation 7-10:

$$\Delta G = G_1 - G_0 = \int_0^1 \left\langle \frac{\partial V}{\partial \lambda} \right\rangle_\lambda \partial\lambda$$

Equation 7-10

In AMBER, the integral is approximated by a summation over discrete intervals using the trapezoidal algorithm, as such as the following equation:

$$\Delta G \approx \sum_0^N \left(\left\langle \frac{\partial V}{\partial \lambda} \right\rangle_{\lambda(i+1)} + \left\langle \frac{\partial V}{\partial \lambda} \right\rangle_{\lambda(i)} \right) \left(\frac{\lambda(i+1) - \lambda(i)}{2} \right)$$

Equation 7-11

[63] Chipot, C.; Kollman, P. A.; Pearlman, D. A. *J. Comp. Chem.* **1996**, *17 (9)*, 1112.

TI, such as FEP, is carried out by systematically varying λ from the initial state 0 to the final state 1. At each λ point, system equilibration is performed, followed by data collection to determine the value of the ensemble for the equilibrated system (Scheme 7-4).

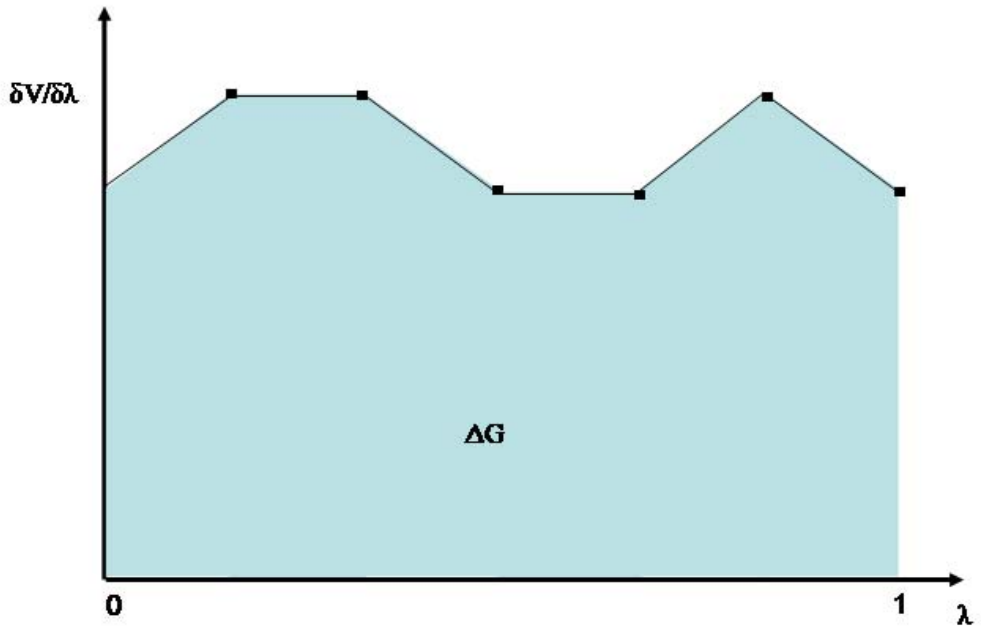

Scheme 7-4

An advantage of TI with respect to the FEP method is that TI avoids the problem in sampling described for FEP. However, TI has its own problem: the driving equation of TI is an integral, which is calculated approximately by evaluating the integrand at finite intervals of λ. In this case, we should need a sufficient finite intervals of lambda to avoid a loss of precision in the integration.

7.2.4.3 Slow growth

Another way to calculate free energy difference from computer simulation is the slow growth method. This method is simply the limiting case of either FEP or TI where the number of λ states is extremely large. Lambda changes slowly enough that it is assumed the system remains in equilibrium at every step. Thus the ensemble average

can be approximated by its instantaneous value (a sample over one step) at each "window". This reduces both equations Equation 7-7 and Equation 7-10 to the following formula (Equation 7-12):

$$\Delta G = \sum_{i=1}^{n} \left(V_{\lambda(i)} - V_{\lambda(i-1)} \right)$$

Equation 7-12

This assertion cannot be rigorously proven, and it can be demonstrated that the configuration will be systematically lag changes in the potential energy function as the simulation progresses. Thus, the validity of this approach has been questioned, although recent work has suggested that the slow growth method may have use in bounding the error on free energy simulations. [64]

7.3 EXPLICIT SOLVATION METHODS

Most of the chemistry processes are carried out in solution. So, it is important to know the function of the solvent and its behaviour around a system.

Acetonitrile is the most common solvent for many [2]pseudorotaxanes and [2]rotaxanes. However, depending on the counterions used, these compounds are better solvated in other solvents. For that reason, one of the purposes of this thesis was to study how these compounds could change their behaviour by modifying the solvent and the counterions.

[64] a) Reddy, M. R.; Erion, M. D. *Free Energy Calculations in Rational Drug Design*. Kluwer Academic/Plenum Publishers: New York, **2001**. b) de Federico de la Rúa, M. *Pseudorotaxanos, catenanos complejos de inclusión con ciclodextrinas: cálculos de energía libre (PhD thesis)*. Universitat Autònoma de Barcelona: Bellaterra, **2006**.

The AMBER program is able to use different solvation methods for solvents (for example, TIP3P and TIP4P for water)[65] with the possibility of generating a box of solvent molecules of different sizes. Knowing that option in AMBER, Xavi Grabuleda developed an explicit solvent method for the acetonitrile during his PhD.[66] Previously, other studies about modelling of liquid acetonitrile existed.[67] However, The Grabuleda's method reproduces better the physical properties of acetonitrile.[68] For that reason, that was the method used in this thesis in the cases where we used acetonitrile as a solvent.[69] Moreover, we also used methanol as a solvent and we used the explicit solvent method developed by J. W. Caldwell. [70]

7.4 AMBER

AMBER (an acronym for Assisted Model Building and Energy Refinement) is a family of force fields for molecular dynamics of biomolecules originally developed by Peter Kollman's group at the University of California in San Francisco. AMBER is also the name for the molecular dynamics simulation package that implements these force fields. It is one of the few programs where the code and force field are separate. Further, the force fields are in the public domain, whereas the codes are distributed under a license agreement.

---

[65] Jorgensen, William L.; Chandrasekhar, Jayaraman; Madura, Jeffry D.; Impey, Roger W.; Klein, Michael L. *J. Chem. Phys*. **1983**, 79(2), 926.

[66] Grabuleda i Salart, X. *Màquines molecular: Estudis teòrics sobre espècies de [2]rotaxans (PhD thesis).* Universitat Autònoma de Barcelona: Barcelona, **2000**.

[67] a) Böhn, H. J.; McDonald, I. R.; Madden, P. A. *Mol. Phys*. **1983**, 49,347. b) Jorgensen, W. L.; Briggs, J. M. Mol. Phys. **1988**, 63, 547. c) Maroncelli, M. *J. Chem. Phys.* **1991**, 94, 2084. d) Troxler, L.; Wipff, G. *J. Am. Chem. Soc.* **1994**, 116, 1468.

[68] Grabuleda, X.; Jaime, C.; Kollman, P. A. *J. Comput. Chem.* **2000**, 21, 901.

[69] Nowadays, an improved acetonitrile model exists whose reference is the following:
Nikitin, A. M.; Lyubartsev, A. P. *J. Comp. Chem*. **2007**, 28, 2020.

[70] Caldwell, J. W.; Kollman, P. A. *J. Phys. Chem*. **1995**, *99*, 6208.

7.4.1 Force Field

The term "AMBER force field" generally refers to the functional form used by the family of AMBER force fields. This form includes a number of parameters; each member of the family of AMBER force fields provides values for these parameters and has its own name, as for example, parm99, gaff (parameter set used in this thesis) and glycam. The basic force field implemented in the AMBER package has the form shown in the Equation 7-13 , which is about the simplest functional form that preserves the essential nature of molecules in condensed phases.[71]

$$U(R) = \sum_{bonds} K_r \left(r - r_{eq}\right)^2 + \sum_{angles} K_\theta \left(\theta - \theta_{eq}\right)^2 + \sum_{dihedrals} \frac{V_n}{2}\left(1 + \cos\left[n\phi - \gamma\right]\right) + \sum_{i<j}^{atoms} \frac{A_{ij}}{R_{ij}^{12}} - \frac{B_{ij}}{R_{ij}^{6}} + \sum_{i<j}^{atoms} \frac{q_i q_j}{\varepsilon R_{ij}}$$

Equation 7-13.- General AMBER equation

7.4.2 Software

AMBER package is composed by many programs which work reasonably well together. The main programs are the following:

sander: Simulated Annealing with NMR-Derived Energy Restraints. This allows for NMR refinement based on NOE-derived distance restraints, torsion angle restraints, and penalty functions based on chemical shifts and NOESY volumes. Sander is also the central simulation program, and is also used for replica-exchange, thermodynamic integration, and potential of mean force (PMF) calculations. Sander also includes QM/MM capability.

[71] Case, D. A.; Pearlman, D. A.; Caldwell, J. W. ; Cheatham III, T. E.; Wang, J.; Ross, W. S.; Simmerling, C.; Darden, T.; Merz, K.M.; Stanton, R.V.; Cheng , A.; Vincent, J. J.; Crowley , M.; Tsui, V.; Gohlke , H.; Radmer, R.; Duan , Y.; Pitera, J.; Massova , I.; Seibel, G. L.; Singh , U. C.; Weiner, P.; Kollman, P. A., *Amber 7 User's Manual*. California: University of California, **2002**.

LEaP: LEaP is an X-windows-based program that provides for basic model building and Amber coordinate and parameter/topology input file creation. It includes a molecular editor which allows for building residues and manipulating molecules.

antechamber: This program suite automates the process of developing force field descriptors for most organic molecules. It starts with structures (usually in PDB format), and generates files that can be read into LEaP for use in molecular modelling. The force field description that is generated is designed to be compatible with the usual Amber force fields for proteins and nucleic acids.

ptraj: This is used to analyse MD trajectories, computing a variety of things, like RMS deviation from a reference structure, hydrogen bonding analysis, time-correlation functions, diffusional behavior, and so on.

mm_pbsa: This script is basically used to automate post-processing of MD trajectories and to analyse energetics using continuum solvent methods.

nmode: It is a normal mode analysis program which gets the first and second derivative information and it is used to search for local minima, perform vibrational analysis, and search for transition states.

In the Scheme 7-5, a general scheme of AMBER with the links between different programs is represented. For starting any simulation, the system coordinates are required, which usually are taken from the X-Ray structure, and the format file is pdb. Using antechamber and LeaP, the amber coordinate files (*prmcrd*) and amber topology files (*prmtop*) can be obtained, which are used as input files for energetic programs. [72]

[72] Pérez, J., *Molecular Modeling with AMBER*. Universitat Autònoma de Barcelona: Barcelona, **2005**.

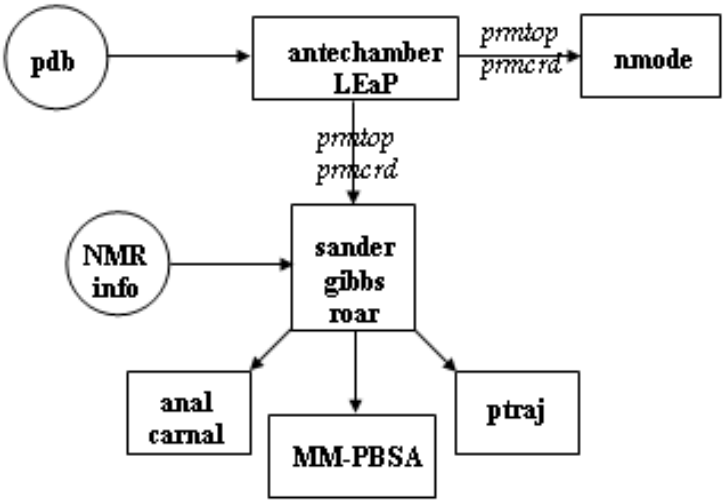

Scheme 7-5.- General scheme of AMBER

In this thesis, the latest versions of AMBER available in our group (versions 7 and 8) were used. These packages contain many programs which are very useful to undertake computational studies based in molecular dynamics. However, the huge number of possibilities makes the use of AMBER difficult for the beginners.

'Time is
a great
story teller.'

Irish proverb

8 CHECKING RESP

8.1 INTRODUCTION ABOUT RESP

AMBER is a huge program that contains a bunch of modules or subprograms. One of them is called RESP (from Restrained Electrostatic Potential) and it fits the quantum mechanically calculated electrostatic potential (ESP) at molecular surfaces using an atom-centered point charge model[73]. We used Gaussian to generate the ESP input for RESP although other quantum mechanical programs such as Jaguar or GAMESS can be used for that purpose. The basic idea with electrostatic potential fit charges is that a least squares fitting algorithm is used to derive a set of atom-centered point charges which best reproduce the electrostatic potential of the molecule. In AMBER, the potential is evaluated at a large number of points defined by four shells of surfaces at 1.4, 1.6, 1.8, and 2.0 times the Van der Waals radii. These distances have been shown to be appropriate for deriving charges which reproduce typical intermolecular interactions (energies and distances). The value of the electrostatic potential at each grid point is calculated from the quantum mechanical wavefunction.

8.2 CHECKING RESP

RESP is a module well known and used. Since many years, all the people from our laboratory have been working with AMBER and have also been using RESP in their studies. However, during this thesis and also in Miguel de Federico's thesis,[74] some problems around RESP calculation were observed. One of them is observed when the RESP calculation is made using more than one conformation.

It is known that the charges obtained from electrostatic potential fitting will depend upon the conformation for which the quantum mechanical calculation was performed. One way to avoid this problem is to perform a series of charge calculations

[73] a) Bayly, C. I.; Cieplak, P.; Cornell, W. D.; Kollman, P. A. *J. Phys. Chem*. **1993**, *97*, 10269. b) Cornell, W. D.; Cieplak, P.; Bayly, C. I.; Kollman, P. A. *J. Am. Chem. Soc.* **1993**, *115*, 9620. c) Cieplak, P.; Cornell, W. D.; Bayly, C.; Kollman, P. A. *J. Computat. Chem.* **1995**, *16*, 1357.

[74] de Federico de la Rúa, M. *Pseudorotaxanos, catenanos complejos de inclusión con ciclodextrinas: cálculos de energía libre (PhD thesis)*. Universitat Autònoma de Barcelona: Bellaterra, **2006**.

for different conformations and then use a charge model in which each charge is weighted according to the relative population of that particular conformation as calculated from the Boltzmann distribution. However, RESP module calculates an average of the potential distribution and not an average of charges taking into account the weight of each conformation. It was easy to see this strange behaviour digging inside the subroutine about RESP in AMBER and also easily calculating the atoms charges of different systems in two different ways. The first way was calculating the atom charges for each conformation and then make an average taking into account the weight of each conformation. The other way was to make the RESP calculation specifying the two conformations and their weights. However, there are differences in results between both methodologies such as it is shown in the following example:

atom	RESP (A)	RESP (B)	Average (C)	RESP (A+B)	Average (C) – RESP(A+B)
1	-0.203551	-0.203551	-0.203551	-0.213683	0.010132
2	0.233820	0.233820	0.233820	0.256143	-0.022323
3	-0.203551	-0.203551	-0.203551	-0.213683	0.010132
4	-0.203551	-0.203551	-0.203551	-0.213683	0.010132
5	0.233820	0.233820	0.233820	0.256143	-0.022323
6	-0.203551	-0.203551	-0.203551	-0.213683	0.010132
7	0.141218	0.141218	0.141218	0.147692	-0.006474
8	-0.342248	-0.342246	-0.342247	-0.368498	0.026251
9	0.141218	0.141218	0.141218	0.147692	-0.006474
10	0.141218	0.141218	0.141218	0.147692	-0.006474
11	-0.342248	-0.342246	-0.342247	-0.368498	0.026251
12	0.141218	0.141218	0.141218	0.147692	-0.006474
13	0.182991	0.182983	0.182987	0.216739	-0.033752
14	0.182991	0.182983	0.182987	0.216739	-0.033752
15	-0.120998	-0.120996	-0.120997	-0.005751	-0.115246
16	0.025635	0.025637	0.025636	0.005675	0.019961
17	0.025635	0.025637	0.025636	0.005675	0.019961
18	0.025635	0.025637	0.025636	0.005675	0.019961
19	-0.120998	-0.120996	-0.120997	-0.005751	-0.115246
20	0.025635	0.025637	0.025636	0.005675	0.019961
21	0.039944	0.039944	0.039944	0.006854	0.033090
22	0.039944	0.039944	0.039944	0.006854	0.033090
23	0.039944	0.039944	0.039944	0.006854	0.033090
24	0.039944	0.039944	0.039944	0.006854	0.033090
25	0.039944	0.039944	0.039944	0.006854	0.033090
26	0.039944	0.039944	0.039944	0.006854	0.033090
				rmsd	0.0392

a)

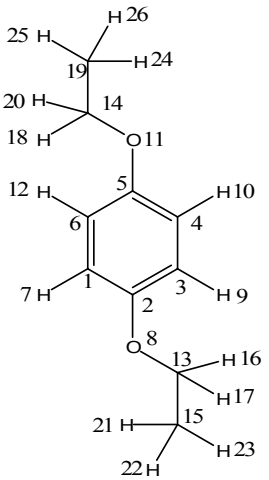

CR1

b)

Scheme 8-1.- a) Atomic charges calculated in RESP using two ways. b) Molecule studied.

It is shown in Scheme 8-1 that there are not big differences in atomic charges between both conformations. The atomic charge average of both conformers [average (C)] is similar to each one [RESP(A) and RESP(B)]. However, the atomic charges from RESP(A+B) method, where RESP takes into account the two conformations, are different comparing to atomic charges obtained from RESP (A), RESP(B) and average (C), specially those for the carbon atoms 15 and 19.

Another problem in RESP appears when a macromolecule is built ensambling two or more residues. In many cases, there is the need of removing some part of these residues to fix them in the final macromolecule. For example, we can use the aromatic molecule CR1 (in Scheme 8-1) for building a crown ether, with a strategy such as follows:

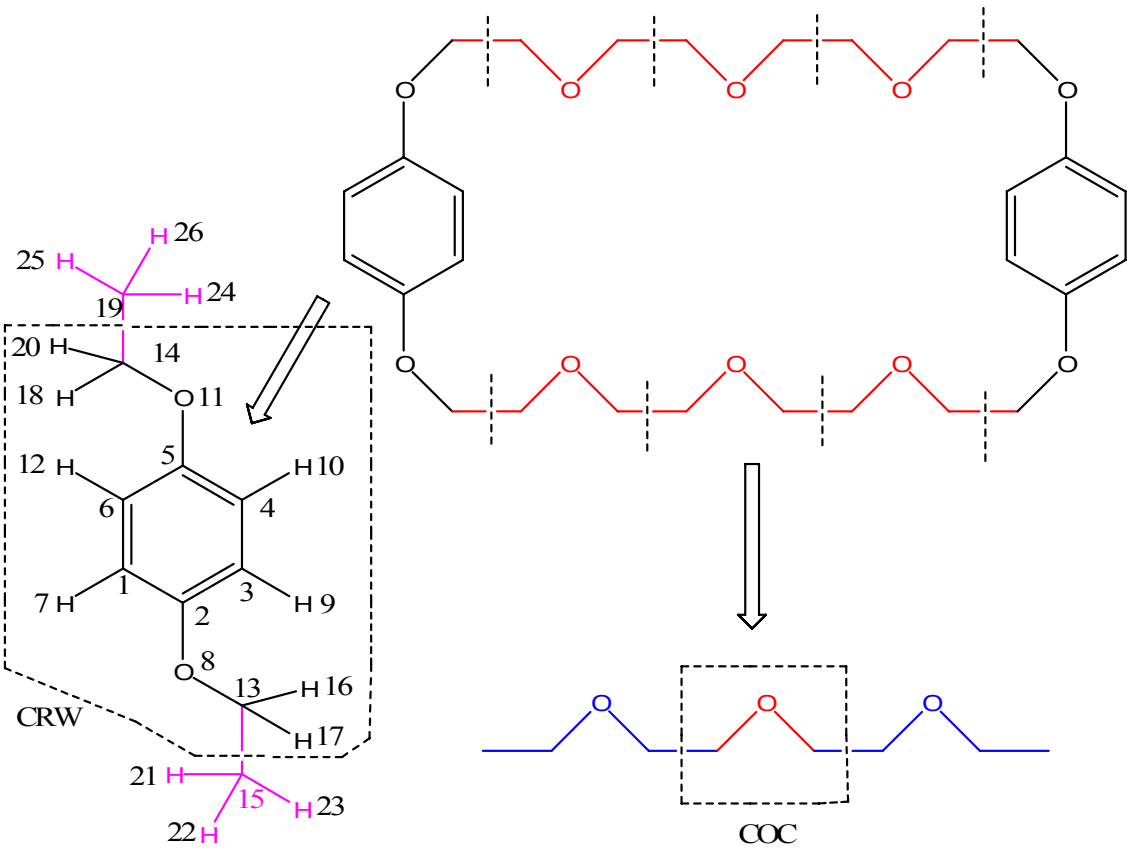

Scheme 8-2.- The crown ether can be built using 2 residues of CRW and 2 polyether chains made by 6 residues of COC.

For building residue CRW, we used the molecule CR1 and removed the two methyl groups. In RESP is necessary to specify the groups that will be deleted (atoms and total charge). In the following table, all the atomic charges are gathered using the same ways as used previously for the molecule CR1:

atom	RESP (A)	RESP (B)	Average (C)	RESP (A+B)	Average (C) – RESP(A+B)
1	-0.188361	-0.188361	-0.188361	-0.186470	-0.001891
2	0.198525	0.198525	0.198525	0.194308	0.004217
3	-0.188361	-0.188361	-0.188361	-0.186470	-0.001891
4	-0.188361	-0.188361	-0.188361	-0.186470	-0.001891
5	0.198525	0.198525	0.198525	0.194308	0.004217
6	-0.188361	-0.188361	-0.188361	-0.186470	-0.001891
7	0.138710	0.138710	0.138710	0.137924	0.000786
8	-0.350282	-0.350282	-0.350282	-0.347131	-0.003151
9	0.138710	0.138710	0.138710	0.137924	0.000786
10	0.138710	0.138710	0.138710	0.137924	0.000786
11	-0.350282	-0.350282	-0.350282	-0.347131	-0.003151
12	0.138710	0.138710	0.138710	0.137924	0.000786
13	0.254728	0.254730	0.254729	0.250564	0.004165
14	0.254728	0.254730	0.254729	0.250564	0.004165
16	-0.001835	-0.001836	-0.001836	-0.000325	-0.001511
17	-0.001835	-0.001836	-0.001836	-0.000325	-0.001511
18	-0.001835	-0.001836	-0.001836	-0.000325	-0.001511
20	-0.001835	-0.001836	-0.001836	-0.000325	-0.001511
				rmsd	0.0025

Table 8-1.- RESP charges used for the building of the CRW residue.

Atomic charges slightly differs depending on the method used (see Table 8-1). Results follow the same tendency as shown in Scheme 8-1a. However, when molecules are studied, the differences between atomic charges calculated using average (C) method and RESP(A+B) method are bigger than for preparing a molecule where some fragments have been removed (compare rmsd from Scheme 8-1 and Table 8-1). However, atom charges values from residue CR1 clearly differs from those from molecule CRW ($rmsd_{average(C)}$=0.0306 if the average (C) values from Scheme 8-1a and Table 8-1 are used. $rmsd_{RESP(A+B)}$ is equal to 0.0282 using the RESP (A+B) value taken from Scheme 8-1a and Table 8-1).

It notices that these fragments must represent well the environment of the residue in the macromolecule. So, it is very important to decide what molecules will be the best for building the residues which will form part of the macromolecule studied.

The macromolecule should be built entirely to avoid cutting the residues for the construction of macromolecules and the associated problems. Moreover, the CPU time for the optimization step in Gaussian is, in many cases, very high. A way to solve these problems, is to use a Single Point Energy calculation instead of running an optimization in Gaussian.

A single point energy calculation is a prediction of the energy and related properties for a molecule with a specified geometric structure. The phrase single point is key, since this calculation is performed at a single, fixed point on the potencial energy surface for the molecule. The validity of results of these calculations depend on having reasonable input structures for the molecules.

Using the previous idea, we tried to build the rotaxanes in one piece. Firstly, we calculated a single point of a minimized structure of a rotaxane. An then, we tried to calculate the atomic charges in RESP. However, the AMBER module did not accept a so big structure (288 atoms) because AMBER limits the number of atoms to MAXATOM = 256 atoms. So, we decided to use as less residues as possible for the contruction of the rotaxane.

The simplest way to divide the rotaxanes used in this thesis is to cut them in four fragments: two residues containing the stoppers and two others with the station areas. However, the residues used in this thesis for building the rotaxane contain, in most cases more than 100 atoms. Single point calculations instead of optimisation were used followed by charge calculation in order to reduce computational time. Before trying to build the full rotaxanes using this approach, we decided to test this methodology using the example previosly shown (molecule CR1 for building residue CRW).

In the next table, RESP charges taken from a single point calculation are gathered:

atom	RESP (A)	RESP (B)	Average (C)	RESP (A+B)	Average (C) – RESP(A+B)
1	-0.194121	-0.194121	-0.194121	-0.193497	-0.000624
2	0.197646	0.197646	0.197646	0.196238	0.001408
3	-0.194121	-0.194121	-0.194121	-0.193497	-0.000624
4	-0.194121	-0.194121	-0.194121	-0.193497	-0.000624
5	0.197646	0.197646	0.197646	0.196238	0.001408
6	-0.194121	-0.194121	-0.194121	-0.193497	-0.000624
7	0.142940	0.142940	0.142940	0.142677	0.000263
8	-0.360378	-0.360378	-0.360378	-0.359215	-0.001163
9	0.142940	0.142940	0.142940	0.142677	0.000263
10	0.142940	0.142940	0.142940	0.142677	0.000263
11	-0.360378	-0.360378	-0.360378	-0.359215	-0.001163
12	0.142940	0.142940	0.142940	0.142677	0.000263
13	0.267043	0.267043	0.267043	0.265216	0.001827
14	0.267043	0.267043	0.267043	0.265216	0.001827
16	-0.000975	-0.000975	-0.000975	-0.000299	-0.000676
17	-0.000975	-0.000975	-0.000975	-0.000299	-0.000676
18	-0.000975	-0.000975	-0.000975	-0.000299	-0.000676
20	-0.000975	-0.000975	-0.000975	-0.000299	-0.000676
				rmsd	0.0010

Table 8-2.- RESP charges for molecule CR1 for building the CRW residue using a single point calculation.

As shown in the Table 8-2, RESP charges taking into account both conformer (RESP (A+B) method) slightly differs from RESP charges for each conformer (RESP (A) and RESP (B)) and from the atomic charges as result of the average of RESP(A) and RESP(B) (average (C)). What is interesting is that atomic charges taken from RESP(A) and RESP(B) using single point calculation are analogous to these obtained using optimization, as shown in Table 8-1 and Table 8-2 ($rmsd_{average(C)}$= 0.0063, $rmsd_{RESP\ (A+B)}$=0.0075). However, atom charges values from residue CR1 are clearly different from those from molecule CRW ($rmsd_{average(C)}$=0.0338 if the average (C) values from Scheme 8-1a and Table 8-2 are used and $rmsd_{RESP(A+B)}$ is equal to 0.0278 using the RESP (A+B) value taken from Scheme 8-1a and Table 8-2).

Faced with these results and to sum up, we decided to carry out the RESP calculations using single point option in Gaussian for the residues used in this thesis. Finally, average (C) charges were used for modelling of the molecules.

'A good laugh and a long sleep
are the best cures
in the doctor's book.'
Irish proverb

9 RESP CHARGES FOR THE SYSTEMS

9.1 INTRODUCTION

All the compounds studied in this thesis were modelled using the AMBER program following the methodology developed in our group.[75] As told in the Chapter 6, AMBER is a package with many modules or subprograms and, most of them do not have graphical interface. In most of the cases, the AMBER user has to create files that contain the commands and parameters that will be read by the module used. Consequently, the user must know well each of the options used. However, to know each parameter used is not an easy job because of the fact that AMBER user manual is difficult for reading and understanding.

For modelling a new molecule in AMBER, there is the need of using other programs as such Gaussian or MacroModel for creating input files which will be read in a AMBER module. In our case, MacroModel is usually used when a conformational search is needed. Afterwards, energies and charges can be calculated using Gaussian program for the most interesting conformers obtained in the conformation search carried out using the Monte Carlo method implemented in MacroModel. The output files from Gaussian will be required in case of doing a RESP charge calculation. RESP charges and atomic coordinates are needed for building a molecule in AMBER.

9.2 ATOMIC CHARGES

The atomic charges used for the modelling of the different molecules studied in this thesis were calculated using RESP methodology. In the following schemes, we can show the RESP charges for the crown ether, PF_6^- and viologens ETH, DIM, CRE, CRD and NET:

[75] Pérez, J., *Molecular Modeling with AMBER*. Universitat Autònoma de Barcelona: Barcelona, **2005**.

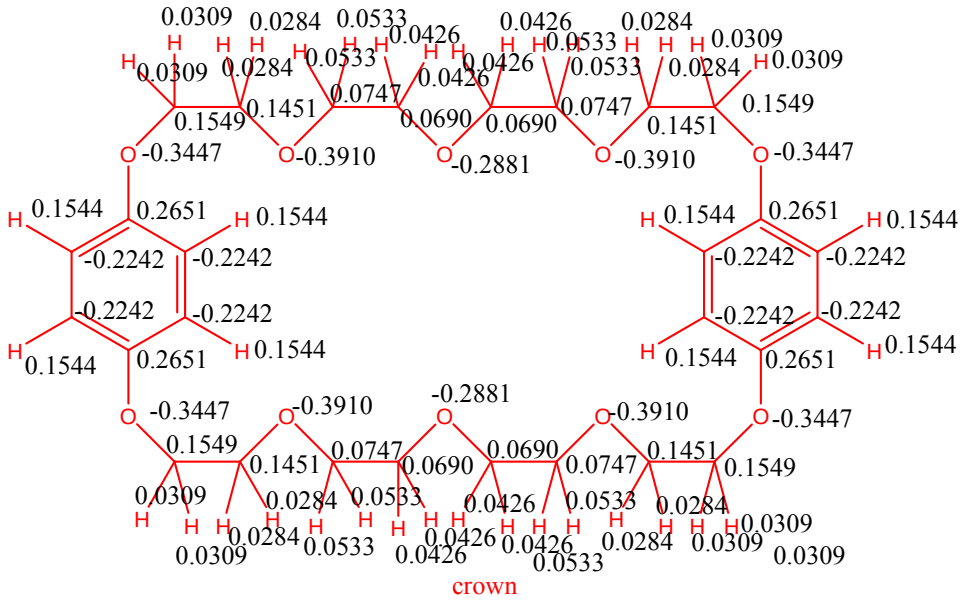

Scheme 9-1.- RESP charges for the bis-*para*-phenyl-34-crown-10 (crown)

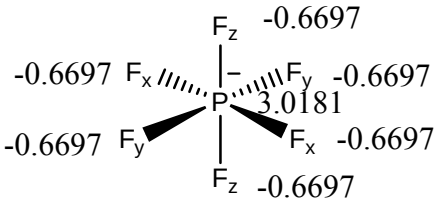

Scheme 9-2.- RESP charges for the hexafluorophosphate anion (PF_6^-)

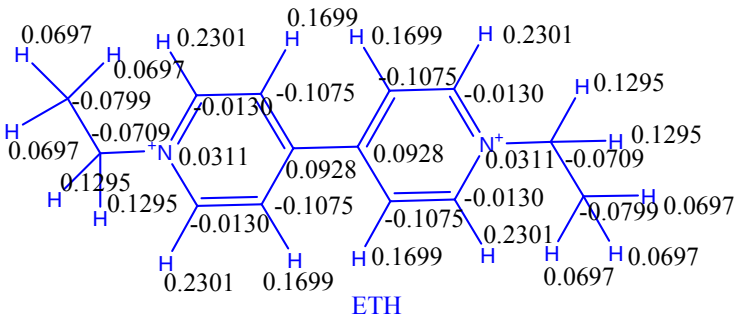

Scheme 9-3.- RESP charges for the 1,1'-diethyl-4,4'-bipyridinium salt (ETH)

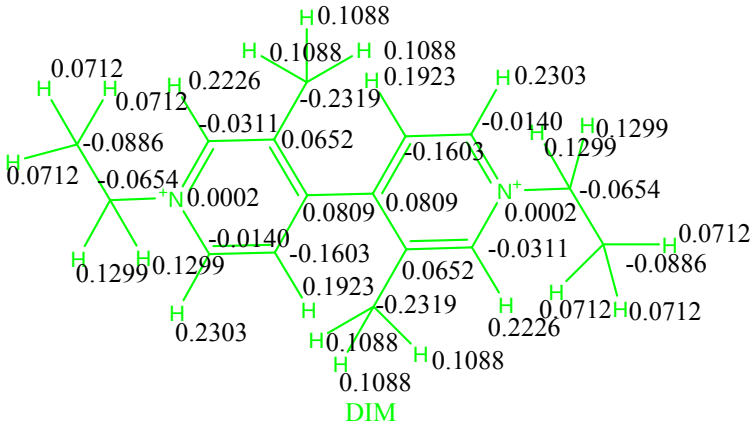

Scheme 9-4.- RESP charges for the 1,1'-diethyl-3,3'-dimethyl-4,4'-bipyridinium salt (DIM)

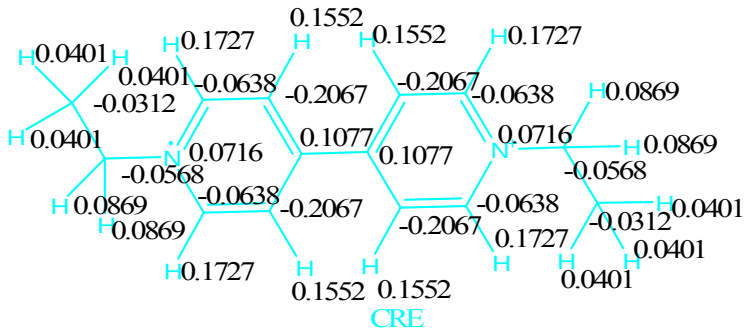

Scheme 9-5.- RESP charges for the 1,1'-diethyl-4,4'-bipyridinium monocation, CRE

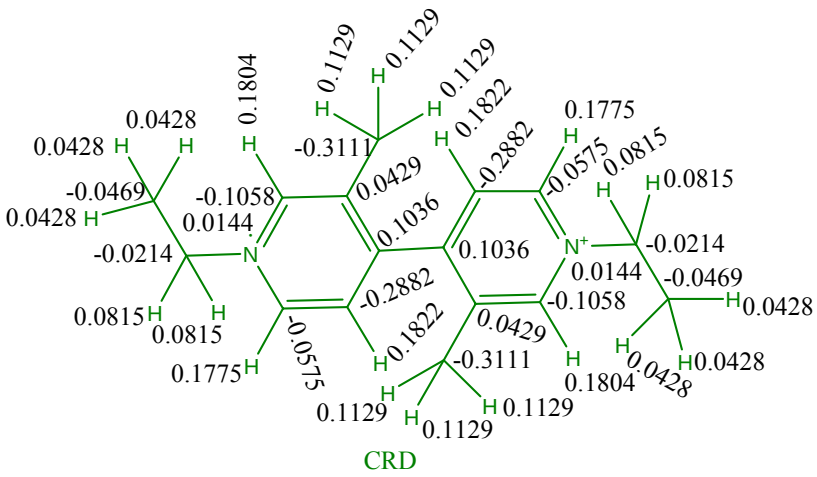

Scheme 9-6.- RESP charges for the molecule CRD

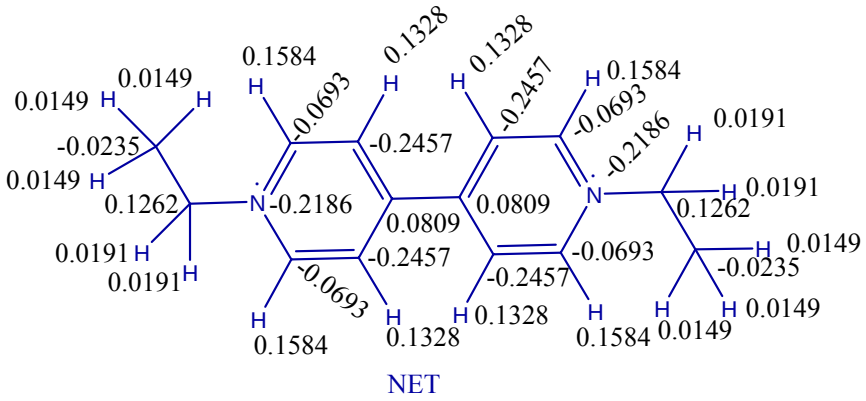

Scheme 9-7.- RESP charges for the molecule NET

The axles studied in this thesis are represented in the Scheme 9-8:

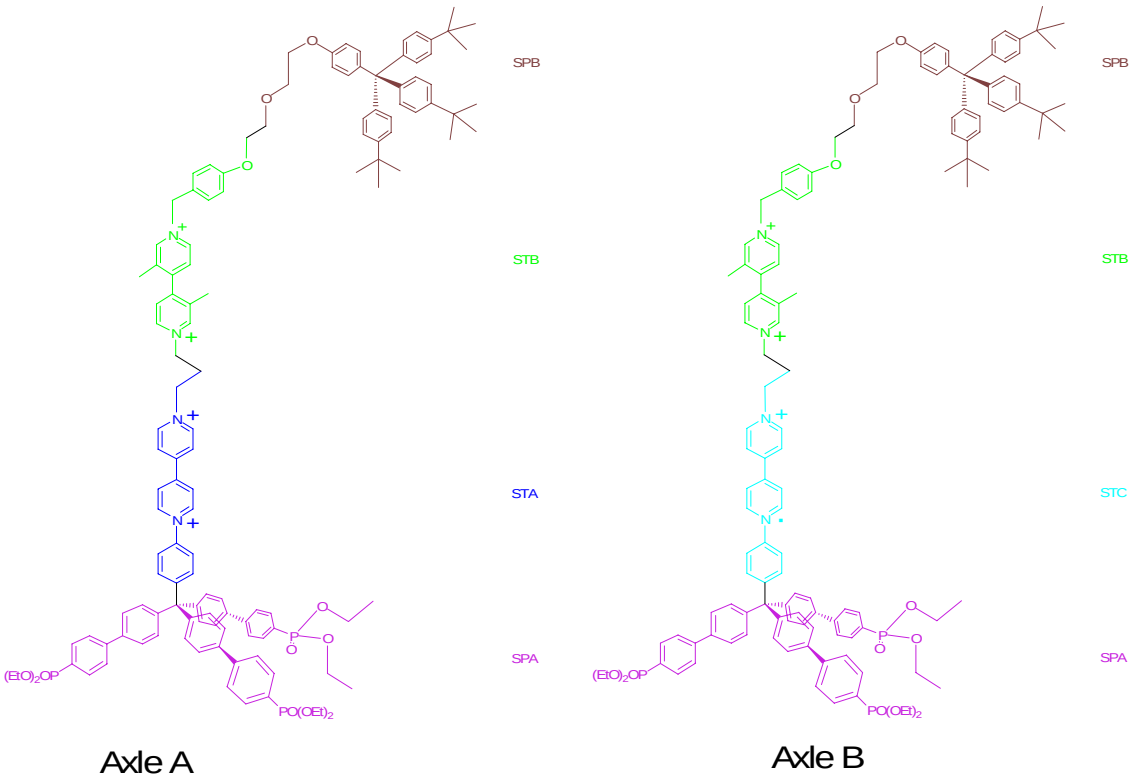

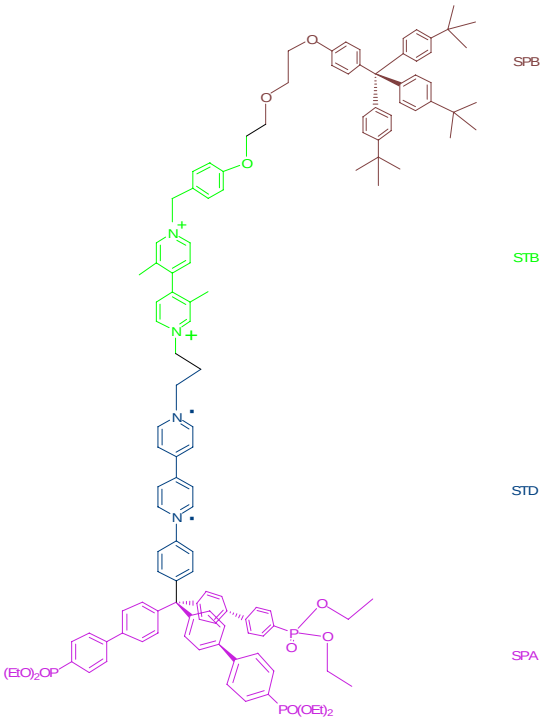

Axle C

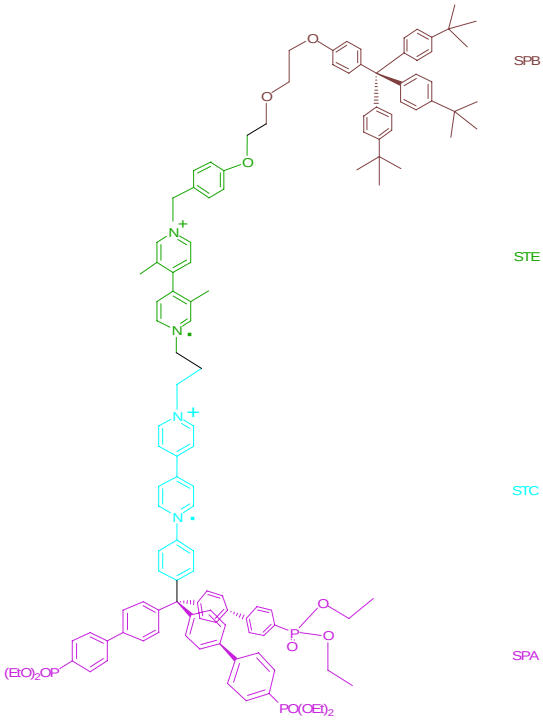

Axle D

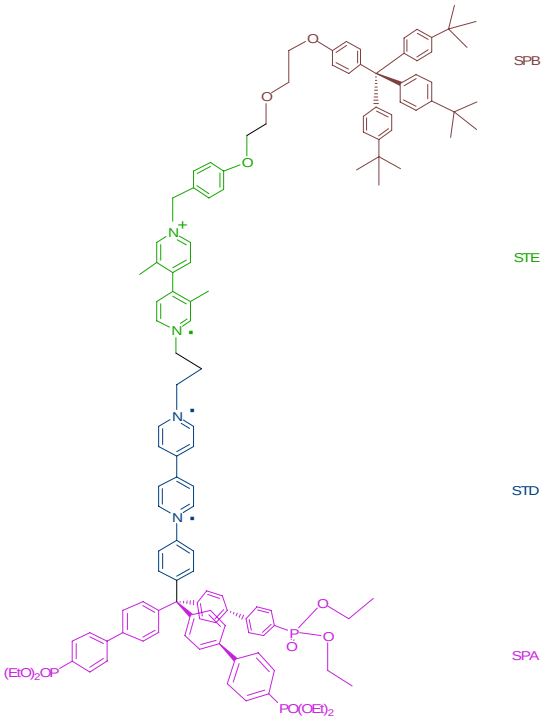

Axle E

Scheme 9-8.- Representation of the different axles used in this thesis.

The electrostatic potential evaluation of each whole axle could not be calculated directly because of its size. Each axle was divided in four fragments or residues (for example, axle A, is built by SPA, STA, STB and SPB residues) and then, each molecule used for building each residue was evaluated following the same RESP methodology as the rest of the components calculated. The residues and its charges used for building the axles studied are represented in the following schemes:

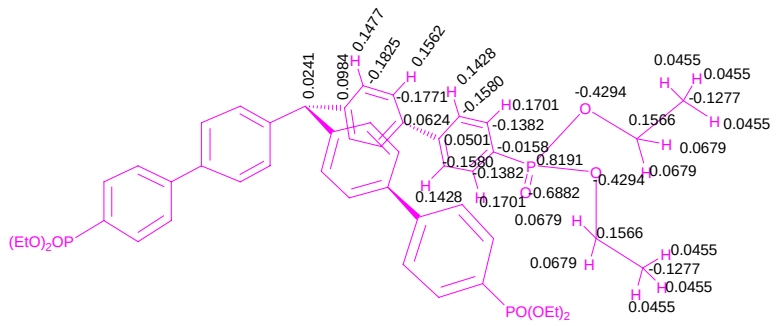

SPA

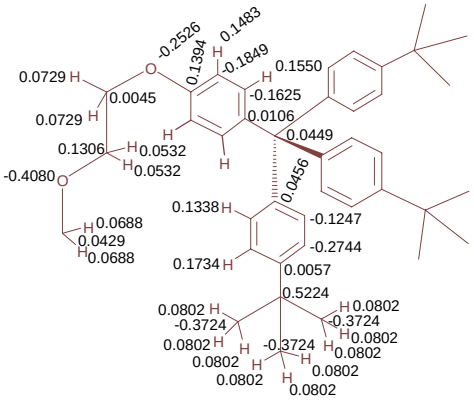

SPB

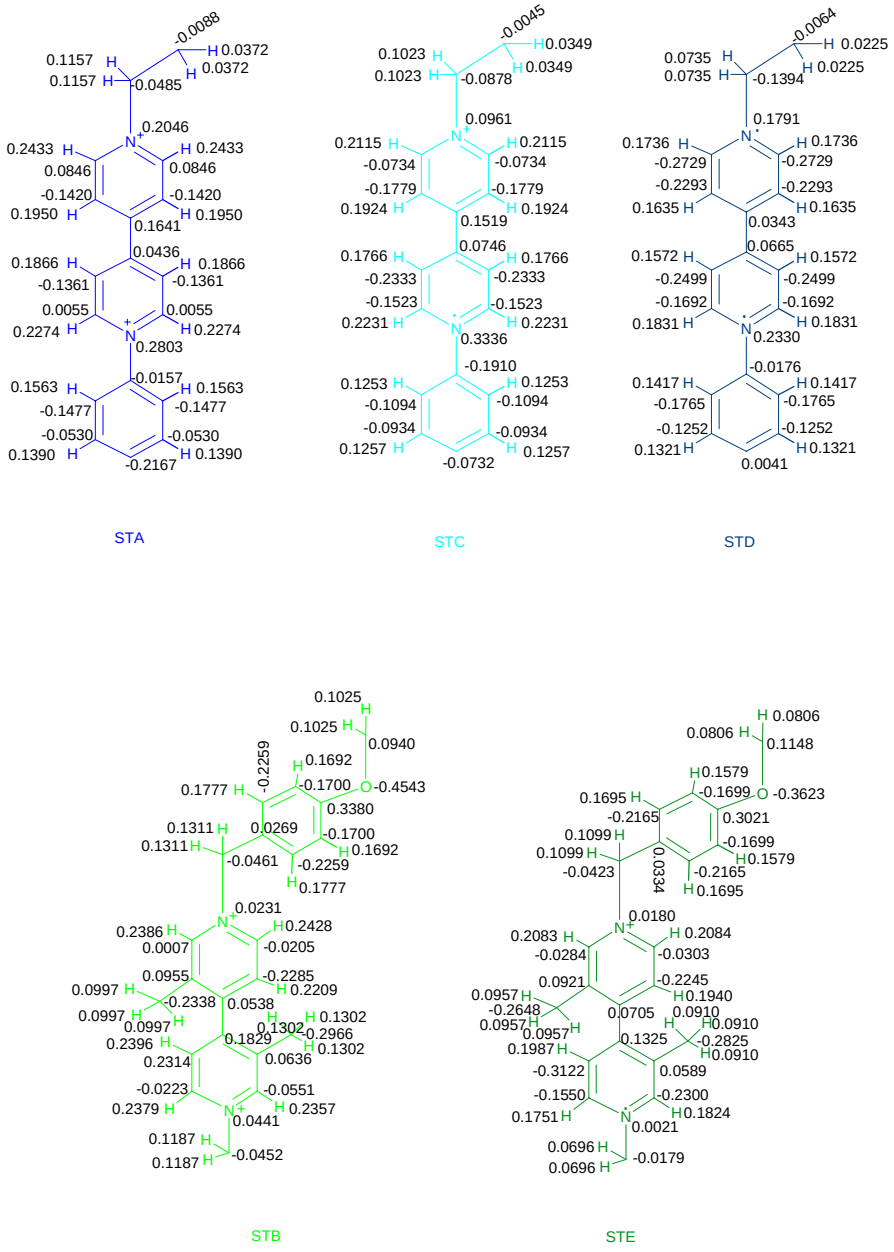

Scheme 9-9.- RESP charges for the residues used for the modelling of the axles shown in Scheme 9-8.

It notices that, for space problems, it was impossible to write all the atom charges in stopper residues SPA and SPB. However, the rest of charges can be deduced thanks to the symmetry presented in these fragments using the charges which are in each representation.

'Better
be safe
than sorry.'

Irish proverb

10 PARAMETERISATION OF PF_6^- AND BR^-

10.1 PARAMETERISATION OF PF_6^-

For a better reliability of results, we decided to model the system using the same counterions as experimentally. In our case, the ions PF_6^- and Br^- were used. However, any of them were include inside any of the AMBER packages.

RESP atomic charges and geometry are needed for modelling any molecule in AMBER. Each atom requires geometric parameters to be modelize properly and most of these parameters are included in parameters files contained in AMBER. However, in some cases, the parameterisation is needed in case of lacking parameters.

All the necessary data to model the bromide were found in the literature.[76] In the following scheme, we can show the parameters file about Br^- used in this thesis:

```
Parameters for bromide anion (Br-)

MASS
bx 79.90         4.530              Markovich, JPC 1996,105(7),page2677

NONB      RE
  bx          2.5950  0.0900            Lybrand,Ghosh,McCammon,JACS,107,7793
```

Scheme 10-1.- Parameters for bromide anion

More complicated was obtaining the parameters needed for creating the hexafluorophosphate ion used in this thesis. To overcome this challenge, we decided to follow the steps of the AMBER 7 manual about parameter development.

[76] a)Lybrand, T. P.; Ghosh, I.; McCammon, J. A. *J. Am. Chem. Soc.* **1985**, 107, 7793-7794. b) Markovich, G.; Perera, L.; Berkowitz, M. L.; Cheshnovsky, O. *J. Chem. Phys.* **1996**, *105(7),* 2675-2685.

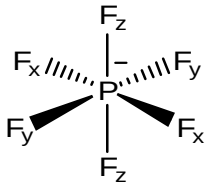

Scheme 10-2.- Representation of the hexafluorophosphate ion

We labelled three types of F (F_x, F_y and F_z) (see Scheme 10-2), depending on the place where are located in the space (x, y or z), just to avoid some warnings and errors which come from the program used in this thesis. Although F_x, F_y and F_z are different atom types, all of them are equivalent and will have the same properties and, then, they will contain the same parameters.

In case of PF_6^-, the parameters for bond F-P and angle F-P-F were not available in parameters files for AMBER. Then, their parameterisation was necessary.

Respecting to the bond F-P, we calculated first the Energy profile along the bond length P-F from 1.5 to 1.70 Å in Gaussian (MP2/6-31G*) (see Scheme 10-3, pink curve). Afterwards, we calculated the Energy *versus* the bond length P-F (from 1.5 to 1.70 Å) in AMBER using different values of bond constant (Kbond) and bond distance (Dbond).

The AMBER curve which better reproduced the *ab initio* results is shown in Scheme 10-3.

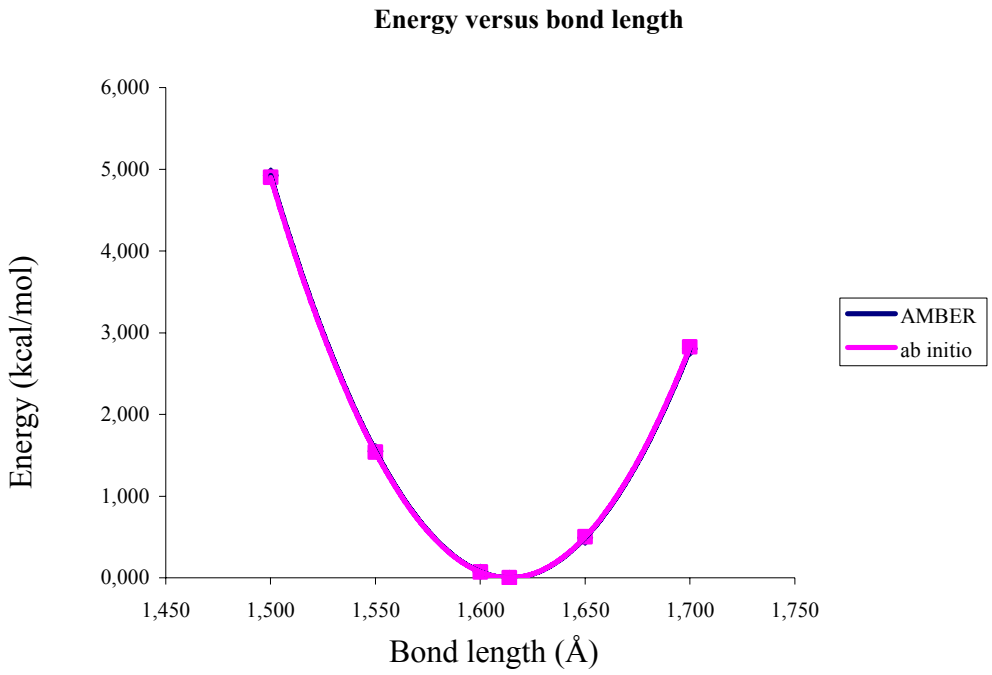

Scheme 10-3.- Representation of the Energy *versus* bond length calculated in AMBER and *ab initio*.

After the parameterisation of the bond P-F, we started to search the best parameters for the angle F-P-F. There are two kind of angles: the angles F-P-F which measure 90 º (F_x-P-F_y, F_x-P-F_z, and F_y-P-F_z) and those angles F-P-F which mesure 180 º (F_x-P-F_x, F_y-P-F_y, and F_z-P-F_z).

For obtaining the parameters for right and straight angles F-P-F in AMBER, we firstly represented the energy along the angle F-P-F in Gaussian (MP2/6-31G*). Afterwards, energy profile *versus* angle F-P-F around 90 º and 180 º were represented in AMBER using different angle parameters. Finally, we chose those conditions which better reproduced the *ab initio* results (see Scheme 10-4 and Scheme 10-5).

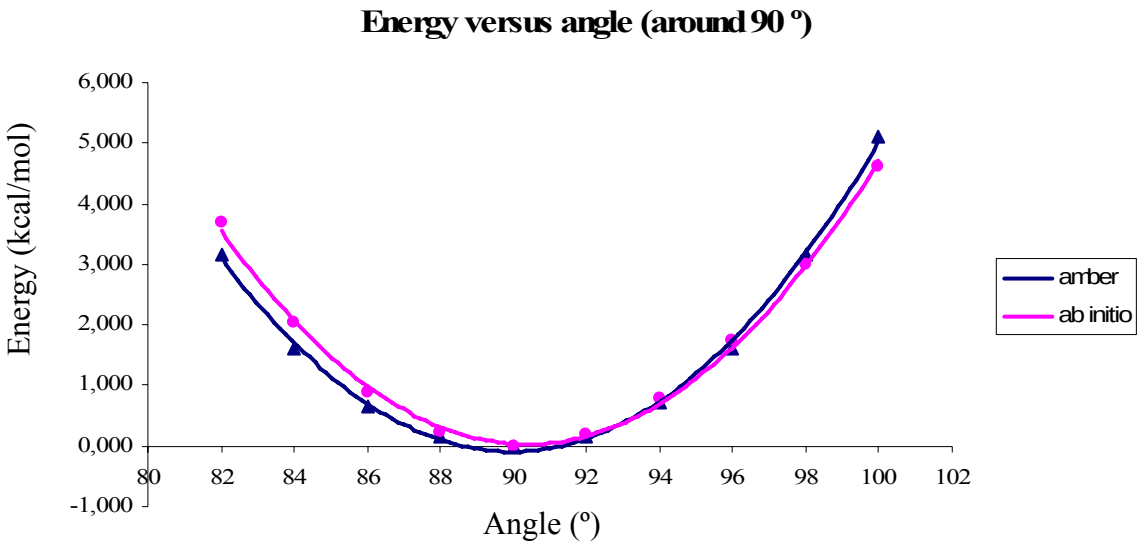

Scheme 10-4.- Energy *versus* angle F-P-F around 90 º.

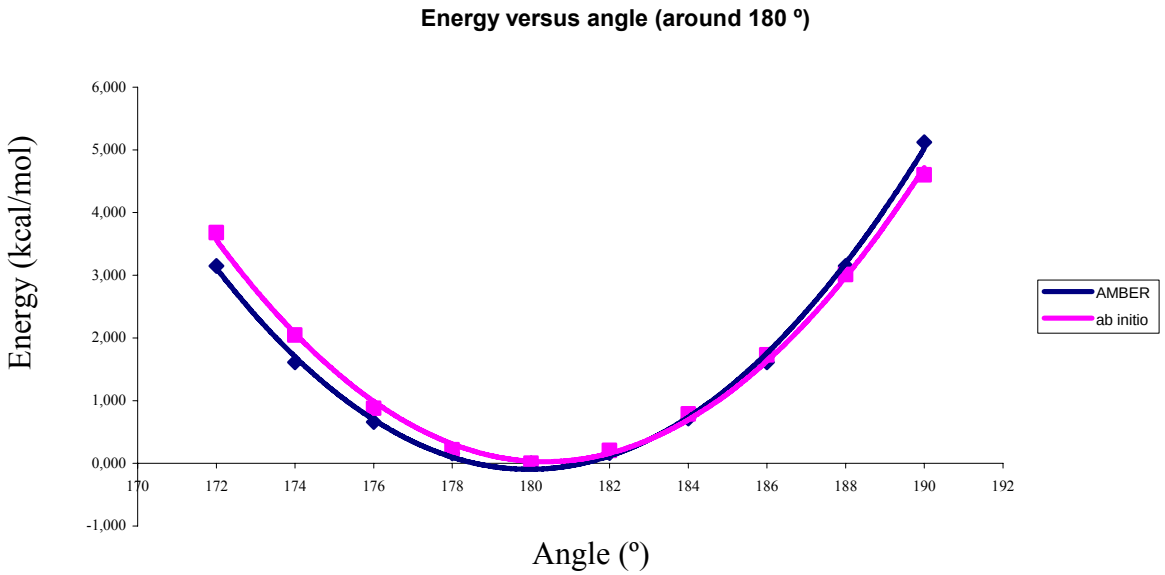

Scheme 10-5.- Energy *versus* angle F-P-F around 180 º.

The parameters calculated for PF_6^- are recollected in the following parameters file:

```
parameters for PF6-
MASS
p6 30.97                          Phosphate
fx 19.00                          Fluorine
fy 19.00                          Fluorine
fz 19.00                          Fluorine

BOND
p6-fx  379.0    1.614             Phosphate with six connected atoms, such as PF6-
p6-fy  379.0    1.614             Phosphate with six connected atoms, such as PF6-
p6-fz  379.0    1.614             Phosphate with six connected atoms, such as PF6-

ANGLE
fx-p6-fy     90.0       90.0      MP2/6-31G*
fx-p6-fz     90.0       90.0      MP2/6-31G*
fy-p6-fz     90.0       90.0      MP2/6-31G*
fx-p6-fx     90.0      180.0      MP2/6-31G*
fy-p6-fy     90.0      180.0      MP2/6-31G*
fz-p6-fz     90.0      180.0      MP2/6-31G*

NONB      RE
  p6          2.10    0.200       JCC,7,(1986),230;
  fx          1.75    0.061       Gough et al. JCC 13,(1992),963.
  fy          1.75    0.061       Gough et al. JCC 13,(1992),963.
  fz          1.75    0.061       Gough et al. JCC 13,(1992),963.
```

Scheme 10-6.- Parameters for hexafluorophosphate anion

'There is no luck
except where
there is discipline.'
Irish proverb

11 PARAMETERISATION OF VIOLOGENS

11.1 INTRODUCTION

One of the main differences between the viologens studied in this thesis is the different flatness which depends on its charge and its substituents. So, it is important to evaluate properly the dihedral angle between the two aromatic rings located in the viologen.

To model any molecule, we firstly calculated its RESP atomic charges (see Chapter 9 "RESP charges for the systems"). Then, its geometry was also necessary.

Geometric parameters for modelling properly the cation viologens ETH and DIM and for the neutral viologen NET were found in the set of parameters gaff used for this thesis. In the following schemes it is shown the atom types used for ETH, DIM and NET viologens:

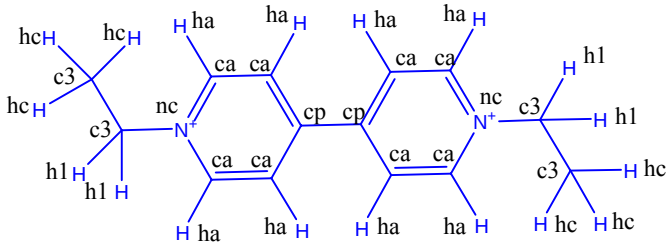

ETH

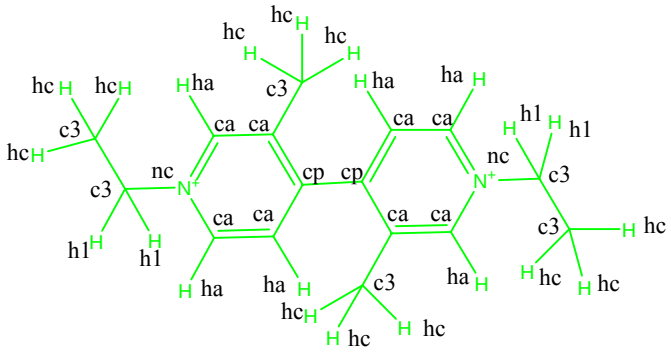

DIM

Scheme 11-1.- Atom types for the cation viologens ETH and DIM.

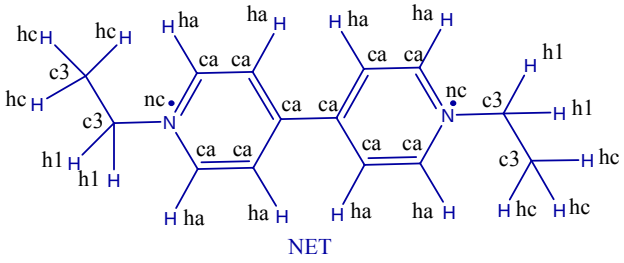

Scheme 11-2.- Atom types for neutral viologen NET.

However, we could not find some geometric parameters associated to radical viologens CRE and CRD in the literature. Therefore, the parameterisation was done for CRE viologen, but the parameters found were used for modelling the CRD viologen as well.

Basically, we needed to find an atom type (and its parameters) for the central carbon atoms (termed in our case such as cr). Then, it was necessary to calculate the bond distance cr-cr and the dihedral angle related to them as well (termed X-cr-cr-X, where X can be any atom. Then, not all atoms are explicit) (see Scheme 11-3). So, we decided to find all these parameters following similar strategy such as in the parameterisation of the PF_6^-.

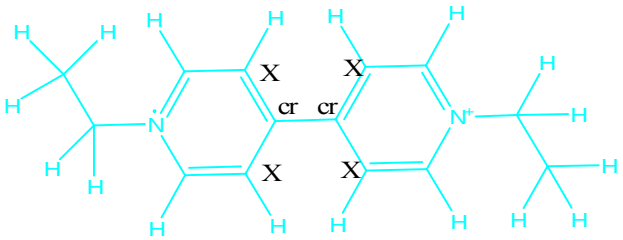

Scheme 11-3.- Scheme for the viologen CRE

11.2 DIHEDRAL PARAMETERS SEARCHING

Taking into account the torsional energy profile calculated previously in Gaussian [BHandHLYP/6-311++G(d,p)] (see Scheme 11-4, red curve), the topology about the dihedral of interest has a two-fold periodicity (PN); it means that there are two potential barriers (around 20 kcal/mol) as the C-C bond is rotated -180 to 180 degrees. These barriers occur at dihedral angles of -90 and 90 degrees (energy minimum at 0 degrees), and can be reproduced by the truncated Fourier series only if a phase shift of 180 degrees (PHASE=180) is used.

AMBER program use the Equation 11-1 to calculate the torsional energy which varies depending on the dihedral angle phi:

$$Etors=(PK/IDIVF)\cdot(1+\cos(PN\cdot phi - PHASE))$$

Equation 11-1

The parameter IDIVF is the total number of torsions about a single bond that the potential applies to. In case of the fact that all atoms are explicit (in that case, we define a dihedral such as ca-cr-cr-ca, where all atoms are well defined), then IDIVF=1 and the total potential for the bond (in our case, 20 kcal/mol) is divided by the number of torsions involved (in our case, thre are 4 torsions around the bond). PK is equal to one-half of the barrier magnitude and would therefore be equal to 20/4/2 = 2.5 kcal/mol. If generic representation (atom label X and it represents any atom) is chosen, the entire potential is used and IDIVF=4. So, the PK= 20/2= 10 kcal/mol.

In our case, the generic representation was used. By default, we used a bond constant of 460.5 $kcal\cdot mol^{-1}\cdot Å^{-2}$ and a bond distance of 1.417 Å for bond cr-cr, which are those found in ab initio calculations.

We represented the torsional energy *versus* the dihedral angle (X-cr-cr-X) in AMBER using different conditions of PK (see Scheme 11-4).

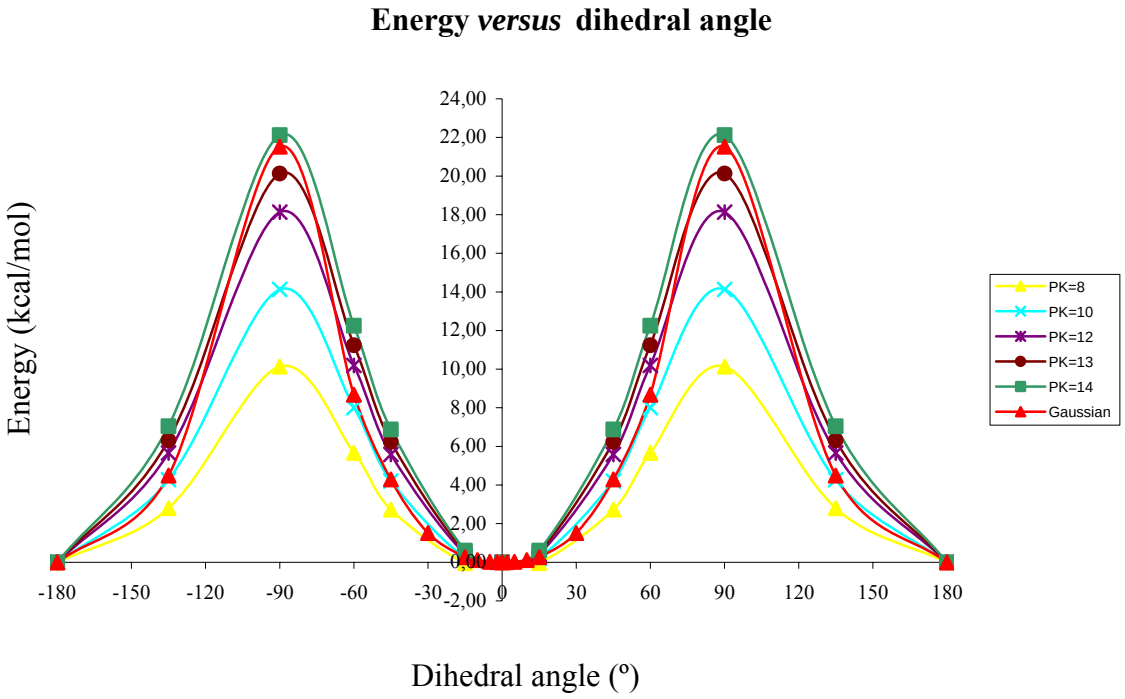

Scheme 11-4.- Energy profile along dihedral angle X-cr-cr-X

Looking in the area between -90 and 90 º (well), we can see better the differences between the set of points obtained in each case.

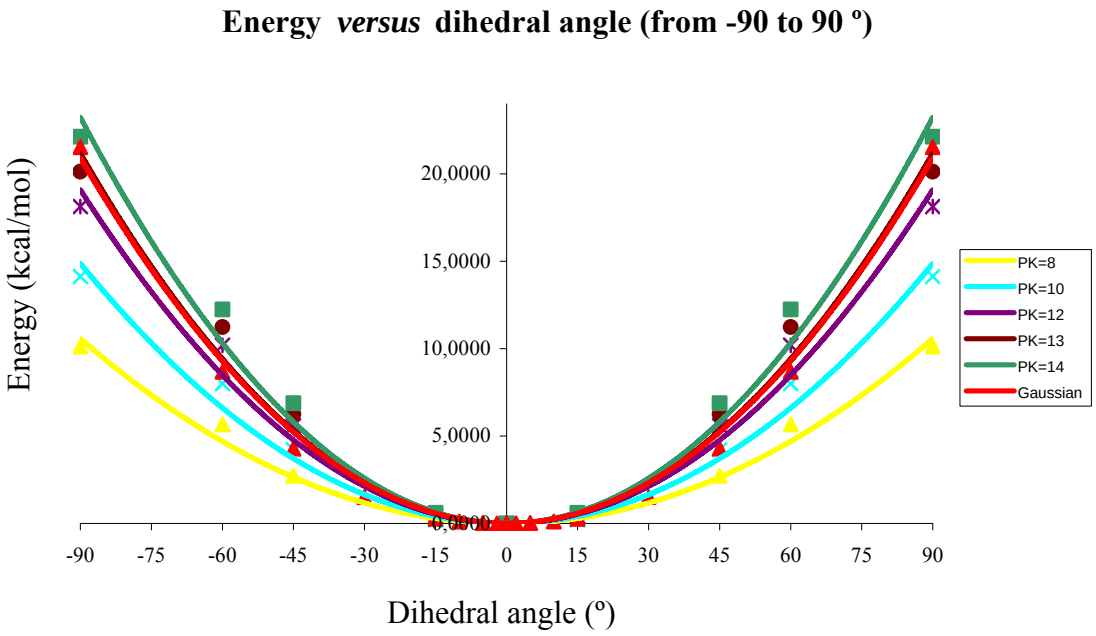

Scheme 11-5.- Energy profile along dihedral angle X-cr-cr-X around 0º (from -90 to 90 degrees).

It notices that the curves represented in Scheme 11-5 follow a quadratic polynom and all of them have a minimum at 0º. It is also shown that using PK=13 give as a results a curve which is similar to that obtained by quantum mechanics.

In conclusion, the best fit is obtained when PK is equal to 13.0 kcal/mol.

11.3 BOND PARAMETERS SEARCHING

In order to find good parameters for bond cr-cr (Kbond and Dbond), we decided to calculate different Bond Energy curves *versus* bond distance modifying Kbond and Dbond.

Firstly, we started using the conditions F found previously (Dbond= 1.417 Å, PK=13.0 kcal/mol) and varying Kbond. Different conditions were tested (see Scheme 11-6).

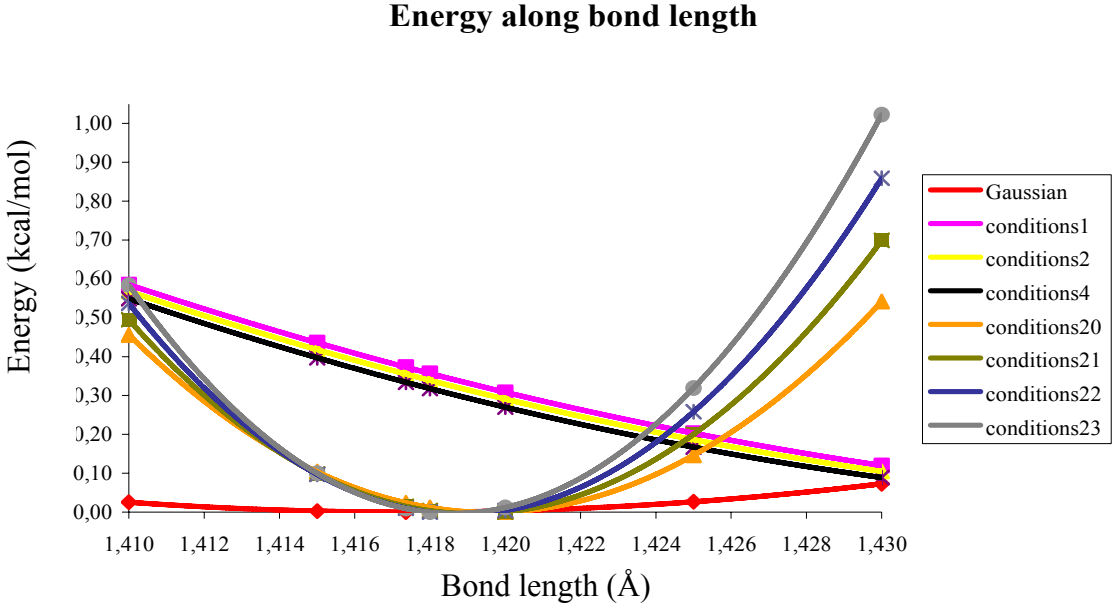

Scheme 11-6.- Energy profile along cr-cr distance.

However, any of them gave good results. Using a Kbond of 423 kcal·mol^{-1}·Å^{-2} (Scheme 11-6, conditions 2), a graph was obtained whose slope was similar to the Gaussian curve. However, the energy minimum was far from 1.417 Å (minimum distance length taken from Gaussian). Increasing the constant value, the energy minimum was getting closer to the minimum observed in the curve calculated in Gaussian. However, the shape of that curve was too much different as that taken from quantum mechanics calculations (see Scheme 11-6, conditions 23, for example).

So, we decided to modify the Dbond value to 1.389 Å. Afterwards, the bond energy profile was calculated using bond constants from 423 up to 426 kcal·mol^{-1}·Å^{-2} (see Scheme 11-7).

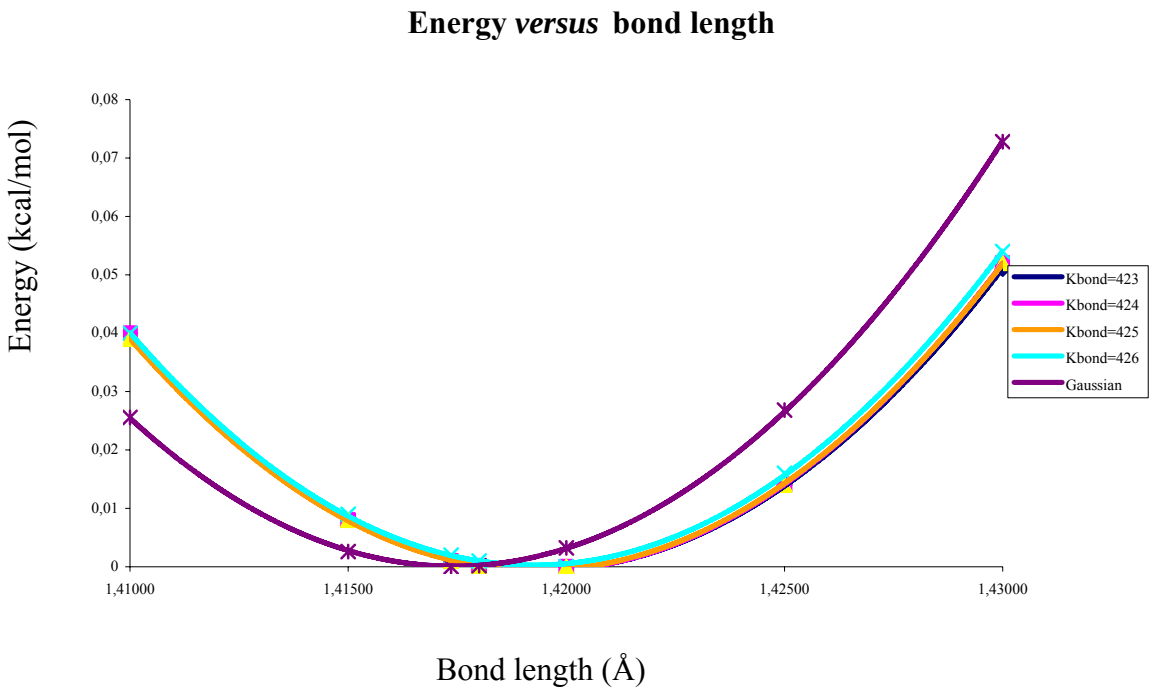

Scheme 11-7.- Representations of the Energy *versus* bond length using a Dbond equal to 1.389 Å.

The curve shape obtained using Kbond=423 kcal·mol^{-1}·Å^{-2} (see Scheme 11-7) were very similar to the curve shape obtained in Gaussian (RMSD calculations were done). However, the minimum distance or equilibrium distance was around 1.419 Å.

Finally, we decided again to change bond distance value and to use Dbond=1.387 Å and then to calculate the bond energy profile along bond length for the following conditions (see Scheme 11-8):

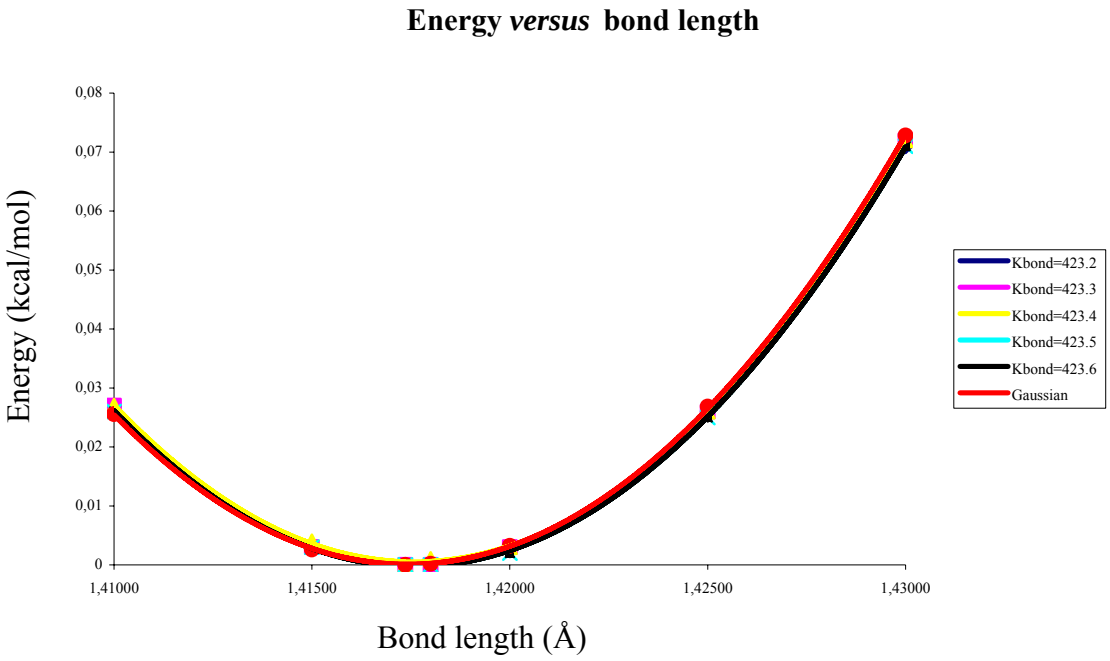

Scheme 11-8.- Energy profile *versus* bond length using Dbond=1.387 Å.

Using a bond constant value of 423.3 kcal·mol^{-1}·Å^{-2}, a curve was obtained whose shape and well is in agreement (RMSD calculations were done) with that obtained using quantum mechanics calculations (see Scheme 11-8, pink curve).

The bond parameters found perfectly reproduce the Gaussian data. In fact, a test was done where all the new parameters found were used to calculate a dihedral energy profile and then, the curve obtained was in agreement with the curve calculated by Gaussian (see Scheme 11-9).

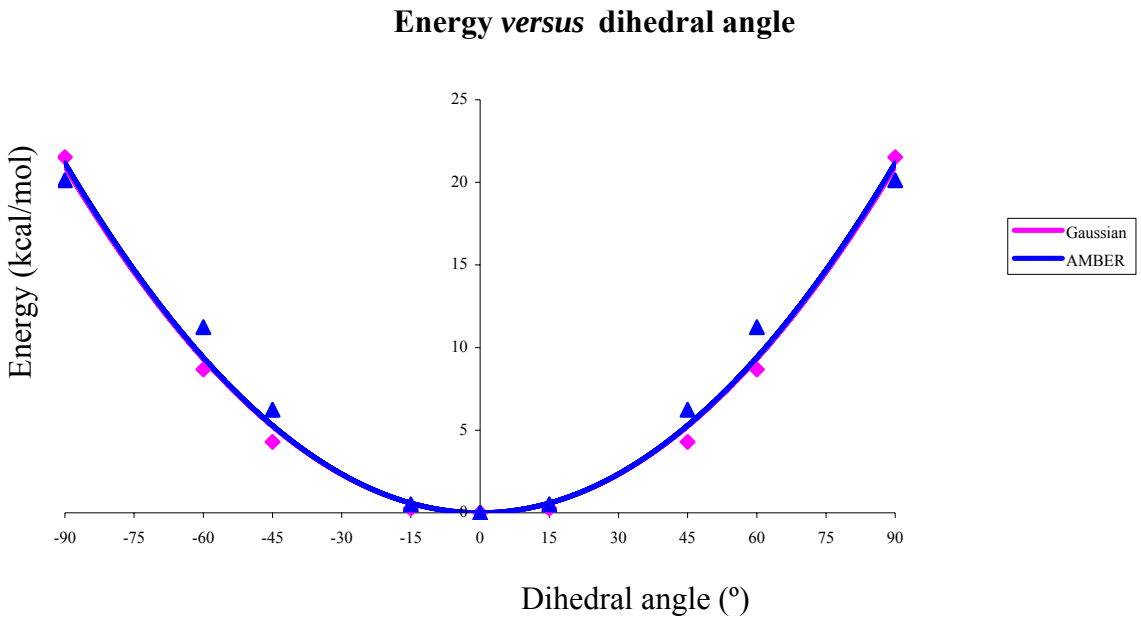

Scheme 11-9.- Energy profiles *versus* dihedral angle for *ab initio* and AMBER.

To sum up, the parameters file related to the radical cation viologens are shown just below :

```
Force Field parameters for cation radicals.Javier & Jacek,2006
MASS
cr 12.01         0.360               same as cp

BOND
ca-cr  466.1    1.395                same as ca-cp
cr-cr  423.3    1.387                Javier Perez

ANGLE
c3-ca-cr    63.7      120.63         same as c3-ca-cp
ca-ca-cr    67.2      119.07         same as ca-ca-cp
cr-ca-ha    48.0      121.08         same as cp-ca-ha
ca-cr-cr    62.6      127.01         same as ca-cp-cp
ca-cr-ca    67.1      118.75         same as ca-cp-ca

DIHE
X -cr-cr-X    4   13.000       180.000          2.000     Javier Perez
X -ca-cr-X    4   14.500       180.000          2.000     same as X -ca-cp-X

NONB      RE
       cr          1.9080  0.0860            OPLS       same as cp
```

Scheme 11-10.- Parameters for the cation viologen CRE and CRD.

And the atom types for the CRE and CRD viologens are in the following scheme:

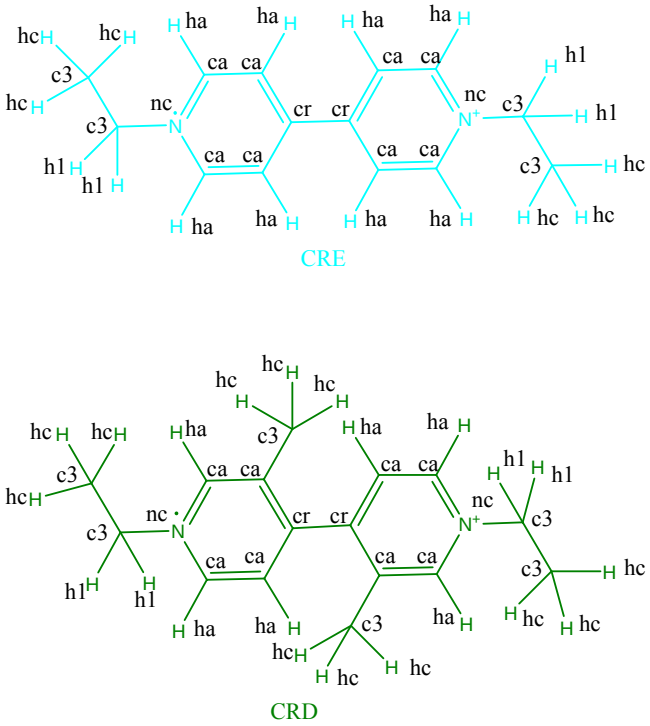

Scheme 11-11.- Atom types for the cation radical viologens CRE and CRD.

'Wisdom is what makes
poor man a king,
a weak person powerful,
a good generation of a bad one,
a foolish man
reasonable.'
Irish proverb

12 SOLVENT-SOLVENT INTERACTION AND COMPLEXATION ENERGY CALCULATION

12.1 SOLVENT-SOLVENT INTERACTION

Molecular dynamic simulation with explicit solvent were run in this thesis and the module xleap implemented in AMBER was used in order to build each system. In xleap, it is possible to specify the size of the solvent box that will appear around the molecule. However, the number of solvent molecules is not a controllable parameter because it depends on the system and the solvent box size. For example, if the same box size is used for the solvation of two different molecules (or two different conformers for the same molecule), two different numbers of solvent molecules will most likely be obtained.

The goal, problem and solution of this chapter are defined just below:

Goal: to obtain the complexation energies calculated from the complex energy and from the energies of its components.

Problem: Each specie has different number of solvent molecules, which makes that the complexation energy cannot be stimated directly because the energy obtained is the sum of that coming from the molecule plus solvent-solvent interaction.

Solution: to obtain the "intrinsic" energy for each specie by removing the energy due to solvent from the energy of the total system (molecule + solvent). However, this solution brings about a new problem: how to evaluate solvent contribution, but this problem has been solved by developing a new methodology.

To take into account the solvent-solvent interaction for the calculation of the complexation energy for each pseudorotaxane, molecular dynamics simulations of different size solvent boxes were done. Solvent-solvent interaction for acetonitrile and methanol were calculated.

Cubic box of different sizes for solvent, number of solvent in each box and total energy for each system are gathered in the following tables:

Box size (Å)	Number of solvent molecules	E total (kcal/mol)
12	124	-1847.57
14	147	-2185.57
16	279	-4125.95
17	251	-3718.21
18	503	-7429.21
19	380	-5613.51
20	487	-7199.04
22	615	-9076.19
23	791	-11666.17
24	897	-13230.67
26	966	-14242.33
28	1077	-15878.39
29	1509	-22231.14
30	1845	-27169.85

Table 12-1.- Data for molecular dynamics simulations for acetonitrile boxes.

Box size (Å)	Number of solvent molecules	E total (kcal/mol)
5	269	874.38
6	306	998.38
7	388	1268.10
8	490	1613.06
9	602	1988.11
10	743	2458.67
11	860	2856.80
12	1006	3346.74
13	1187	3949.40
14	1381	4600.07
16	1822	6088.74
18	2308	7704.19
20	2911	9716.54

Table 12-2.- Data for molecular dynamics simulations for methanol boxes.

Taking into account the data shown in Table 12-1, the energy per solvent molecule *versus* the number of acetonitrile molecules was represented (Scheme 12-1).

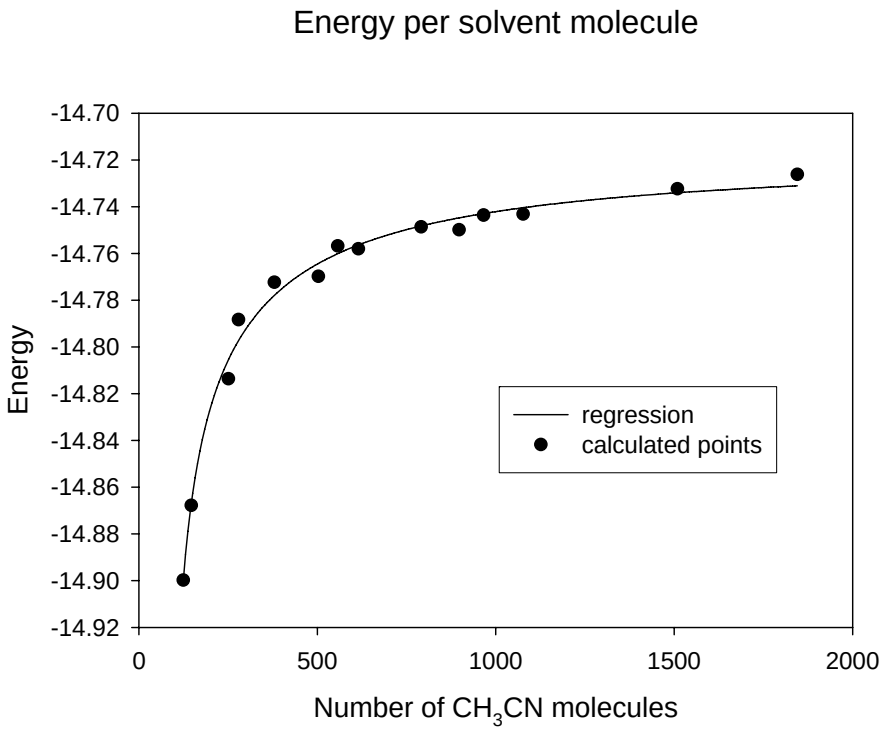

Scheme 12-1.- Representation of the Energy per molecule *versus* number of CH_3CN molecules.

In Scheme 12-1 is shown that Energy is no linearly dependent. Energy increases with number of solvent molecules (*n*) and the best fit follows the next equation:

$$G_{n(solvent)} = A + \frac{B}{n} + \frac{C}{n^2} + \frac{D}{n^3}$$

Equation 12-1

This function will be used to calculate the energy term associated to the solvent-solvent interaction for each system designed. Over 1000 acetonitrile molecules, energy remains almost constant or this increases slightly.

The variation of the energy per methanol molecule is represented in the Scheme 12-2:

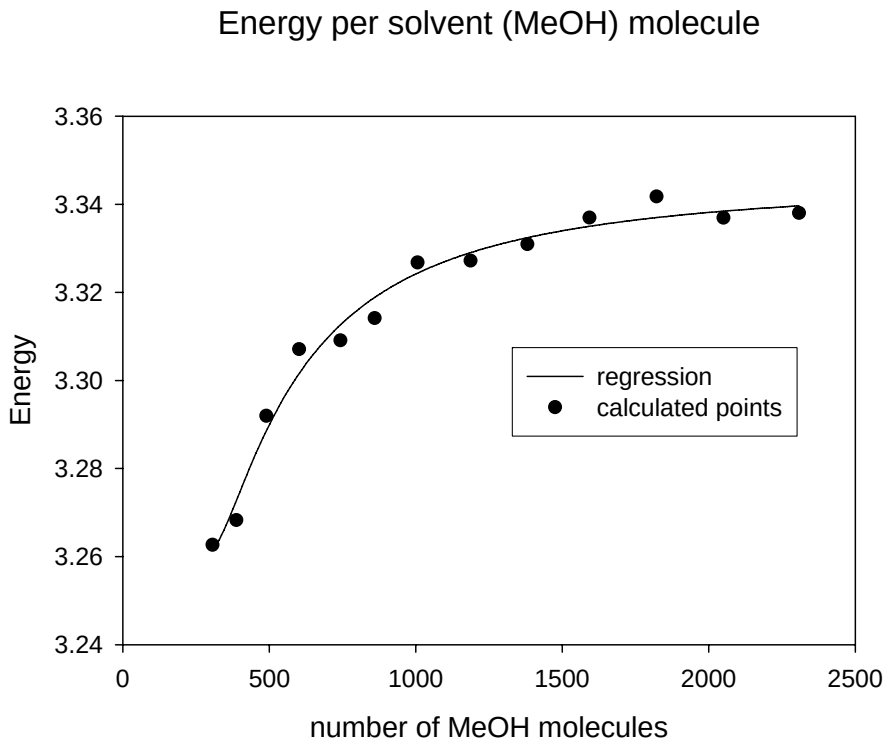

Scheme 12-2.- Representation of the energy per molecule *versus* number of methanol molecules.

Analogously to the acetonitrile case, it is shown that energy varies depending on the number of molecules following the polynomial equation Equation 12-1, whose constants parameters A, B, C and D for methanol and acetonitrile are gathered in the following table:

solvent	A	B	C	D
Acetonitrile	-14.71726	-26.36338	1654.307	-148869
methanol	3.345866	-10.62908	-13577.8	2611037

Table 12-3.- Constants parameters for acetonitrile and methanol in the equation Equation 12-1.

12.2 COMPLEXATION ENERGY CALCULATION

Energy for any system can be calculated using the next equation:

$$G_i = G_i^S - n \cdot G_{n(solvent)}$$

Equation 12-2

Where, in our case, i can be *complex*, *viologen (or guest)* or *crown (or host), n* is the number of solvent molecules used, G_i^S is the total energy from the system i taken from the molecular dynamic simulation, $G_{n(solvent)}$ is the energy associated to the solvent molecules and G_i is the energy from the system, which will not depend on the number of molecules of solvent.

Finally, complexation energy ΔG can be calculated such as follows:

$$\Delta G = G_{complex} - G_{viologen} - G_{crown}$$

Equation 12-3

In Chapter 3, each complexation energy term was calculated taking into account different sizes of solvent and the value of energy given is an average. For example, in the calculation of the complexation energy for the system ETH·crown·$2PF_6^-$ in acetonitrile, 7 molecular dynamics simulations of crown, 7 MD simulations of ETH·$2PF_6^-$ and 7 MD simulations of the complex ETH·crown·$2PF_6^-$ were run using different sizes of solvent (from 12 to 24 Å). Then, energies resulted from viologen, crown and complex were averaged, $G_{complex}$, $G_{viologen}$ and G_{crown} were obtained and finally, complexation energy for system ETH·crown·$2PF_6^-$ in acetonitrile was calculated. In total, 126 Molecular Dynamics simulations were used to calculate all the complexation energies given in Table 3-1.

In Chapter 4, complexation energies were calculated. In that case, 4 MD simulations were run using acetonitrile as a solvent (box size, 16 Å).

In the following table, total energy, solvent molecules and energy per molecule for each system are gathered:

System	G_i^S (kcal/mol)	Number of solvent Molecules (*n*)	G_i (kcal/mol)
Crown	-7091.5882	488	114.03
AxleA·4PF_6^-	-25878.0812	1767	152.80
AxleA·4PF_6^-·crownV1	-25622.8189	1757	260.88
AxleA·4PF_6^-·crownV2	-25646.2924	1759	266.84

Table 12-4.- Total energy taken from MD simulation (G_i^S), number of solvent molecules and G_i for different systems in acetonitrile (box size= 16 Å).

The complexation energy for each translational conformation was calculated taking into account the study performed with solvents in this chapter and using the Equation 12-3.

Finally, in Chapter 5, 42 MD simulations with different box size of acetonitrile (from 12 to 24 Å) were used to calculate the complexation energies for all radical viologens.

'The early bird catches the worm.'

Irish proverb

13 POTENTIAL ENERGY PROFILE

13.1 INTRODUCTION

One of the objectives in this thesis was to calculate a curve where we could show the energy changes depending on the position of the complex components. We wanted to observe the change of energy during the processes of threading and unthreading. To predict that fact, we decided to develop a script run in AMBER which obtained the Energies (kinetic, potential and total energy) of the system along the center-of-mass distance between the complex components.

Basically, the script shown in Scheme 13-1 is mainly divided in seven steps. In the first step, the program converts an amber .crd file to a .pdb file. PDB is a standard format which can be opened by many programs where the user can visualize and check the geometry for each system structure created. The distance between the center of mass of the host and guest is calculated in the second step. Afterwards, that distance is restrained. In step 3, the file that contains the restraints is created. Then, the system is minimized, heated and equilibrated with restraints (see steps 4 and 5). Later, a molecular dynamics simulation where we can recollect energies and distances data is run (registration step, step 6). When registration step is finished, an average of the distances between host and guest along all the simulation is done (step 7). At the end, kinetic energy, potential energy, total energy and average distance between station and crown are recorded, and a structure taken from the registration step is used to repeat the same process, but now, using a new distance between the host and guest. The program finishes when all the shifts (translations) that were specified by the user just at the execution of the script are done.

The script used for this job is shown just below.

```
##############################################################################################
#
#                                      ENERGY PROFILE SCRIPT
#                                      BY JAVIER PEREZ MIRON
#
##############################################################################################


# Execution command
# Eprofile.exe [name of the system] [number of translations]
#!/bin/csh
set currentdir = `pwd`
cd ${currentdir}



##############################################################################################
#
#              creation report.err  and analytical files
#
##############################################################################################



date > report.err

echo "001dCM         "      > 001new_dCM.txt
echo " 104Ek  "      > 104Ek.txt
echo " 104Ep  "      > 104Ep.txt
echo " 104Etot"     > 104Etot.txt
echo " 104dCM "    > 104CM.txt
echo " Std    "    > 104CM_Std.txt



##############################################################################################



set n = 1
set num1 = 1
while($n <= $2)



##############################################################################################
#
#              crd to pdb using ambpdb. step 1
#
##############################################################################################



/usr/local/amber7/exe/ambpdb -p 001${1}_min1.TOP <001${1}_min${n}.CRD>
001${1}_min${n}.pdb

echo crd to pdb using ambpdb FINISHED.                                    >> report.err
echo structure number "${n}".                                             >> report.err
echo step 1                                                               >> report.err
echo " "                                                                  >> report.err



##############################################################################################
#
#              calculate center-of-mass distance. step 2
#
##############################################################################################



# 001CM.trajin file is created
```

```
echo "trajin ${currentdir}/001${1}_min${n}.CRD"                          > 001CM.trajin
echo "distance CM :ETH@* :COC@*-:CR1@* out 001CM_min${n}.out"           >> 001CM.trajin
echo "go"                                                               >> 001CM.trajin


/usr/local/amber7/exe/ptraj ${currentdir}/001${1}_min1.TOP 001CM.trajin

echo 001CM.trajin file and 001CM_min1.out are  created FINISHED.       >> report.err
echo structure number "${n}".                                          >> report.err
echo step 2                                                            >> report.err
echo " "                                                               >> report.err



##############################################################################################
#
#              Calculate min.file. step 3
#
##############################################################################################



# num1 variable contains the value of the distance between station and macrocycle.

echo "${num1}"                                                 > 001new_dCM${n}.txt

#min.file is created
#min.file. This file contains the parameters needed to define the distance between
#the station and the macrocycle.

echo "&rst"                                                                  > min.file
echo "iat=-1,-1,"                                                            >> min.file
echo "ir6=0,"                                                                >> min.file
echo "r1=0.0,"                                                               >> min.file
echo r2="$num1"","                                                           >> min.file
echo r3="$num1"","                                                           >> min.file
echo "r4=99.0,"                                                              >> min.file
echo "rk2=100.0,"                                                            >> min.file
echo "rk3=100.0,"                                                            >> min.file
echo "igr1=39,44,57,62,"                                                     >> min.file
echo "igr2=17,18,"                                                           >> min.file
echo "&end"                                                                  >> min.file
echo " "                                                                     >> min.file

echo min.file is created FINISHED.                                           >> report.err
echo structure number "${n}"                                                 >> report.err
echo step 3                                                                  >> report.err
echo " "                                                                     >> report.err

cp min.file  min.file${n}



##############################################################################################
#
#              minimization. step 4
#
##############################################################################################



#/prod/AMBER/amber7/exe/sander -O \
/usr/local/amber7/exe/sander -O \
-i 001min.in \
-o 001${1}_min${n}.out \
-p 001${1}_min1.TOP \
-c 001${1}_min${n}.CRD \
-r 001${1}_min${n}.rst \
-inf 001${1}_min${n}.inf         ||goto error1

echo minimization FINISHED.                                                  >> report.err
echo structure number "$n"                                                   >> report.err
echo step 4                                                                  >> report.err
echo " "                                                                     >> report.err
```

```
#############################################################################################
#
#              Heating and Equilibration step. step 5
#
#############################################################################################


#/prod/AMBER/amber7/exe/sander -O \
/usr/local/amber7/exe/sander -O \
-i 103min.in \
-o 103${1}_min${n}.out \
-p 001${1}_min1.TOP \
-c 001${1}_min${n}.rst \
-x 103${1}_min${n}.trj \
-r 103${1}_min${n}.rst \
-inf 103${1}_min${n}.inf         ||goto error2


echo Heating and Equilibration step FINISHED.                                  >> report.err
echo structure number "$n"                                                     >> report.err
echo step 5                                                                    >> report.err
echo " "                                                                       >> report.err


#############################################################################################
#
#                                        Registration Step. step 6
#
#############################################################################################


#/prod/AMBER/amber7/exe/sander -O \
/usr/local/amber7/exe/sander -O \
-i 104min.in \
-o 104${1}_min${n}.out \
-p 001${1}_min1.TOP \
-c 103${1}_min${n}.rst \
-x 104${1}_min${n}.trj \
-r 104${1}_min${n}.rst \
-inf 104${1}_min${n}.inf         ||goto error3

echo registration  step FINISHED.                                              >> report.err
echo structure number "$n"                                                     >> report.err
echo step 6                                                                    >> report.err
echo " "                                                                       >> report.err


#############################################################################################
#
#              calculate center-of-mass distance from Registration Step. step 7
#
#############################################################################################


echo "trajin ${currentdir}/104${1}_min"${n}".trj"                               > 104CM.trajin
echo "distance CM :ETH@* :COC@*-:CR1@* out 104CM_min"${n}".out"                >> 104CM.trajin
echo "go"                                                                      >> 104CM.trajin

/usr/local/amber7/exe/ptraj ${currentdir}/001${1}_min1.TOP 104CM.trajin

media.com 104CM_min${n}

echo center-of-mass distance from Registration Step FINISHED.                  >> report.err
echo structure number "$n"                                                     >> report.err
echo step 7                                                                    >> report.err
echo " "                                                                       >> report.err
```

```
#############################################################################################
#
# preparing .CRD file for next step
#
#############################################################################################



set m = `expr $n + 1`

cp 104${1}_min${n}.rst 001${1}_min${m}.CRD



#############################################################################################
#
# analytical files
#
#############################################################################################


cat 001new_dCM${n}.txt |awk '{print $1}'  >> 001new_dCM.txt
grep 'Etot' 104${1}_min${n}.out | tail -2 | head -1 | cut -c39-46  >> 104Ek.txt
grep 'Etot' 104${1}_min${n}.out | tail -2 | head -1 | cut -c66-73 >> 104Ep.txt
grep 'Etot' 104${1}_min${n}.out | tail -2 | head -1 | cut -c15-22 >> 104Etot.txt
cat 104CM_min${n}.media |head -1 |awk '{print $1}' >> 104CM.txt
cat 104CM_min${n}.media |tail -1 |awk '{print $1}' >> 104CM_Std.txt


########################################


       @ n = $n + 1

       @ num1 = $num1 + 1

end

paste 001new_dCM.txt 104Ek.txt 104Ep.txt 104Etot.txt 104CM.txt 104CM_Std.txt >
analyse.txt


goto final

exit



#############################################################################################
#
#                                     errors
#
#############################################################################################



error1:
date >> report.err
echo 'There was an error in minimization step'                  >> report.err
echo 'Check the files and try again'                            >> report.err
exit
#
error2:
date >> report.err
echo 'There was an error in the heating and equilibration step' >> report.err
echo 'Check the files and try again'                            >> report.err
exit
#
error3:
date >> report.err
echo 'There was an error in the registration step'              >> report.err
echo 'Check the files and try again'                            >> report.err
exit
#
error4:
```

```
date >> report.err
echo 'There was an error in the average structure minimization'  >> report.err
echo 'Check the files and try again'                             >> report.err
exit
#
final:
date >> report.err
echo 'The calculation is finished'                               >> report.err
echo 'Good job'                                                  >> report.err
exit
#

##############################################################################################
#
#                                       END
#
##############################################################################################
```

Scheme 13-1.- Script for Energy profile calculation.

'Humor to a man
is like a feather pillow.
It is filled with what is
easy to get
but gives
great comfort.'
Irish proverb

14 HOMO AND SPIN DELOCALISATION (GAUSSIAN)

14.1 HOMO CALCULATIONS

The calculations of HOMO done in this thesis were carried out with Gaussian 03 program in two steps.

Firstly, the most stable conformation taken from Molecular Dynamics simulation was used then for a single point calculation. The command used was the following:

```
#P mp2/6-31G* SP geom=connectivity maxdisk=40GB test
```

Afterwards, the checkpoint generated (file.chk) was converted to a formatted checkpoint file.

```
formchk file.chk file.fchk
```

Finally, a .cub file, which contains the molecular orbital data, was created using the following command:

```
cubegen 512MB MO=Homo file.fchk file.cub 0 h
```

14.2 SPIN DELOCALISATION CALCULATION

It is possible to observe how the electrons are delocalised around the molecule creating a .cub file using the following command:

```
cubegen 512MB spin=Spin file.fchk file2.cub 0 h
```